Check for updates

Advanced Functional Materials

ADVANCED FUNCTIONAL MATERIALS
www.afm-journal.de

REVIEW

The Evolution and Integrated Systems of Microbatteries

Sheng Wang[1] | Huajian Xu[2] | Xiaopan Song[3] | Yang Gu[3] | Linwei Yu[1,3]

[1]College of Electronic and Optical Engineering, College of Flexible Electronics (Future Technology), Nanjing University of Posts and Telecommunications, Nanjing, P. R. China | [2]School of Electronic and Information Engineering, Soochow University, Suzhou, P. R. China | [3]School of Electronics Science and Engineering, Nanjing University, Nanjing, P. R. China

Correspondence: Sheng Wang (shengwang@njupt.edu.cn) | Xiaopan Song (songxiaopan@nju.edu.cn) | Linwei Yu (yulinwei@nju.edu.cn)

Received: 18 September 2025 | **Revised:** 23 December 2025 | **Accepted:** 24 December 2025

Keywords: integrated arrays | microbatteries | nanowire | on-chip integration

ABSTRACT

Advances in microbatteries (MBs) technology drive miniaturization and on-chip integration, embedding energy storage directly within semiconductor substrates to deliver compact power solutions for portable electronics. This progress meets growing demands across applications such as Internet of Things (IoT) sensors and wearable devices. However, MBs remain in an early developmental stage compared to commercial lithium-ion batteries, requiring breakthroughs in materials science, manufacturing methods, and structural engineering to improve performance. A comprehensive understanding of these aspects is critical for advancing the field. This review meticulously examines the historical evolution of MBs technologies, emphasizing pivotal advancements in nanostructured systems, particularly focusing on thin-film architectures and self-aligned nanowire growth techniques. Furthermore, the review delves into the integration of artificial intelligence (AI) within the realm of MBs, alongside exploring advanced fabrication techniques and optimization strategies. Subsequently, we conduct a systematic analysis of several specific application scenarios. Based on the extant developmental status, this paper proposes prospective research avenues, with particular emphasis on high-density integrated arrays and flexible MBs, thereby providing strategic guidance for further augmenting MBs performance. The key challenges and technical pathways are elucidated, deepening understanding of current paradigms while establishing a foundation for future innovations.

1 | Introduction

The exponential expansion of Internet of Things (IoT) infrastructure, anticipated to exceed 30 billion interconnected edge devices by 2025, has precipitated a critical need for advanced miniaturized electrochemical energy storage solutions capable of sustaining operationally autonomous microelectronic systems [1–3]. Core IoT subsystems—including microelectromechanical systems (MEMS), implantable biotelemetric sensors, and passive radio frequency identification (RFID) transponders—demand microscale energy harvesting systems with monolithic integration capabilities that ensure energy autonomy while maintaining operational stability across extended thermal cycling regimes (−40°C to 85°C) without periodic maintenance interventions [4–7]. These operational constraints have catalyzed the emergence of microsupercapacitors (MSCs) and solid-state microbatteries (MBs) as dual vanguards in next-generation energy storage development, each leveraging divergent charge storage modalities to service discrete application domains within the IoT power continuum [8–12]. The diversity of application scenarios and performance requirements serves as the core driving force behind the diversification and refinement of microbattery technologies. For instance, the urgent demand for power sources that are thin, lightweight, flexible, and deformation-tolerant in flexible wearable electronics directly fuels the continuous advancement and optimization of thin-film battery technology in terms of material selection, structural design, and integration processes. In the medical implant

© 2026 Wiley-VCH GmbH

sector, stringent standards for device biocompatibility, long-term stability, and utmost safety strongly propel innovation in miniaturized, high-safety MB systems designed for in vivo applications. Meanwhile, for applications such as micro-drones and remote sensors that require high energy density, the associated demands continually spur and accelerate research progress in new MB systems, such as those incorporating nanowire anode materials. This research aims to shorten ion transport pathways and enhance material utilization efficiency through nanostructure engineering.

MBs development has undergone three distinct technological paradigms: initial efforts employed geometric scaling of conventional Li-ion architectures, followed by solid-state electrolyte integration enabling 3–5 mAh cm^{-2} areal capacities under 0.1C discharge regimes, with current third-generation systems achieving breakthrough energy densities (>800 Wh L^{-1}) through architecturally engineered three-dimensional (3D) interdigitated current collectors. State-of-the-art solid-state Li MBs demonstrate 500–800 Wh L^{-1} volumetric energy densities-doubling conventional Li-polymer counterparts–while maintaining mechanically compliant architectures suitable for epidermal sensor arrays, with recent prototypes sustaining >90% capacity retention after 2000 bending cycles at minimum radii < 500 μm [13–20]. Crucially, innovations like liquid-droplet-based soft MBs merge energy storage with therapeutic functionality, enabling applications in cardiac defibrillation and neural stimulation. The integration of these technologies with energy harvesting systems (e.g., microscale photovoltaics or piezoelectrics) is redefining autonomous operation paradigms. The hybrid MB-MSC architecture, governed by AI-driven energy management algorithms, now achieves 24/7 operation in environmental sensors by dynamically allocating energy reserves. Furthermore, emerging "skin-powered" systems eliminate traditional batteries entirely, utilizing human-body RF energy transmission to sustain low-power IoT nodes-a paradigm shift toward batteryless wearables [21–24].

The evolution of MBs is characterized by sustained advancements in key performance indicators, including energy and power densities, cycle life, safety, and scalability. Early research efforts were primarily directed toward downsizing conventional battery chemistries, a process that introduced unique challenges concerning electrode design, electrolyte stability, and manufacturing methodology [16, 25–27]. As the field progressed, investigations expanded to encompass novel materials and innovative architectures, which have not only elevated electrochemical performance but also enabled seamless integration with microelectronic systems. This progression has culminated in the development of integrated power systems, wherein MBs are seamlessly embedded as integral components of the device structure, thereby optimizing spatial efficiency and enhancing overall system performance. As the preferred power solution for advanced miniaturized devices, MBs provide adequate energy density and ensure a stable voltage output. Typically, a rechargeable battery comprises a cathode, an anode, and an electrolyte layer interposed between them. The challenge of miniaturization primarily focuses on reducing the dimensions of these electrodes from centimeters to micrometers without compromising performance [28–30]. Contemporary innovations in MBs technology emphasize multiscale heterogeneous co-integration across physical, material, and system domains. At the architectural innovation frontier, atomic layer deposition-enabled solid-state MBs with sub-50μm thickness demonstrate direct backside integration on system-on-chip (SoC) platforms through 3D heterogenous integration techniques. Utilizing sulfur–argyrodite solid electrolytes ($Li_7P_3S_{11}$, 5–15 mS cm^{-1} ionic conductivity) paired with lithographically defined through-silicon vias (TSVs < 10 μm diameter), these monolithic systems achieve 18–25 mAh cm^{-2} areal capacities with volumetric energy densities reaching 450 Wh L^{-1} under 0.5C cycling conditions, while maintaining 82% capacity retention after 2000 cycles through interface-engineered Li/electrolyte interphases [31]. Meanwhile, breakthroughs in integration strategies have enabled novel energy architectures. For instance, implantable MBs utilize biocompatible encapsulation materials, such as polyimide/silicon nitride composite coatings, in conjunction with flexible electrode architectures, including carbon nanotube/lithium composite fibers, to enable seamless integration within cardiac pacemakers or neural stimulators. These systems are capable of delivering stable power outputs for durations exceeding a decade [13]. Hybrid systems combining "solar cell-microbattery" configurations further demonstrate vertical stacking of perovskite photovoltaic(PV) layers and miniature lithium-ion batteries (LIBs), achieving >22% efficiency and >90% area utilization to enable 24/7 power supply for wireless sensor nodes [32]. More ambitiously, on-chip MBs, fabricated via MEMS processes and 3D heterogeneous integration, embed energy storage units directly into processor or sensor chips, creating "memory-compute-energy" unified architectures that boost system energy efficiency by over 30% [33].

Nevertheless, the scalable deployment of micro-batteries in hyper-integrated systems faces multifaceted challenges. Technologically, on-chip integration must address thermal management (e.g., capacity degradation at chip temperatures >80°C) and interfacial compatibility (e.g., microcracks caused by thermal expansion mismatches between silicon substrates and battery materials). In system-level integration, dynamic coupling of multi-energy sources (e.g., solar, RF energy harvesting, and MBs) and cross-scale management (spanning nanoscale electrodes to centimeter-scale packaging) demand adaptive energy routing algorithms. From an application perspective, stringent biosafety certifications for implantable devices (e.g., long-term ion leakage rates <0.1 μg cm^{-2}) and manufacturing yield targets for on-chip integration (>95%) require breakthroughs in precision engineering. Addressing these challenges necessitates a holistic innovation framework that integrates material genome engineering (e.g., high-throughput screening of solid electrolytes), heterogeneous packaging (e.g., wafer-scale MBs arrays), and system-level co-design (leveraging digital twin-enabled multiphysics simulations). Such a "material devices-systems" co-optimization paradigm is critical to unlocking the full potential of MBs in next-generation intelligent microsystems [34–36].

To date, comprehensive reviews on micro-power sources have predominantly centered on MSCs, whereas comparatively limited research attention has been directed toward MBs. However, given the groundbreaking advancements achieved in the field of MBs over recent years, a systematic synthesis of their latest developments has become critically imperative. In this review, we present a comprehensive retrospective analysis of

16163028, 2026, 33, Downloaded from https://advanced.onlinelibrary.wiley.com/doi/10.1002/adfm.202524957 by Nanjing University, Wiley Online Library on [03/11/2026]. See the Terms and Conditions (https://onlinelibrary.wiley.com/terms-and-conditions) on Wiley Online Library for rules of use; OA articles are governed by the applicable Creative Commons License

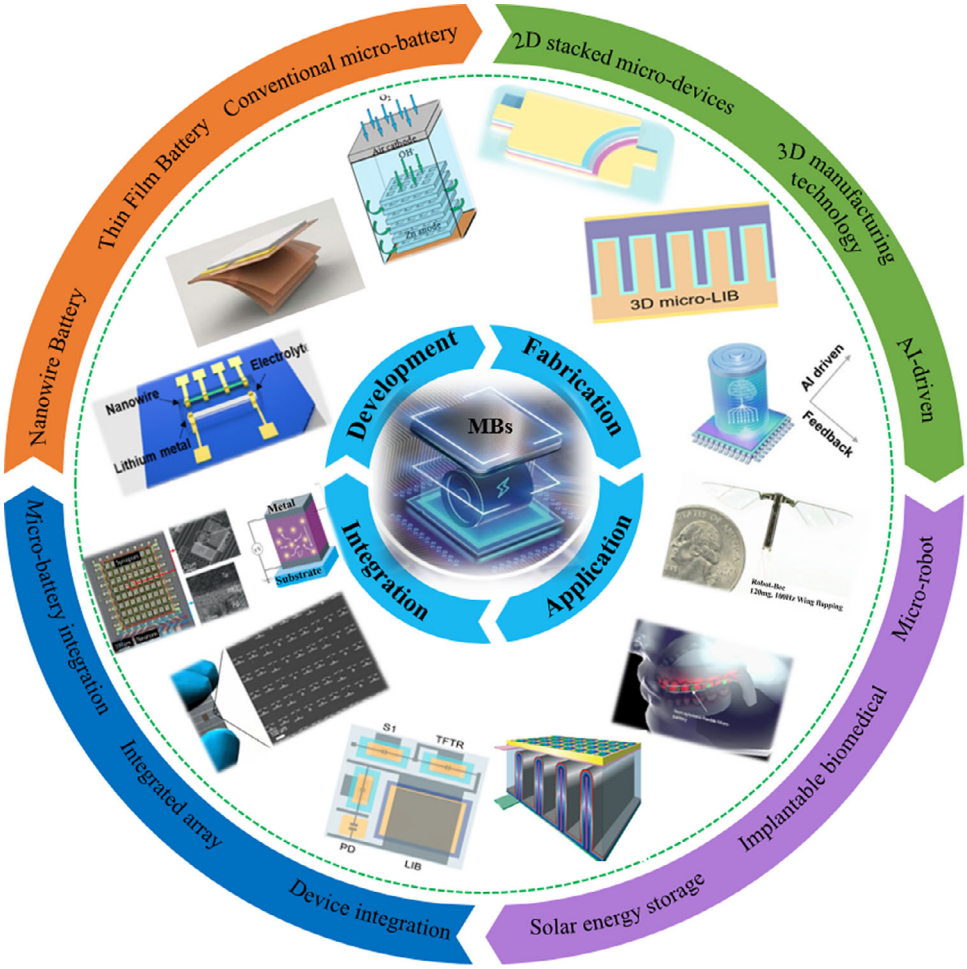


FIGURE 1 | Development, fabrication, integration, and applications of MBs. Conventional micro-battery. Reproduced with permission [37]. Copyright 2011, IOP Publishing. Thin Film Battery. Reproduced with permission [38]. Copyright 2018, Elsevier. Nanowire Battery. Reproduced with permission [39]. Copyright 2019, Elsevier. 2D stacked micro-devices. 3D manufacturing technology. Reproduced with permission [40]. Copyright 2024, Nature Publishing Group. AI-driven. Reproduced with permission [41]. Copyright 2024, Elsevier. Micro-robot. Reproduced with permission [42]. Copyright 2017, IEEE. Implantable biomedical. Reproduced with permission [43]. Copyright 2017, Springer Nature. Solar energy storage. Reproduced with permission [44]. Copyright 2007, Wiley-VCH. Device integration. Integrated array. Micro-battery integration. Reproduced with permission [45]. Copyright 2020, Springer Nature.

the evolution of MBs, alongside an in-depth exploration of their cutting-edge achievements and challenges in fabrication, functionalization, intelligent integration, and practical applications. The review begins with a concise overview of the historical progression of MBs, emphasizing the technological evolution of thin-film batteries and nanowire-based architectures. Subsequently, we elaborate on advanced manufacturing techniques and the application of artificial intelligence (AI) in MBs, including an evaluation of key performance parameters and metrics that define their operational efficacy. Furthermore, the article highlights frontier research in intelligent integrated systems, particularly focusing on the synergistic integration of MBs with solar cells and multifunctional sensors (Figure 1). Finally, we underscore the principal technical challenges confronting MBs, spanning design optimization, system-level integration, and performance enhancement strategies. Through this structured analysis, this review aims to provide valuable insights and references to guide future research and innovation in the field.

2 | The Development and Manufacturing of Microbatteries

2.1 | The Development of Microbatteries

The rapid advancement of technology has fueled the evolution of MBs as compact, high-performance energy sources. Originating in the 1950s with mercury-based systems, early MBs were quickly rendered obsolete due to environmental toxicity concerns, prompting a shift toward lithium-based chemistries. Key breakthroughs in the 1970s and 1980s, such as the development of lithium-iodine batteries for medical implants and Sony's commercialization of lithium-ion technology, laid the groundwork for architectures with enhanced safety and energy density. In subsequent decades, material innovations—ranging from nanostructured electrodes to solid-state electrolytes—have enabled ultrathin, flexible, and high-power designs tailored for IoT and wearable devices. In contemporary research, there is an increasing emphasis on developing sustainable and intelligent

16163028, 2026, 33, Downloaded from https://advanced.onlinelibrary.wiley.com/doi/10.1002/adfm.202524957 by Nanjing University, Wiley Online Library on [03/11/2026]. See the Terms and Conditions (https://onlinelibrary.wiley.com/terms-and-conditions) on Wiley Online Library for rules of use; OA articles are governed by the applicable Creative Commons License

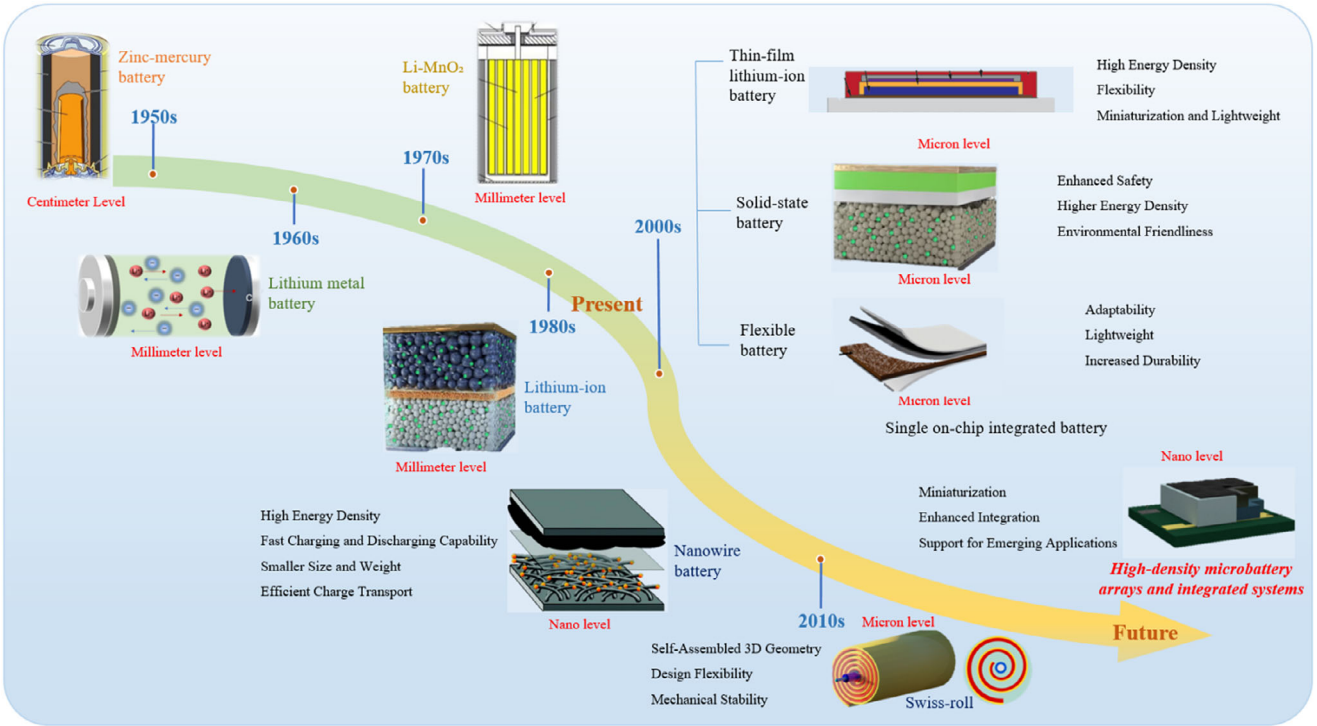


FIGURE 2 | Developmental trajectory and evolution of batteries. Zinc–mercury battery. Lithium metal battery. Li-MnO_2 battery. Lithium-ion battery. Thin-film lithium-ion battery. Solid-state battery. Flexible battery. Reproduced with permission [49]. Copyright 2021, Royal Society of Chemistry. Swiss-roll. Reproduced with permission. Copyright 2024, American Chemical Society. Nanowire battery. Single on-chip integrated battery. Reproduced with permission [50]. Copyright 2021, American Chemical Society.

energy solutions, exemplified by biodegradable systems and interface-engineered solid-state batteries. This trend signifies a paradigm shift from standalone energy storage devices toward multifunctional, integrated power architectures. Such advancements underscore the critical importance of MBs in enabling the digital transformation and interconnectivity of modern technologies, positioning them as pivotal components in the future development of sophisticated microsystems [46–48].

The evolution of MBs technology traces a transformative trajectory shaped by interdisciplinary advancements (Figure 2). The 1950s semiconductor revolution catalyzed electronics miniaturization, creating critical demand for compact power solutions. Early zinc-mercury batteries addressed this need but faced rapid obsolescence due to mercury's environmental persistence and bioaccumulative risks, prompting urgent exploration of sustainable alternatives. Lithium emerged as a prime candidate in the 1960s, leveraging its exceptional electrochemical attributes — −3.04 V redox potential and 3860 mAh g^{-1} theoretical capacity. However, commercialization barriers persisted due to dendritic lithium growth during cycling, causing catastrophic thermal failures. Lithium–manganese dioxide (Li–MnO_2) systems, which became key power sources in aerospace applications due to their stable 3 V discharge profiles, marked a period of technological diversification in the 1970s. At the same time, lithium–iodine (Li–I_2) batteries demonstrated exceptional operational stability—delivering over a decade of reliable performance in cardiac pacemakers—and significantly advanced the field of implantable medical devices [51]. Sony's 1991 commercialization of LIBs marked a paradigm shift, employing graphite anodes and lithium cobalt oxide ($LiCoO_2$) cathodes in a "rocking-chair" ion-shuttling mechanism. This architecture achieved 4V operation with 100–150 Wh kg^{-1} energy densities while eliminating metallic lithium deposition hazards. Mobile technology proliferation in the 1990s drove dual material engineering strategies: Olivine-structured lithium iron phosphate ($LiFePO_4$) cathodes enhanced thermal stability beyond 300°C through robust 3D frameworks, while advanced liquid electrolytes incorporating $LiPF_6$ in EC-DMC solvents achieved stable solid electrolyte interphase (SEI) formation, enabling 500-cycle durability with 80% capacity retention [52]. The wearable electronics and IoT revolutions of the 21st century have driven significant structural advancements in energy storage. Thin-film batteries, fabricated through vapor deposition techniques, have achieved micron-scale thicknesses, while solid-state systems utilizing LLZO and LATP ceramic electrolytes have exceeded energy densities of 400 Wh kg^{-1}, offering enhanced safety performance. Nanoscale material engineering breakthroughs in the 2010s redefined performance boundaries: Stress-engineered silicon nanowire anodes delivered 4200 mAh g^{-1} capacities through volumetric expansion mitigation, while MXene materials leveraged surface redox pseudocapacitance to achieve power densities exceeding 10 kW kg^{-1} [53]. Concurrently, 3D printing enabled precise fabrication of gradient electrode architectures and porous current collectors, optimizing ion diffusion pathways [54]. Current research frontiers focus on solid-state electrolyte interface engineering to achieve 10^{-3} S cm^{-1} ionic conductivity for automotive-grade applications, alongside biodegradable systems employing cellulose matrices with magnesium and zinc electrodes for transient power applications in environmental sensing. These developments underscore MBs'

16163028, 2026, 33, Downloaded from https://advanced.onlinelibrary.wiley.com/doi/10.1002/adfm.202524957 by Nanjing University, Wiley Online Library on [03/11/2026]. See the Terms and Conditions (https://onlinelibrary.wiley.com/terms-and-conditions) on Wiley Online Library for rules of use; OA articles are governed by the applicable Creative Commons License

evolution from basic energy storage devices to sophisticated platforms integrating materials innovation, nanofabrication, and systems engineering.

Within the realm of advancing miniaturized energy storage technologies, LIMBs have distinguished themselves as leading candidates, showcasing remarkable potential for high-efficiency micropower applications. Notably, in the context of energy density, Hur et al. [55] demonstrated a remarkable areal energy density of 5.2 mWh cm^{-2}, even under spatially constrained conditions. By leveraging semiconductor fabrication techniques, the study introduced a fully three-dimensional battery architecture. Selective etching methods were employed to fabricate stable silicon anode arrays, while the cathode was prepared through slurry casting. Additionally, SU-8 photoresist was utilized as the solid electrolyte, applied via coating processes to ensure structural integrity and performance. The constructed LIMBs effectively harnessed the high lithium storage capacity, significantly enhancing energy loading. Additionally, miniaturized devices for other alkali metal ion batteries were also fully developed to complement these advancements. Wang et al. [56] introduced a high-voltage sodium-ion MBs based on a dual-ion battery architecture. This design, which involves the intercalation of anions into graphite, demonstrates significant potential for high-voltage applications. By employing exfoliated graphene for both the anode and cathode, in-plane thin-film MBs achieve an exceptional operating voltage range of 4.3 to 4.7 V, which is comparable to the performance of commercial LIBs. The miniaturization of LIBs exhibits significant promise, attributed to their high-voltage platforms and superior specific capacities, rendering them highly advantageous for integration into micro-energy storage systems. However, this advancement also introduces critical safety considerations. Given the reduced dimensions, the electrodes in MBs can be positioned extremely close together, which intensifies issues related to the combustion risks of organic electrolytes and the propensity for dendritic lithium growth. These factors underscore the necessity for innovative solutions to enhance safety while maintaining performance.

Unlike the previously discussed alkali metal ion batteries, high-performance aqueous batteries have attracted considerable attention owing to their notable advantages in cost efficiency, safety, and ionic conductivity. Within this domain, various ion reaction mechanisms have been widely explored, utilizing charge carriers such as Zn^{2+}, NH_4^+, and Al^{3+}. These features make aqueous batteries an attractive option for research and development in energy storage systems. Characterized by their rapid charge and discharge capabilities, aqueous zinc batteries demonstrate an amplified performance advantage in miniaturized designs, primarily due to the thinner structural dimensions that enhance these properties [37, 57–59]. Lai et al. [60] reported an environmentally benign and integrable zinc–manganese dioxide ($Zn//MnO_2$) MB system, which demonstrated a remarkable volumetric energy density of 71.3 mWh cm^{-3} and achieved a peak power density as high as 1621.4 mW cm^{-2}. The study revealed that aqueous zinc-based MBs are capable of delivering high-power performance comparable to that of electrochemical capacitors at similar power densities, while maintaining energy densities that are competitive with conventional LIBs. Such outcomes underscore the potential for miniaturized aqueous batteries to leverage their inherent advantages, thereby demonstrating superior performance characteristics in compact form factors. Exploiting the potential of 3D nanostructures significantly eased the compromise between achieving high active material loading and sustaining elevated power density. Hao's [58] development of a hierarchically ordered microelectrode (HOP) serves as a prime example, illustrating how advanced electrode design can harmonize these competing requirements. Nanostructured microelectrodes of comparable thickness exhibit both enhanced rate capability and increased capacity relative to solid electrodes, suggesting concurrent advancements in energy and power densities. In contrast to miniaturized LIBs, aqueous zinc MBs typically deliver superior power density, although their energy density tends to be comparatively lower. Carefully optimizing material loading in a vertically dense arrangement can lead to significant advancements in both energy and power densities, thereby addressing these limitations.

Over the past decade, driven by the increasing demand for miniaturization and integration, thin-film batteries and nanowire batteries have garnered significant attention as research hotspots due to their compact size and excellent compatibility with microdevices and on-chip integration. Innovative TFBs, featuring on-chip configurations, scalable dimensions, and high power density despite modest capacity, have been recognized as viable power solutions for enduring, low-power microelectronic devices, including MEMS, detectors, and sensors. For instance, West et al. [68] successfully developed TFBs with areas ranging from 50 to 100 μm^2, aligning with the ongoing trend toward the miniaturization of spacecraft components. By virtue of their distinctive structural design, micro-nanowire batteries exhibit substantially higher energy and power densities than conventional batteries, positioning them as an optimal choice for miniature devices that demand high-performance power solutions. The nanowire structure substantially increases the surface area of electrode materials, thereby enhancing electrochemical reaction efficiency and further improving the battery's charge–discharge rate and cycle life. Additionally, the compact size of micro-nanowire batteries makes them highly suitable for integration into various miniature devices, such as wireless sensors, implantable medical devices, and IoT applications, providing a reliable power supply for these technologies. Moreover, due to their customizable physical properties, such as flexibility and transparency, micro-nanowire batteries are considered an excellent option for emerging fields, particularly in applications like wearable electronics and transparent electronics, where they demonstrate immense potential. Consequently, these batteries not only improve the performance of existing electronic devices but also pave the way for the development of next-generation electronics. They offer vast potential for future innovations across various technological domains. For instance, Mai et al. [69] developed a single nanowire (NW) electrode device to conduct in situ investigations into the capacity fading mechanisms of electrodes in lithium-ion-based energy storage systems. This work represented the first microcell example aimed at elucidating the interplay between material structural evolution, transport characteristics, and electrochemical performance. Beyond nanowire materials, on-chip microcell technology has been successfully adapted for use with two-dimensional (2D) nanosheet materials. For instance, Chowalla et al. [70] developed a low-resistance contact microcell on monolayer molybdenum disulfide (MoS_2) to assess and compare the electrochemical activity at edge

16163028, 2026, 33, Downloaded from https://advanced.onlinelibrary.wiley.com/doi/10.1002/adfm.202524957 by Nanjing University, Wiley Online Library on [03/11/2026]. See the Terms and Conditions (https://onlinelibrary.wiley.com/terms-and-conditions) on Wiley Online Library for rules of use; OA articles are governed by the applicable Creative Commons License

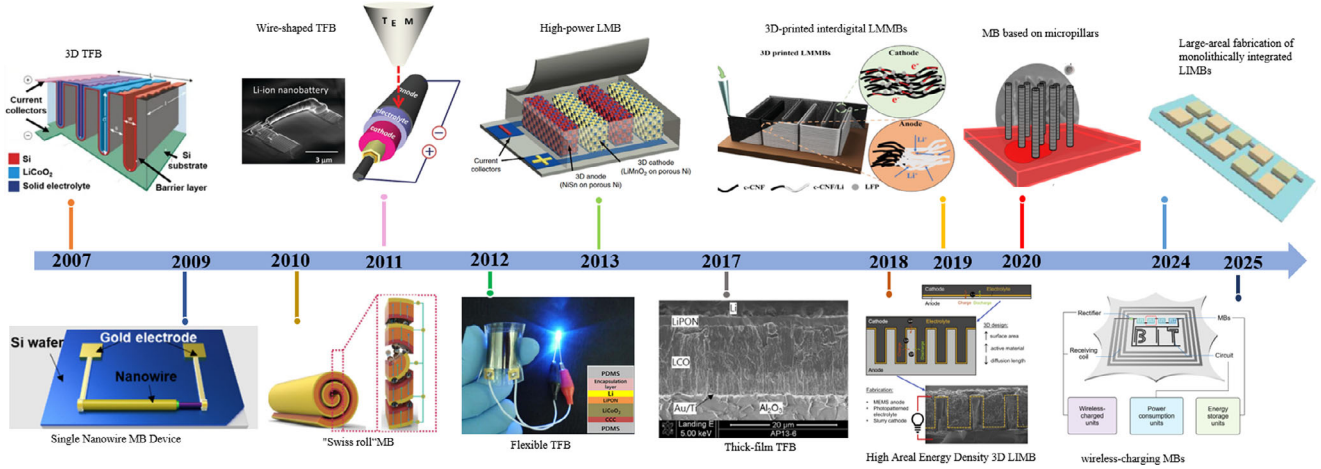


FIGURE 3 | A Brief Roadmap of Representative MB Technologies. 3D TFB. Swiss roll MB. Reproduced with permission [40]. Copyright 2024, Springer Nature. Single Nanowire MB Device. Reproduced with permission [39]. Copyright 2019, Elsevier. Wire-shaped TFB. Reproduced with permission [61]. Copyright 2012, American Chemical Society. Flexible TFMB. Reproduced with permission [57]. Copyright 2012, American Chemical Society. High-power LMB. Reproduced with permission [62]. Copyright 2013, Springer Nature. Thick-film TFB. Reproduced with permission [63]. Copyright 2017, Elsevier. High Areal Energy Density 3D LIMB. Reproduced with permission [55]. Copyright 2018, Elsevier. 3D-printed interdigital LMMBs. Reproduced with permission [64]. Copyright 2019, Wiley-VCH. MB based on micropillars. Reproduced with permission [65]. Copyright 2018, Elsevier. Large-areal fabrication of monolithically integrated LIMBs. Reproduced with permission [66]. Copyright 2025, Elsevier. Wireless-charging MBs. Reproduced with permission [67]. Copyright 2025, AAAS.

sites and the basal plane. Propelled by the escalating demand for progressively miniaturized and high-performance electronic devices, the research and development endeavors in micro-nanowire batteries are advancing pertinent technologies. These advancements include the exploration of cutting-edge materials and innovations in fabrication methodologies, thereby facilitating breakthroughs in the field. Such progress is paving the way for novel application paradigms and sophisticated technological solutions. In the foreseeable future, the evolution of micro-batteries will concentrate on on-chip integration and high-density array architectures to accommodate the increasing intricacies of operational demands and catalyze technological innovation. This trajectory not only promises to enhance the efficacy of existing devices but also furnishes indispensable support for nascent technological sectors. Figure 3 employs a timeline flowchart to outline the development trajectory of MBs, specifically highlighting key milestones in the miniaturization of material dimensions, optimization of fabrication processes, and advancement toward high-density system integration.

2.2 | 3D Thin Film Microbattery

An innovative and highly promising strategy for micropower solutions lies in all-solid-state thin-film lithium/lithium-ion microbatteries (TFBs). These MBs, characterized by their fully solid-state architecture, exhibit compatibility with conventional thin-film fabrication processes, facilitate straightforward miniaturization, and allow precise size adjustability. As a result, they enable seamless on-chip power integration for wireless microelectronic systems, effectively meeting the rigorous demands of contemporary miniaturized technologies [71]. TFBs represent a class of solid-state batteries distinguished by their compact form factor, typically featuring either a stacked (layered) or interdigitated structural configuration. By capitalizing on the flexibility of on-chip design and enabling precise dimensional control, these advanced TFBs deliver a unique combination of moderate capacity and high-power density. Such characteristics make these power sources highly suitable for long-endurance, low-energy microelectronic devices, including MEMS, detectors, and sensors [72–74].

For instance, Zhang et al. [42] introduced a fully integrated SoC tailored for an insect-scale flapping-wing pico-aerial vehicle, utilizing a TFB as the power source. By integrating TFBs with energy-harvesting technologies—such as solar cells, piezoelectric generators, and thermoelectric device self-sustaining power systems can be realized, paving the way for future autonomous applications. A notable example is an 8.75-mm energy-autonomous microsystem that integrates a silicon-based solar cell with a 12-μAh TFB to power a temperature sensor connected to a central processing unit. Such self-powered architecture enables the efficient incorporation of wireless microdevices into networked systems, thereby expanding the scope of potential applications across various domains. Autonomous wireless sensors can be effectively utilized in a wide range of applications, including smart building management, industrial automation, and factory automation. In addition to their role in microelectronics, TFBs are also regarded as promising energy solutions for RFID devices, smart cards, and implantable medical systems, such as biomedical implants and electronic contact lenses. This suitability originates from their inherently compact form factor, superior electrochemical stability, enhanced safety characteristics, and extended cycle life. Acknowledging this potential, several companies—such as Cymbet, Front Edge Technology, and STMicroelectronics—have recently introduced commercial TFB products with diverse sizes and capacities, primarily targeting applications in microelectronics, smart cards, and implantable medical devices. Furthermore, by engineering specific physical properties, TFBs exhibit considerable versatility and can be

16163028, 2026, 33, Downloaded from https://advanced.onlinelibrary.wiley.com/doi/10.1002/adfm.202524957 by Nanjing University, Wiley Online Library on [03/11/2026]. See the Terms and Conditions (https://onlinelibrary.wiley.com/terms-and-conditions) on Wiley Online Library for rules of use; OA articles are governed by the applicable Creative Commons License

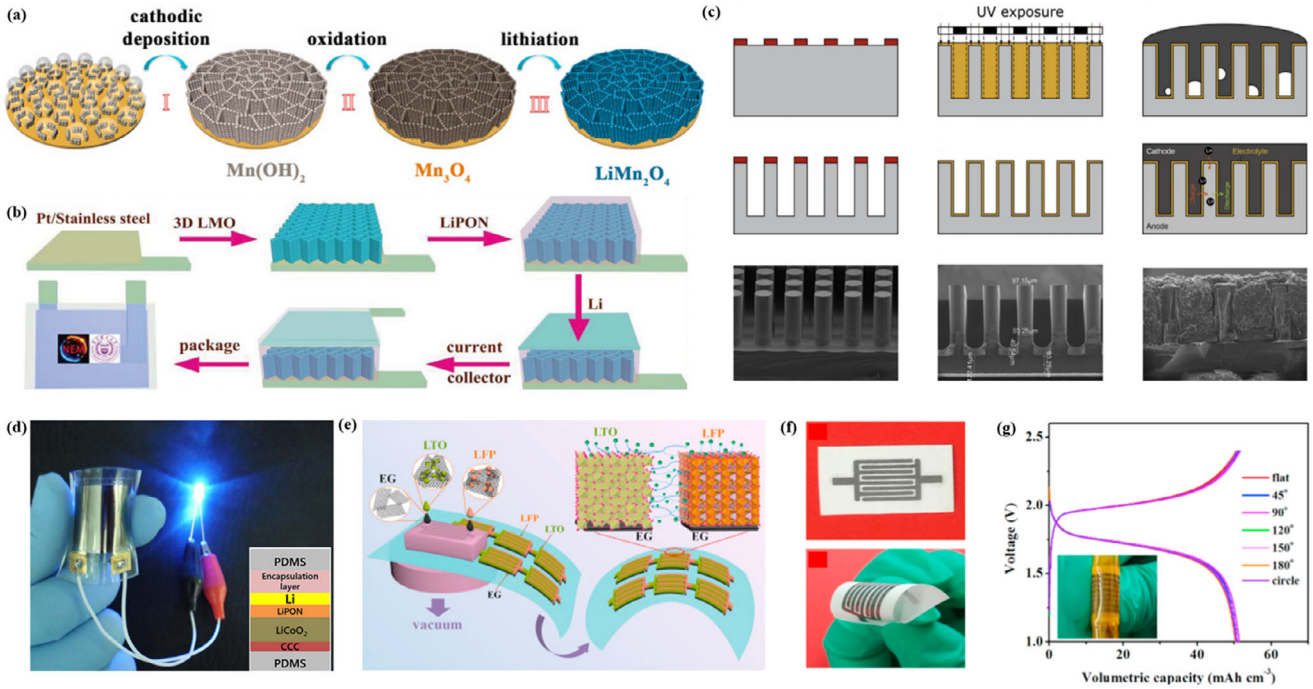


FIGURE 4 | (a) Fabrication schematic of three-dimensional porous $LiMn_2O_4$ nanowall arrays on Au substrate. Reproduced with permission [81]. Copyright 2016, Elsevier. (b) Fabrication schematic of flexible 3D TFB. Reproduced with permission [79]. Copyright 2018, Wiley-VCH. (c) Fabrication schematic of three-dimensional battery architectures using SU-8-coated silicon arrays. Reproduced with permission [55]. Copyright 2018, Elsevier. (d) Operational demonstration of a bendable lithium-ion battery powering a blue LED under mechanical bending. Reproduced with permission [57]. Copyright 2012, American Chemical Society. (e) Diagram depicting the mask-assisted fabrication steps for creating integrated LTO/LFP LIMBs. (f) Visual representations of a single LIMB cell showing its flexibility through flat and twisted states. (g) GCD profiles of LTO/LFP-LIMBs under 0–180° bending and full-circle deformation (inset: cell optical image during bending). Reproduced with permission [38]. Copyright 2018, Elsevier.

effectively adapted for use in communication systems and consumer electronics. Flexible TFBs offer a compelling power solution for wearable electronics—such as wristbands, smartwatches, and augmented-reality glasses—due to their lightweight construction and intrinsic safety features. Likewise, transparent TFBs exhibit significant potential as embedded energy storage elements in next-generation transparent electronic systems, including optoelectronic devices, smart windows, and transparent display technologies.

Significant advancements have been achieved in the development and optimization of TFBs. However, conventional planar-structured TFBs still face limitations in terms of insufficient energy and power output per unit area. These limitations are largely ascribed to the restricted electrode–electrolyte reaction interface and relatively slow ion transport kinetics, challenges that become more pronounced with increasing film thickness. To overcome these challenges, 3D TFB architectures have been introduced. By significantly expanding the electrode/electrolyte interface area, 3D TFBs achieve concurrent improvements in both energy density and power density. This design not only mitigates the intrinsic limitations of planar configurations but also establishes a foundation for more efficient and high-performance micro-battery solutions, catering to applications that demand compact yet highly capable energy storage systems. Xia et al. [75–78] proposed a "hydrothermal lithiation" technique, enabling the fabrication of vertically aligned nanoarrays of lithium cobalt oxide (LCO) and lithium manganese oxide (LMO) on various substrates at reduced temperatures. As shown in Figure 4a, the hydrothermal lithiation process converts tetragonal spinel Mn_3O_4 nanowall arrays into cubic spinel lithium manganese oxide (LMO) nanowall arrays, with minimal morphological changes. The distinctive nanostructured architecture imparts the resulting 3D LMO electrodes with a high reversible capacity of 0.29 mAh cm^{-2} (131 mAh g^{-1}), as well as excellent rate performance and cycling stability. While this hydrothermal lithiation approach shows considerable promise for the fabrication of three-dimensional cathodes for TFBs, it currently presents limitations in terms of compatibility with standard on-chip integration and microfabrication processes. Recently, Xia et al. [79] presented a simple yet effective physical vapor deposition (PVD) approach for fabricating three-dimensional (3D) cathodes through precise control of the thin-film growth mode. During DC sputtering under optimized pressure and power conditions, adatoms ejected from the LMO target exhibit a tendency to aggregate on the substrate at 300°C, primarily due to their reduced kinetic energy. These clusters subsequently evolve into 3D islands through the Volmer–Weber growth mechanism. Utilizing this 3D LMO cathode architecture, a semi-three-dimensional (semi-3D) TFB was fabricated, exhibiting significantly reduced interfacial resistance and improved specific capacity compared to conventional planar TFBs. A similar approach was applied to deposit 3D α-MoO_{3-X} and MnO_{2-X} nanostructures directly onto conductive substrates via reactive DC sputtering, highlighting the versatility of this method in fabricating high-performance 3D electrode architectures. These results demonstrate the versatility and effectiveness of the physical vapor deposition (PVD) method in fabricating 3D cathodes through precise control over the thin-film growth

16163028, 2026, 33, Downloaded from https://advanced.onlinelibrary.wiley.com/doi/10.1002/adfm.202524957 by Nanjing University, Wiley Online Library on [03/11/2026]. See the Terms and Conditions (https://onlinelibrary.wiley.com/terms-and-conditions) on Wiley Online Library for rules of use; OA articles are governed by the applicable Creative Commons License

mode (Figure 4b). In a recent advancement, Dunn et al. [80] have pioneered the application of semiconductor processing techniques to the creation of 3D TFBs. The approach utilizes partially lithiated 3D silicon pillars, fabricated via dry etching of crystalline silicon wafers, which serve simultaneously as the structural framework and anode material. A conformal solid electrolyte layer is then deposited around these high-aspect-ratio structures through photopatterning based on SU-8 photoresist. For cathode formation, a slurry of $LiNi_{0.8}Co_{0.15}Al_{0.05}O_2$ is applied, followed by vacuum-assisted infiltration to complete the battery assembly (as illustrated in Figure 4c).

The rapid advancement of flexible optoelectronic technologies—such as rollable displays, smart electronic systems, and wearable devices—has spurred increasing demand for miniaturized, lightweight, and mechanically robust TFBs that can serve as stable, integrated power sources. These next-generation TFBs are required to deliver high performance while meeting rigorous safety standards to support the evolving needs of advanced flexible electronics. Koo et al. [57] introduced a versatile transfer methodology for the fabrication of flexible LCO/LiPON/Li TFBs, as illustrated in Figure 4d. The fabrication process involves first constructing the battery cell on a thermally stable sacrificial substrate, followed by a transfer process onto a flexible polydimethylsiloxane (PDMS) substrate. The resulting flexible TFB exhibited a high areal capacity of 106 μAh cm^{-2} under standard operating conditions. Moreover, it demonstrated outstanding mechanical flexibility, maintaining over 94.5% of its initial capacity after 100 bending cycles at various curvature radii. Zheng et al. [38] developed a planar-integrated TFB architecture employing an ionogel electrolyte, lithographically patterned LTO nanosphere anodes fabricated via mask-assisted interdigital processing, and LFP microsphere cathodes. In this configuration, exfoliated graphene nanosheets serve dual roles as both current collectors and conductive additives, as illustrated in Figure 4e. The resulting LTO/LFP TFBs exhibit excellent mechanical flexibility, with no discernible structural degradation or delamination between the microelectrodes and the substrate, even under significant bending, as illustrated in Figure 4f. In addition to their robust mechanical performance, these flexible TFBs deliver a stable volumetric capacity of 50 mAh cm^{-3} and maintain a Coulombic efficiency of over 99.3% across multiple charge–discharge cycles, from the planar state to a fully bent configuration with a curvature of 180° (Figure 4g). The non-vacuum coating method employed, characterized by its simplicity and cost-effectiveness, suggests potential avenues for the fabrication of flexible TFBs, opening up new possibilities in this field.

2.3 | Nanowire Microbattery

While the thin-film technologies have laid critical groundwork for miniaturized energy storage, their performance ceilings in energy density, rate capability, and mechanical flexibility have spurred exploration into one-dimensional nanostructured materials. Nanowires, characterized by their high aspect ratio, tunable surface chemistry, and direct ion-transport pathways, have emerged as a paradigm-shifting platform for next-generation electrodes. One-dimensional (1D) nanomaterials, such as nanowires (NWs), nanorods, nanotubes, and nanofibers, have attracted significant research attention owing to their unique functional properties. Among these materials, nanowires stand out because of their high crystallinity, precisely adjustable dimensions, and efficient radial charge transport properties. These unique properties enable the development of nanoscale systems and functional devices, particularly in the domain of electrochemical energy storage. To enhance the energy storage performance of NWs, various morphologies and structural designs have been developed, building upon the foundational architecture of these one-dimensional nanostructures. NWs can be categorized into two hierarchical levels. At the individual level, modifications lead to the creation of NWs with diverse shapes, including porous NWs and coaxially coated NWs. Furthermore, by integrating multiple individual NWs through various assembly methods, macroscopic architectures such as arrays or networks can be achieved, presenting an overall structural organization. Based on their morphological and structural features, NWs can be classified into several distinct categories, including simple NWs, core–shell or coated NWs, hierarchical or heterostructured NWs, porous/mesoporous NWs, and hollow-structured NWs, as schematically depicted in Figure 5a. Additionally, depending on their mode of assembly, NWs can form organized architectures such as nanowire arrays, networks, and bundled configurations [82–85].

The Silicon Nanowires (SiNWs) are poised to become essential components for the development of future electronic and optoelectronic nanodevices, functioning both as active elements and as electrical interconnects. Unlike zero-dimensional quantum dots and 2D well structures, 1D nanostructures such as SiNWs provide an additional spatial degree of freedom, enabling them to be integrated directly into more complex functional networks or circuits. Achieving full utilization of this potential necessitates precise manipulation of SiNW growth pathways, directing them into well-defined linear arrangements as well as interconnected, non-overlapping network structures to optimize their functional performance. This approach allows for the formation of a predetermined layout of SiNWs tailored to specific functionalities in a single growth process [86–92]. Yu et al. [93] introduced and experimentally validated an in-plane SLS (Solution–Liquid–Solid) growth mechanism, termed IPSLS, for the fabrication of SiNWs oriented within the plane of the substrate. In this process, a nanoscale liquid indium droplet serves as a catalyst, facilitating the transformation of hydrogenated amorphous silicon (a-Si:H) into crystalline SiNWs through consumption and crystallization. Notably, this innovative approach employs an entirely in situ annealing procedure that does not require reactive gases. The transformation is driven by the Gibbs energy difference between hydrogenated a-Si:H and crystalline silicon. A defining feature of in-plane nanowire growth is the ability to direct the movement of catalyst droplets using fine surface features, such as individual step edges. This characteristic allows for precise control over both the positioning and growth direction of SiNWs, providing a promising strategy for achieving aligned in-plane SiNWs during synthesis while preserving the integrity of the vacuum environment. In this approach, indium (In) catalyst droplets were generated via the surface reduction of an indium tin oxide (ITO) layer through H_2 plasma treatment. A thin hydrogenated a-Si:H layer (15–120 nm in thickness) was deposited over the catalyst, and SiNW growth was subsequently initiated via annealing at temperatures ranging from 300 to 500°C (Figure 5b) [94].

16163028, 2026, 33, Downloaded from https://advanced.onlinelibrary.wiley.com/doi/10.1002/adfm.202524957 by Nanjing University, Wiley Online Library on [03/11/2026]. See the Terms and Conditions (https://onlinelibrary.wiley.com/terms-and-conditions) on Wiley Online Library for rules of use; OA articles are governed by the applicable Creative Commons License

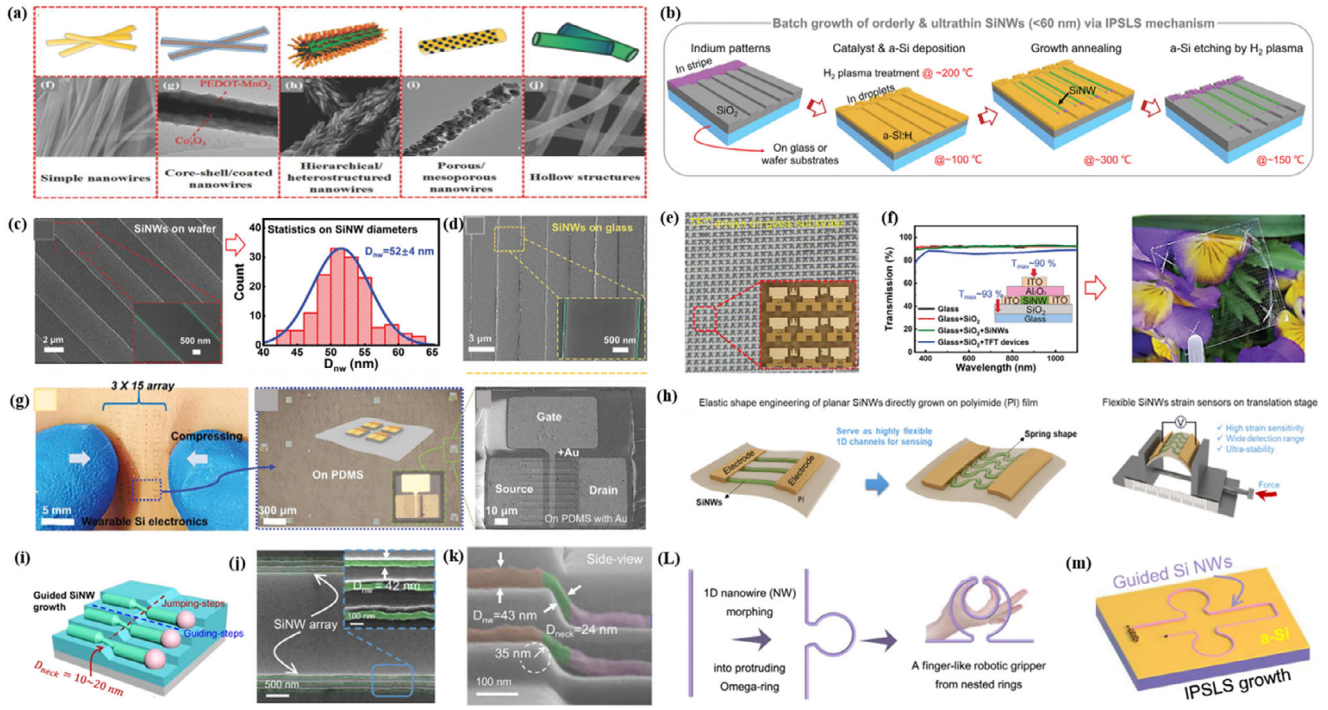


FIGURE 5 | (a) Different morphologies and structures of NWs. Reproduced with permission [82]. Copyright 2018, Wiley-VCH. (b) Schematic of IPSLS-directed growth of ordered ultrathin SiNW arrays on glass or wafer substrates. (c) SEM image of edge-guided SiNWs on a wafer, displaying diameter distribution in the inset. (d) SEM image of SiNWs on a glass substrate, with an enlarged inset. (e) Optical image of SiNW array on glass. Inset: Close-up of the device. (f) Optical image of SiNW array on glass. Inset: Device close-up. Reproduced with permission [95]. Copyright 2023, Wiley-VCH GmbH. (g) Optical images: SiNW-FET arrays on PDMS film attached to skin, with discrete islands analyzed by microscope/SEM. Reproduced with permission [96]. Copyright 2022, Wiley-VCH GmbH. (h) Schematic of straight vs. spring-shaped SiNWs on flexible PI substrate; Spring-shaped sensor mounted on custom stretch platform. Reproduced with permission [97]. Copyright 2025, American Chemical Society. (i) Schematic of guided growth of parallel IPSLS SiNW arrays across a step junction, forming necked structures (middle diameter < 20 nm; channel length < 100 nm). (j) SEM images showing typical SiNW growth on flat guiding steps. (k) SEM micrograph of step-necked SiNWs, showing a necked segment diameter reduced by half compared to the thicker ends. Reproduced with permission [98]. Copyright 2025, Springer Nature. (l) Illustration of geometric transformation from a straight nanowire to single and nested omega-ring structures, serving as a basic pairwise gripper. (m) IPSLS-mode ultralong SiNWs shaped into robotic designs via In-guided droplet movement and a-Si crystallization. Reproduced with permission [99]. Copyright 2023, Springer Nature.

Song et al. [95] demonstrated a scalable and effective strategy for the ordered integration of SiNW arrays with highly uniform diameters (52 ± 4 nm). The SiNWs were synthesized directly on glass and wafer substrates through a guided in-plane solid–liquid–solid (IPSLS) growth process, followed by passivation using a novel solution-phase oxidation/etching cycling technique. A representative field-emission scanning electron microscopy (FE-SEM, Zeiss Sigma) image of the nanowires, grown along pre-defined guiding edges on the wafer substrate, is shown in Figure 5c. The SiNW array, highlighted in green for clarity, exhibits a highly ordered and uniform morphology, with an average diameter of D_{NW} = 52 ± 4 nm. Moreover, the IPSLS-grown SiNWs can be directly synthesized on glass substrates, as illustrated in Figure 5d, where a 300 nm SiO_2 buffer layer was pre-deposited onto the surface of Corning glass to facilitate the growth process. However, the resulting nanowires exhibit a somewhat broader diameter distribution, with an average diameter of D_{NW} = 56 ± 8. The SiNW-based SiNW-TFTs fabricated on glass substrates, such as the one shown in Figure 5e, demonstrate a visibly transparent appearance, particularly when metallic electrodes are substituted with indium tin oxide (ITO) contacts. Transmission characterization, illustrated in Figure 5f, indicates that glass substrates integrated with SiNW arrays achieve an optical transparency of nearly 90% across the visible to near-infrared spectrum (400–1200 nm). For SiNW-based TFTs fabricated with ITO electrodes on glass, the overall transparency is further enhanced, yielding highly transparent devices. In cases where opaque metal electrodes are used, the average transparency remains high at ≈73 %, which is sufficient for numerous applications in transparent electronics and AR/VR display technologies.

In their follow-up study, the research group further demonstrated that slender SiNW channels with diameters below 80 nm can be selectively grown at predefined positions through an IPSLS mechanism. These nanowires were subsequently transferred in a scalable and efficient manner onto large-area PDMS elastomer substrates, enabling reliable integration for flexible device applications [96]. As illustrated in Figure 5g, a well-ordered 3 × 15 array of FET units can conformally adhere to soft skin and endure substantial compressive deformation without delamination or structural failure. An optical microscopy image of the SiNW-FET devices transferred onto PDMS confirms that the positional accuracy and structural integrity of the individual island structures are well maintained. This preservation is further corroborated by detailed scanning electron microscopy (SEM) analysis of the transferred FET units. The direct growth and monolithic

16163028, 2026, 33, Downloaded from https://advanced.onlinelibrary.wiley.com/doi/10.1002/adfm.202524957 by Nanjing University, Wiley Online Library on [03/11/2026]. See the Terms and Conditions (https://onlinelibrary.wiley.com/terms-and-conditions) on Wiley Online Library for rules of use; OA articles are governed by the applicable Creative Commons License

integration of position-controlled, morphology-tunable SiNWs on low-cost polymer substrates—without requiring post-growth transfer processes—holds significant promise for the development of high-performance flexible sensors and logic circuits. To the best of our knowledge, this study demonstrates, for the first time, the successful synthesis of SiNWs at a low temperature of 200°C on flexible polyimide (PI) films through a planar IPSLS growth mechanism [97]. SiNWs with an average diameter of approximately 146 nm were selectively grown at predefined positions on polyimide (PI) substrates in a well-ordered array configuration, adopting a preferred helical or spring-like morphology. A strain sensor array fabricated from the coiled SiNWs exhibited exceptional electromechanical performance, achieving a gauge factor (GF) of approximately 90, withstanding tensile strains up to 3.3% (corresponding to a bending radius of 1.5 mm), and maintaining stable functionality over 30 000 mechanical bending cycles. The sensors were successfully attached to a human finger for real-time motion monitoring, demonstrating high sensitivity and remarkable mechanical durability, underscoring their strong potential for integration into wearable health-monitoring systems, as shown in Figure 5h.

Wu et al. [98] demonstrated the fabrication of ultrathin, short SiNW channels through a local-curvature-modulated catalytic growth process, in which planar nanowires are guided across step edges. During this dynamic "jumping" growth mechanism, the leading catalyst droplet undergoes significant elongation, resulting in a sub-100 nm necking segment with diameter modulation decreasing from approximately 45 nm to below 25 nm. The fabricated FETs exhibit outstanding electrical performance, featuring an on/off current ratio exceeding 8×10^7 and a subthreshold swing as low as 70 mV/dec. These enhancements are attributed to improved gate control over the narrowed channel and better contact resistance at the thicker source/drain regions (Figure 5i–k). Such ultracompact and flexible microgrippers hold significant potential for enabling high-precision manipulation, assembly, and processing of microscale objects, facilitated by fast, large-amplitude, and multidirectional actuation capabilities. Yan et al. [99] fabricated minimalistic robotic nanostructures based on single-nanowire morphing, with actuation enabled through geometry-engineered Lorentz forces. This approach leveraged a programmable folding growth technique to direct ultralong, ultrathin SiNWs into discrete and nested ω-shaped ring configurations. The resulting structures were integrated across microfabricated electrode frames and coated with a conductive silver layer to establish controlled current paths. Under an applied magnetic field, the devices were activated via Lorentz-force-driven motion, allowing for rapid and large-scale deformations, including grasping, flapping, and torsional manipulation of microscale objects. Moreover, high-frequency or resonant excitation could be employed to counteract adhesion forces such as van der Waals interactions, thereby enabling controlled payload release. More complex operations—such as mutual alignment, precise object transfer, and selective testing and installation of LED units—were also successfully demonstrated through coordinated pairwise gripper interactions. This single-nanowire morphing approach offers a versatile and efficient platform for the rapid design, fabrication, and prototyping of diverse ultracompact nanorobotic systems, mechanical sensors, and tools for biological manipulation, as illustrated in Figure 5l,m. The advancement of these sophisticated nanowire technologies is expected to significantly promote the development of MBs integration, laying a solid foundation for further innovation.

In nanowire batteries, the in-plane solid–liquid–solid growth mechanism establishes deterministic morphological regulation of nanowire architectures in MBs systems, ensuring optimal electrochemical compatibility through crystallographic orientation alignment. This bottom–up synthesis paradigm fundamentally addresses interfacial heterogeneity challenges while establishing a scalable fabrication framework for next-generation nanowire-based energy storage technologies.

Mai et al. [69] reported the development of a novel single-nanowire electrode device, specifically designed as a model platform for in situ investigations into the fundamental mechanisms responsible for capacity fading in lithium-ion-based energy storage systems. In their device configuration, either an individual vanadium oxide nanowire or a Si/a-Si core/shell nanowire serves as the working electrode, enabling precise electrochemical analysis at the single-particle level (Figure 6a). The electrical transport characteristics of individual nanowires are continuously monitored in real time to track structural and conductive variations occurring during charge–discharge cycling. The findings reveal that, accompanying shallow discharge-induced lithium-ion intercalation, the conductance of the vanadium oxide nanowire diminishes by more than two orders of magnitude. This approach offers valuable insights into the mechanisms underlying capacity fade at the nanoscale, highlighting the potential of single nanowire devices for detailed electrochemical studies. As shown in Figure 6b, the cyclic voltammogram (CV) of the vanadium oxide nanowire electrode is presented alongside a control CV obtained from highly oriented pyrolytic graphite (HOPG) and passivated Cr/Au current collectors in the absence of nanowires, allowing for a direct comparative assessment of electrochemical behavior. It is evident that distinct oxidation and reduction peaks, characteristic of lithium-ion intercalation and deintercalation processes, are observable only for the vanadium oxide nanowire electrode. The current associated with these peaks is approximately four to five times higher than that observed in the control, highlighting the active involvement of the nanowire in electrochemical reactions. Figure 6c displays the voltage profile of a vanadium oxide nanowire cathode versus HOPG anode during a single charge–discharge cycle. The cell voltage exhibits a steady increase during charging at –150 pA and reaches a stable value of approximately 3.9 V. Upon discharge at 50 pA, a continuous voltage decay is observed. The sloping discharge curve suggests the presence of either a substantial internal resistance within the cell or a relatively fast discharge process.

In summary, the SiNWs demonstrate great potential for next-generation high-performance gate-all-around field-effect transistors and thin-film transistor display drivers. They also provide a crucial foundation for the integration of multifunctional chip architectures that incorporate micro and nanoscale energy systems, sensors, memory devices, and micro/nanoelectromechanical systems. The in-plane solid–liquid–solid growth mode, as a positionable and integrable nanowire fabrication approach, opens up new pathways for the large-scale integration and customized design of nanowire-based lithium-ion battery applications.

16163028, 2026, 33, Downloaded from https://advanced.onlinelibrary.wiley.com/doi/10.1002/adfm.202524957 by Nanjing University, Wiley Online Library on [03/11/2026]. See the Terms and Conditions (https://onlinelibrary.wiley.com/terms-and-conditions) on Wiley Online Library for rules of use; OA articles are governed by the applicable Creative Commons License

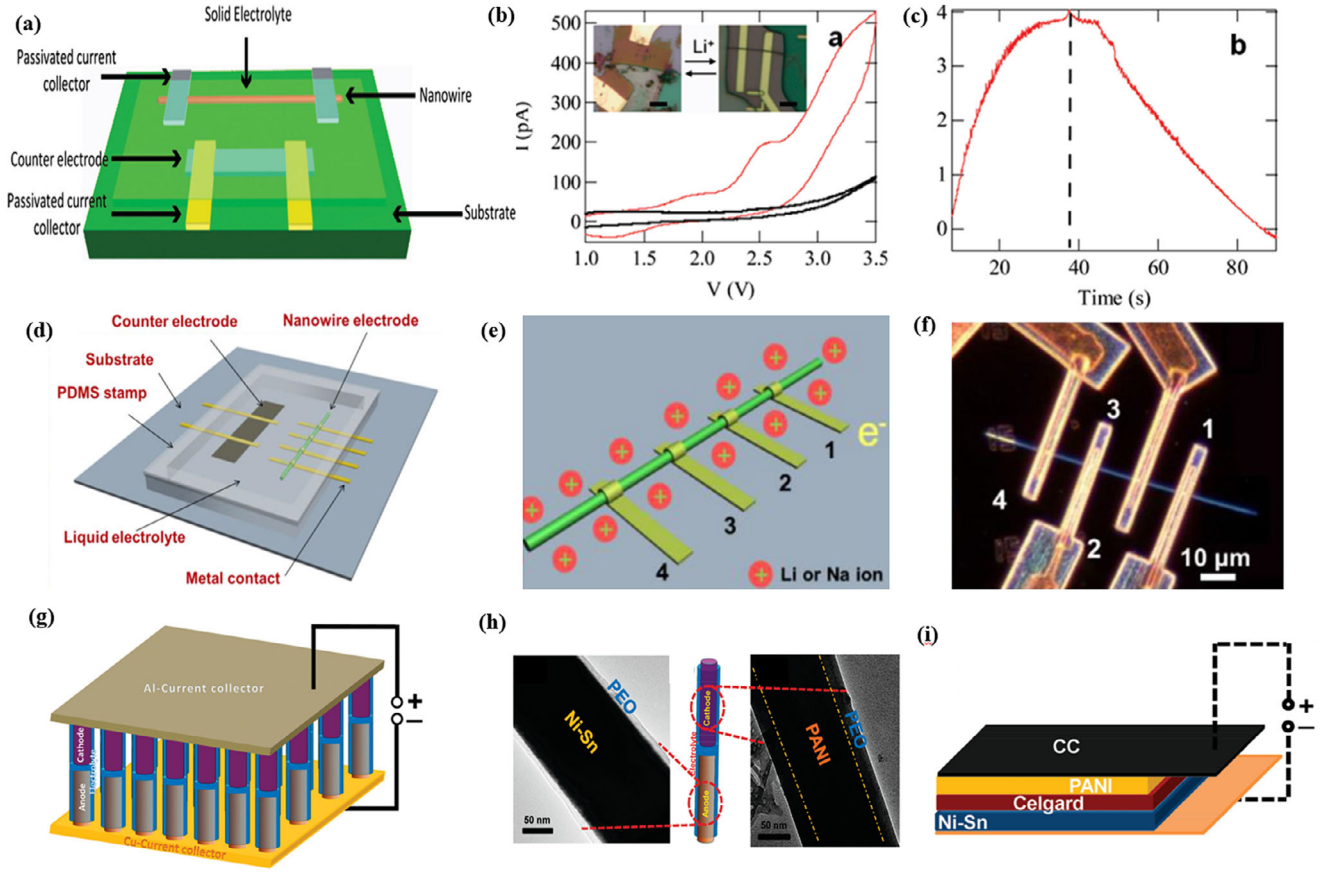


FIGURE 6 | (a) Device-level schematic of individual nanowire electrode architecture. (b) Cyclic voltammetry of individual V_xO_γ nanowire (1.0–3.5 V vs. HOPG @ 50 mV/s); control with Cr/Au electrode (black). (c) Voltage profiles of individual V_xO_γ nanowire cathode vs. HOPG during galvanostatic cycling. Reproduced with permission [69]. Copyright 2010, American Chemical Society. (d) Device schematic highlighting quadruple-terminal nanowire integration and microfluidic PDMS confinement of liquid electrolyte. (e) **Configuration I: Full electrolyte immersion of the nanowire**. (f) Dark-field optical microscopy (DF-OM) imaging of a nanowire electrode. Reproduced with permission [100]. Copyright 2015, American Chemical Society. (g) Schematic of alumina-templated fabrication for nanowire-based energy storage devices. (h) Structural characterization and device schematic: TEM image of anode/electrolyte core–shell NWs (Ni-Sn/PEO); Schematic of nanowire energy storage architecture; TEM image of cathode/electrolyte core–shell NWs (PANI/PEO). (i) Schematic of thin-film device architecture: Ni–Sn anode | Celgard separator | PANI cathode. Reproduced with permission [101]. Copyright 2011, American Chemical Society.

Despite recent advances, the fundamental mechanisms governing Li^+ and Na^+ ion transport within nanoscale battery electrodes remain poorly understood, primarily due to a lack of comprehensive experimental studies. A clear understanding of these processes is crucial for guiding the rational design and optimization of high-performance electrode materials. NWs offer unique geometric advantages that make them ideal candidates for in situ electrochemical investigations. With lengths extending over tens of micrometers and diameters in the tens-of-nanometers range, individual nanowires can be configured as model electrodes, enabling real-time, high-resolution monitoring of structural and electronic changes during battery operation—free from interference by non-active components. To gain deeper insights into the transport characteristics of Li and Na ions within the nanoscale electrodes of batteries, Xu et al. [100] designed a multi-contact configuration on single nanowire electrodes (Figure 6d). This setup allows for the recording of conductance across various segments of the nanowire during charge and discharge cycles, thereby providing detailed information on ion transport dynamics. As shown in Figure 6e,f, contact 1 was employed for all electrochemical measurements. The electrical transport properties of the three nanowire segments were recorded in situ before and after the electrochemical processes. Following the reactions, the conductance of the nanowire decreased by 96.5 %, 9.2 %, and 1.9 % in segments 1–2, 2–3, and 3–4, respectively. Gowda et al. [101] reported a composite nanostructured electrochemical device consisting of a Ni–Sn anode and a polyaniline (PANI) nanowire cathode, encapsulated within a conformal polymer core–shell separator, as illustrated in Figure 6g. A parallel array of these nanowire-based devices achieves a reversible areal capacity of approximately 3 μAh cm^{-2} at a current density of 0.03 mA cm^{-2}. As shown in Figure 6h, both the Ni–Sn anode and the PANI cathode are coated with a thin layer of poly (ethylene oxide) (PEO)-based electrolyte material. This electrolyte layer ensures stable ionic contact and facilitates efficient electrochemical reactions at the electrode interfaces. As shown in Figure 6i, the fabrication and electrochemical evaluation of the cells involved stacking a thin-film Ni–Sn anode and a PANI cathode, with a Celgard separator infused with a $LiPF_6$-based electrolyte placed between the two electrodes. Galvanostatic charge–discharge tests were carried out at current densities of approximately 0.2, 0.3, and 0.4 mA cm^{-2}. After about 20 cycles, the system delivered

16163028, 2026, 33, Downloaded from https://advanced.onlinelibrary.wiley.com/doi/10.1002/adfm.202524957 by Nanjing University, Wiley Online Library on [03/11/2026]. See the Terms and Conditions (https://onlinelibrary.wiley.com/terms-and-conditions) on Wiley Online Library for rules of use; OA articles are governed by the applicable Creative Commons License

reversible areal capacities of approximately 100, 75, and 56 μAh cm^{-2} at the respective current densities.

2.4 | Artificial Intelligence-Driven

The advent of the intelligent era has driven breakthrough advancements in smart devices, raising higher demands for energy supply applications. Despite notable progress in MBs research, their electrochemical performance and adaptability remain constrained by inherent material limitations and the complexities of technological innovation. Driven by the progress in information technology and artificial intelligence, the Fourth Industrial Revolution facilitates the development of next-generation batteries through the incorporation of cutting-edge materials and technologies. This approach enables the creation of batteries with superior electrochemical properties and unmatched reliability, representing a major advancement in the field of energy storage. Notably, the concept of intelligence has begun to permeate both battery design and energy management systems, enabling smarter and more adaptive energy storage solutions. Recent years have witnessed rapid progress in artificial intelligence (AI), especially in the domain of machine learning (ML). Leveraging ML's powerful capabilities in classification and regression tasks has led to substantial breakthroughs across various aspects of rechargeable battery research. These advancements have yielded several significant outcomes. Looking forward, it is anticipated that AI will be pivotal in further revolutionizing the development of materials and technologies for rechargeable batteries.

Rechargeable batteries, as essential components in energy storage, have been extensively integrated into a wide variety of electronic devices, including new-energy vehicles, medical devices, and portable electronics. They play a crucial role in mitigating global energy consumption and are key to promoting sustainable energy solutions. Nevertheless, current limitations in rechargeable battery performance pose significant challenges to meeting the escalating requirements of modern applications. AI, particularly due to its powerful data analysis capabilities, has seen rapid advancements and is driving progress across multiple domains of rechargeable battery research, significantly accelerating the pace of innovation. In the area of materials discovery, each material possesses a distinct structural configuration, which can be effectively captured as unique features by ML models. By establishing nonlinear relationships between material structures and target properties, ML enables the prediction of previously unrecognized characteristics, facilitating targeted design efforts. Wang and colleagues developed a deep learning (DL) model incorporating transfer learning (TL) to predict the band gap values of thousands of metal oxides, sulfides, and other materials within milliseconds, demonstrating the potential of AI-driven approaches in high-throughput material screening. Wang et al. [102] identified four classes of energy materials based on electron conductivity (as shown in Figure 7a). In contrast to traditional high-precision generalized computing methods that are typically resource-intensive and slow, DL models offer significant benefits in terms of computational efficiency, precision, and economic viability. Additionally, this research employed band gap values as an intermediary link between the crystal structures of materials and their targeted classifications, providing a deeper understanding of how strongly correlated intrinsic material properties can be harnessed to improve predictive models in subsequent studies. Apart from conventional energy materials, there has been increasing attention toward porous materials owing to their distinctive structural and functional properties beneficial for energy-related applications. One promising approach to addressing the high-dimensional complexity inherent in material systems involves the digitization of materials—transforming material structures into mathematical representations through data reconstruction and imaging techniques powered by advanced algorithms. Inspired by the strong image-processing capabilities of convolutional neural networks, researchers are exploring strategies to convert material architectures into image-based formats, which can then be translated into numerical data and processed as computational models for predictive analysis and design.

The Battery Management System (BMS) in battery-powered energy storage systems is tasked with critical functions such as estimating the State of Charge (SOC) and State of Health (SOH), monitoring safety, regulating temperature, and balancing cells to ensure reliable and safe battery operation. Despite its importance, achieving optimal BMS performance is increasingly challenging due to the inherent limitations of embedded hardware in terms of memory and computational power, a problem that is well-supported by both theoretical analyses and practical findings. With the exponential growth in battery data generated throughout its lifecycle, there is a growing trend within the scientific community to leverage cloud computing for scalable storage and advanced data analysis. Compared to conventional approaches that rely heavily on local infrastructure, cloud-based solutions offer greater flexibility, cost efficiency, and computational scalability. Furthermore, the incorporation of ML has become indispensable for uncovering meaningful patterns and predictive insights from large-scale observational datasets. Consequently, the evolution of cloud-enabled, AI-integrated BMS represents a promising direction for future research and development. By combining the strengths of physics-based process models with the adaptability of ML techniques, this hybrid approach is anticipated to substantially improve predictive accuracy and modeling capabilities for long-range dependencies across multiple timescales. Although ML has become a powerful tool for analyzing extensive time-series datasets, its application to complex spatio–temporal systems remains challenging due to the influence of physical constraints and nonlinear interactions. To address these challenges, deep learning has garnered substantial attention in recent years due to its capability to automatically extract spatio–temporal features from complex datasets. It has demonstrated significant progress in tackling problems that have long posed difficulties for the artificial intelligence community, particularly in capturing intricate patterns and dependencies in high-dimensional data. Within the realm of battery systems, deep learning techniques have demonstrated exceptional capability in detecting hidden patterns and correlations within large datasets, thereby enhancing the precision of modeling and predictive analytics (Figure 7b). This approach not only enhances the accuracy of predictive models by capturing long-range spatial correlations across multiple timescales but also facilitates a deeper understanding of the underlying complex physical mechanisms [103]. Accurate and real-time estimation of the battery's current health status—such as its aging trajectory and remaining useful life—is essential for reliable monitoring of its

16163028, 2026, 33, Downloaded from https://advanced.onlinelibrary.wiley.com/doi/10.1002/adfm.202524957 by Nanjing University, Wiley Online Library on [03/11/2026]. See the Terms and Conditions (https://onlinelibrary.wiley.com/terms-and-conditions) on Wiley Online Library for rules of use; OA articles are governed by the applicable Creative Commons License

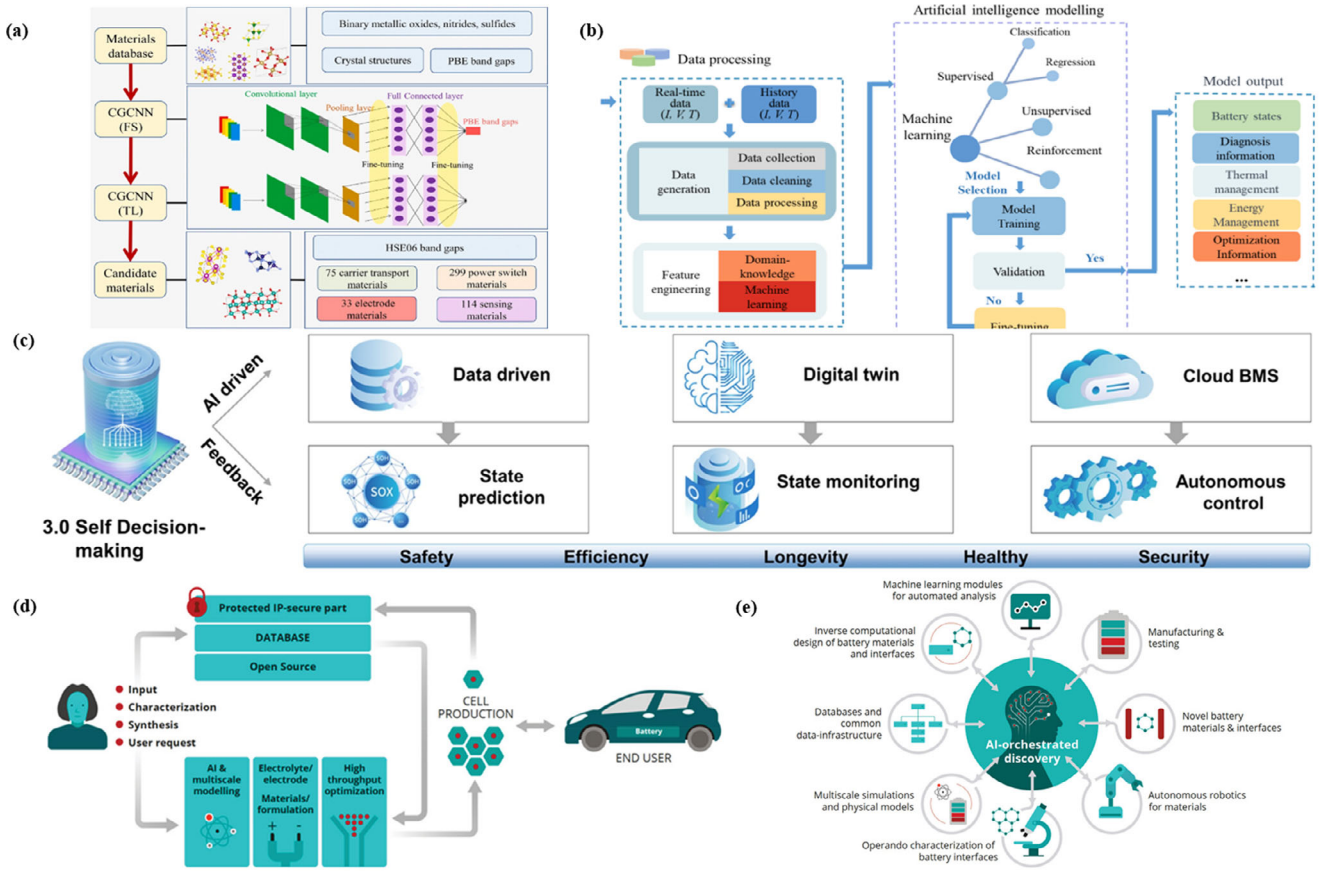


FIGURE 7 | (a) ML-optimized energy material discovery framework with bandgap-driven screening. Reproduced with permission [102]. Copyright 2023, Elsevier. (b) AI and ML for modelling and predicting battery states. Reproduced with permission [103]. Copyright 2023, Multidisciplinary Digital Publishing Institute. (c) Smart Batteries 3.0: Autonomous decision-making architecture integrating big data analytics, digital twin simulations, and cloud-based BMS networks. Reproduced with permission [41]. Copyright 2024, Elsevier. (d) The BIG-MAP project employs autonomous workflows and integrates diverse, multi-fidelity data across the battery value chain to enable closed-loop discovery of advanced battery materials and interfaces. (e) Data flow framework for autonomous AI-integrated battery development cycles within the BIG-MAP and BATTERY 2030+ initiatives. Reproduced with permission [104]. Copyright 2021, Wiley-VCH.

operational condition. Such information enables the implementation of effective control strategies that enhance safety and extend service life. To further improve state awareness, enable real-time data visualization, and support more accurate prediction and fault diagnosis, big-data-driven smart batteries incorporate self-decision-making capabilities. These technologies collectively facilitate advanced autonomous control and optimized system-level decision-making. Based on this, Meng et al. [41] introduced a comprehensive self-decision-making framework tailored for managing the complete lifecycle of smart batteries (Figure 7c).

Next-generation battery systems are being enhanced with integrated multisensory and self-healing capabilities. When combined with AI-powered, physics-informed ML models designed to predict the spatio–temporal dynamics of battery materials and interfaces, this integration enables the preemptive detection, prediction, and mitigation of possible degradation and failure modes. This integrated approach is expected to significantly enhance battery quality, reliability, and lifespan. The efficient acquisition and utilization of the vast amounts of battery data generated daily in academic, industrial, and end-user settings—such as from electric vehicle owners—offer significant potential to enhance battery performance and longevity, paving the way toward million-mile battery systems. ML-based models enable closed-loop charging optimization (Figure 7d), improving efficiency and lifespan. Combined with high-throughput and electrochemical data, they support inverse design of advanced battery components. Achieving this requires a comprehensive framework to model key interfacial processes. Within the BATTERY 2030+ initiative, this concept is encapsulated in the "Battery Interface Genome (BIG)." DL models capable of forecasting the dynamic changes in battery materials and interfaces over space and time are emerging as key enablers for the development of next-generation energy storage technologies [104]. Autonomous, data-driven workflows for battery research are advancing through collaborations like Batteries Europe and contributions from key journals such as the Journal of Power Sources and Joule. These initiatives promote the integration of comparable and interoperable datasets from both experimental and computational sources. Using computational tools like ASE and workflow managers such as FireWorks, AiiDA, and MyQueue, platforms can integrate experimental data with full provenance tracking. This accelerates the development of next-generation battery materials. These tools will be accessible via the BIG-MAP App Store and a public GitHub repository. Furthermore, they are designed to enhance experimental

16163028, 2026, 33, Downloaded from https://advanced.onlinelibrary.wiley.com/doi/10.1002/adfm.202524957 by Nanjing University, Wiley Online Library on [03/11/2026]. See the Terms and Conditions (https://onlinelibrary.wiley.com/terms-and-conditions) on Wiley Online Library for rules of use; OA articles are governed by the applicable Creative Commons License

efficiency by enabling the autonomous execution of simulations and supporting the initiation and control of physical experiments via the BIG-MAP orchestration infrastructure (Figure 7e).

The convergence of MBs (characterized by milliampere-hour capacity and sub-millimeter thickness) with AI is driving transformative advancements in miniaturized intelligent electronics. In implantable medical devices, AI algorithms dynamically optimize energy allocation from MBs by analyzing physiological data, extending the operational lifespan of intelligent pacemakers by approximately 30%. Within industrial IoT systems, sensors powered by MBs leverage ultra-lightweight AI frameworks such as Tiny ML to enable localized data processing, reducing transmission energy consumption by 60%. Core advantages of this integration include enhanced energy efficiency through AI-managed charge/discharge cycling, which minimizes parasitic losses, and ML-driven prediction of battery degradation that improves cycle life by 20–40%. Real-time health monitoring further enhances system reliability by preemptively identifying failure risks.

Nevertheless, significant challenges persist. The limited energy density of MBs (<100 mAh) restricts the prolonged operation of computationally intensive AI models. Thermal management complexities arise from compounded heat generation during AI inference and battery discharge within confined spaces. Additionally, constrained processing capabilities of microcontrollers impede real-time execution of deep learning algorithms. Future advancements require developing solid-state electrolytes and 3D electrode architectures to boost energy density, integrating hybrid power systems combining MBs with micro-energy harvesters (e.g., solar/kinetic), and implementing algorithm compression techniques to reduce computational demands.

The development of AI technology is experiencing exponential growth and has demonstrated a profound impact across diverse fields. Core branches of AI, such as ML and deep learning, possess an exceptional capability to process vast datasets. Through sophisticated algorithmic models, these techniques can uncover intricate patterns, regularities, and trends hidden within the data. Subsequently, they facilitate highly accurate predictions and intelligent decision-making based on these insights. This capability has rendered the screening of solid-state battery materials and the prediction of their performance not only possible but also a highly efficient and promising research avenue [105–108].

In the realm of material screening for solid-state batteries, identifying an ideal combination of s electrolytes and electrode materials necessitates a comprehensive and profound exploration within vast and diverse material systems. Each stage of this process—from experimental design to sample preparation and performance characterization—traditionally demands considerable investments of time and financial resources. Conventional trial-and-error approaches, being inherently slow and inefficient, struggle to match the rapid pace of technological evolution. In contrast, the application of AI and ML models has established an efficient and precise strategic framework for screening SSEs and electrode materials. This paradigm shift significantly accelerates the screening process, enhances its success rate, and substantially shortens the overall research and development cycle. AI algorithms are playing a dual role in advancing solid-state battery technology: significantly accelerating material development and enabling accurate predictions of key performance indicators. A pertinent example is the work by Zahid et al. [109], who developed a SOC estimation method utilizing a neuro-fuzzy system integrated with subtractive clustering. Their results demonstrate that the proposed model achieves high estimation accuracy, with a maximum error of less than 0.1%. This high-fidelity prediction capability lays a crucial foundation for the development of real-time adaptive BMS, which can leverage such data for dynamic performance optimization.

The fundamental requirements imposed by artificial intelligence on microsystems and edge intelligence find their core logical starting point and ultimate physical constraint in energy supply. Consequently, as a key enabling technology for deep integration and extreme miniaturization, the performance evolution of MBs—such as high energy density, low self-discharge rate, and long cycle life—directly defines the physical boundaries of intelligent systems.

Specifically, the milliwatt-level continuous power consumption and instantaneous peak power demands of AI inference, MB technology must break through the current energy-power density trade-off. This pursuit forms a mutually driven, closed-loop relationship with the development of high-efficiency AI chips and low-power heterogeneous computing architectures. Simultaneously, the three-dimensional heterogeneous integration of MBs with sensors and processors at the packaging level (e.g., on-chip Swiss-roll structures) represents an inevitable path toward achieving ultrahigh spatial efficiency and functional density at the system level. Furthermore, in line with the evolutionary trend toward agent-based AI and autonomous collaboration, the long-term cycling stability, wide-temperature-range operational capability, and fast-charging characteristics of MBs constitute the foundational layer supporting the reliable, sustained, and self-organizing operation of distributed intelligent agents [110–112].

Ultimately, the AI-driven design of microsystems logically forms a tightly coupled, co-optimization chain: energy foundation (MB) → computing (heterogeneous chip) → intelligent paradigm (edge AI). The goal is to construct next-generation integrated systems that maximize intelligent efficiency, autonomy, and reliability within the finite energy boundaries delineated by MBs.

2.5 | Manufacturing Process

Contrary to conventional energy storage devices, MBs require large-scale construction and assembly in a compact, miniaturized form. Within the realm of advancing miniaturization techniques, two principal categories—etching and printing—have gained prominence due to their respective advantages in resolution and material flexibility. Etching excels in achieving high-resolution patterns, whereas printing offers a wider selection of materials. These methodologies not only broaden the application scope of MBs but also emphasize key development themes such as high-resolution fabrication, high material loading, and the inherent trade-offs between these performance metrics. Printing electronics technologies—encompassing both 2D and 3D printing approaches—offer a range of advantages, including low manufacturing costs, compatibility with diverse printable materials,

16163028, 2026, 33, Downloaded from https://advanced.onlinelibrary.wiley.com/doi/10.1002/adfm.202524957 by Nanjing University, Wiley Online Library on [03/11/2026]. See the Terms and Conditions (https://onlinelibrary.wiley.com/terms-and-conditions) on Wiley Online Library for rules of use; OA articles are governed by the applicable Creative Commons License

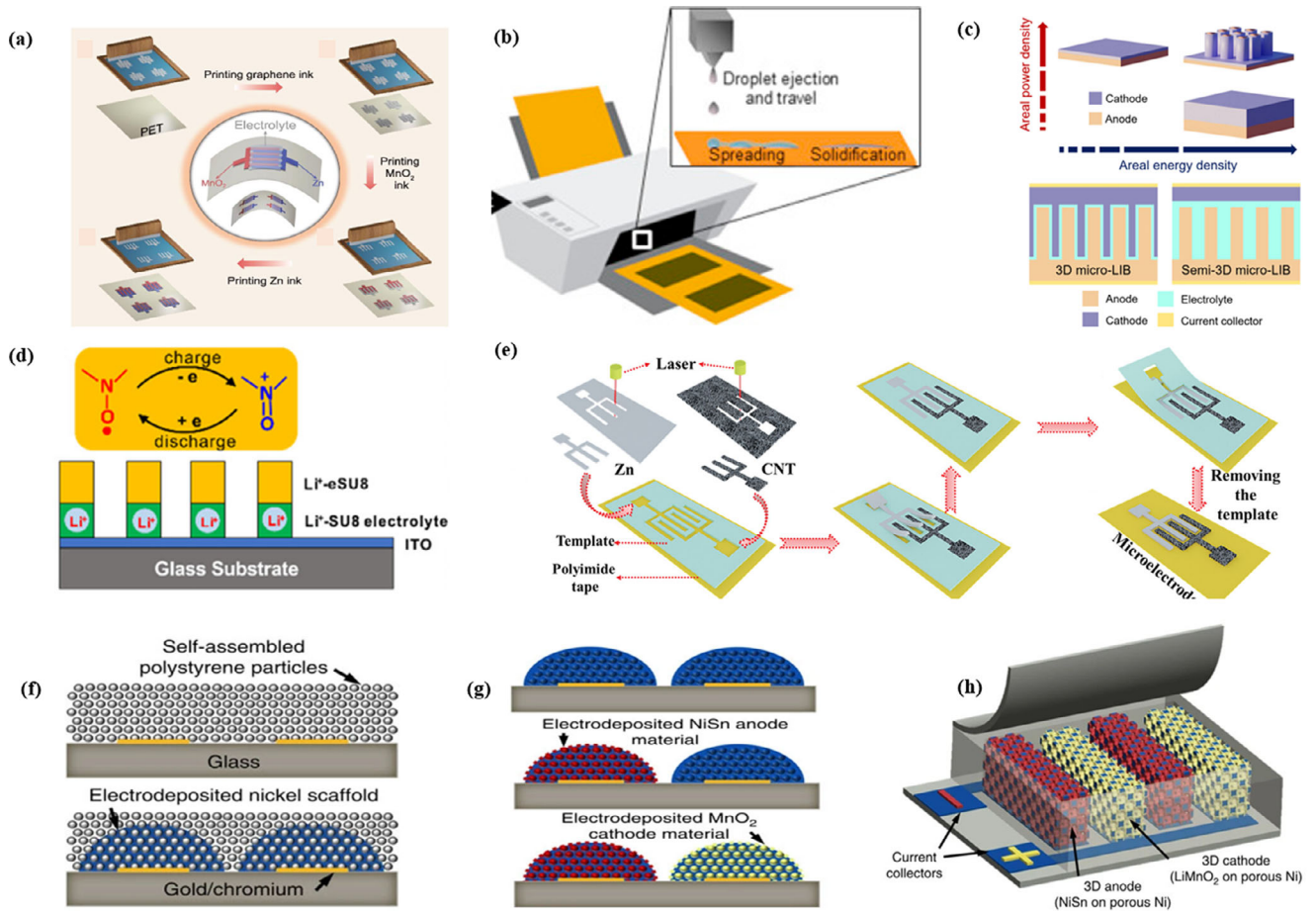


FIGURE 8 | (a) Schematic of the fabrication process of printed Zn//MnO_2 IMBs based on screen-printing technology. Reproduced with permission [113]. Copyright 2020, Oxford University Press. (b) Injected into an inkjet printer cartridge and printed. Reproduced with permission [114]. Copyright 2017, Elsevier. (c) Synergistic areal P–E density enhancement enabled by 3D-architected electrode design. Reproduced with permission [40]. Copyright 2024, Nature Publishing Group. (d) MB half-cell photolithographic patterning on silicon wafer: fabrication schematic and device architecture. Reproduced with permission [115]. Copyright 2019, American Chemical Society. (e) Schematic diagram of the fabrication process of the microelectrode. Reproduced with permission [116]. Copyright 2022, Wiley-VCH. (f,g) Fabrication schematic of architecture-defining Ni scaffold for single-substrate electrodeposition-guided electrode integration. (h) MB architecture integrating bicontinuous Ni scaffold (blue) as current collector with electroactive layers: Ni–Sn anode (red) | lithiated MnO_x cathode (yellow) in nanoporous electrode configuration. Reproduced with permission [62]. Copyright 2013, Springer Nature.

substrate flexibility, structural integrity of printed components, and process scalability. While 2D printing facilitates the realization of lightweight, high-power in-plane MBs, 3D printing enables the fabrication of complex, highly integrated three-dimensional architectures. Each technique contributes unique capabilities that are instrumental in advancing the design and scalable manufacturing of next-generation MBs.

Screen printing is an efficient and cost-effective fabrication technique that involves the use of a squeegee to force conductive ink through a pre-patterned stencil or screen, thereby transferring a desired microscale pattern onto a target substrate. A variety of nanomaterial-based inks have been successfully deposited through this process to fabricate interdigitated microelectrodes on diverse flexible substrates, including polymer films, textiles, and paper, enabling applications in wearable and disposable electronic devices. Wang et al. [113] employed a cost-effective screen printing technique to rapidly fabricate flexible planar interdigitated MBs, comprising a zinc anode (6.4 μm thick), a c-MnO_2 cathode (9.8 μm thick), and a neutral aqueous electrolyte composed of 2 M $ZnSO_4$ and 0.5 M $MnSO_4$ (Figure 8a). Notably, the graphene ink, Zn-based ink, and MnO_2 ink exhibited typical thixotropic behavior—characterized by a decrease in viscosity under increasing shear rate—enabling smooth and uniform printing on a variety of substrates, including textiles, A4 paper, rigid glass, and flexible polyethylene terephthalate (PET). The as-fabricated Zn//MnO_2 interdigitated MBs exhibited a high volumetric capacity of 19.3 mA h cm^{-3} at a current density of 7.5 mA cm^{-3}, an energy density of 17.4 m Wh cm^{-3}, along with good cycling stability (retaining approximately 83.9% of initial capacity after 1300 cycles) and excellent mechanical flexibility. While screen printing offers clear advantages for large-scale manufacturing, inkjet printing is more commonly employed in small-batch or customized applications due to its high spatial resolution and design flexibility.

However, the print quality achieved by both techniques is strongly influenced by the solubility (intravolumetric homogeneity) and chemical stability of the employed inks. Inkjet printing achieves high-efficiency fabrication of electrode arrays by depositing

16163028, 2026, 33, Downloaded from https://advanced.onlinelibrary.wiley.com/doi/10.1002/adfm.202524957 by Nanjing University, Wiley Online Library on [03/11/2026]. See the Terms and Conditions (https://onlinelibrary.wiley.com/terms-and-conditions) on Wiley Online Library for rules of use; OA articles are governed by the applicable Creative Commons License

individual droplets of liquid materials through a nozzle onto various substrates. Lawes et al. [114] developed a thin-film silicon nanoparticle (SiNP) anode using a conductive binder, as shown in Figure 8b. After ink formulation and printing deposition, the resulting anode incorporating a PEDOT: PSS binder demonstrated outstanding cycling stability, effectively mitigating the substantial volume changes undergone by SiNPs during repeated lithiation and delithiation processes. The printed electrodes not only enabled precise control over thickness but also exhibited excellent cycling stability, retaining a stable capacity over 1000 charge-discharge cycles. As an emerging advanced manufacturing technology, 3D printing is catalyzing transformative progress across a wide array of disciplines. Compared to traditional planar fabrication techniques, 3D printing enables a significantly higher areal loading of active materials, thereby boosting the overall areal capacity. This method effectively mitigates the reduction in specific surface area typically caused by disordered material stacking, allowing for enhanced power density even at elevated loading levels. Moreover, 3D printing facilitates the direct integration or co-fabrication of MBs, eliminating the need for separate assembly and packaging steps, thus simplifying the overall manufacturing process. To address the intrinsic limitations of conventional planar micro-lithium-ion battery architectures, the concept of three-dimensional electrode structures has been proposed, offering two primary advantages. By engineering the electrode morphology while maintaining the standard sandwich configuration of electrode/electrolyte/electrode, a much greater electrochemically active surface area can be achieved within the same planar dimensions. Consequently, this design enhances the battery's capacity without increasing the diffusion distance for Li^+ ions. Moreover, it allows for a higher areal energy density to be attained without compromising the areal power density, thus delivering superior performance with preserved functionality (Figure 8c). Additionally, the 3D structure facilitates improved ion diffusion pathways and maximizes the utilization of available space, contributing to overall performance enhancement.

The fabrication of battery-on-chip devices could potentially be achieved through the photopatterning of electrochemical energy storage materials directly onto electronic substrates via lithographic techniques. However, this approach is predominantly constrained to transparent, photocurable resins. The use of insoluble inorganic battery components and conductive materials can negatively impact the optical transparency of the photoresist, which is a critical factor in optically integrated systems. In comparison, radical polymers offer a range of advantageous features such as excellent solubility, high optical clarity, and robust resistance to radical-induced degradation. Consequently, these materials are considered highly promising for use in on-chip energy storage, transport, and conversion technologies [115, 117–121]. Thus, leveraging the unique attributes of radical polymers may offer a viable solution to overcome the limitations associated with traditional photocurable resins, thereby enhancing the functionality and performance of integrated micro-energy systems. Cao et al. [115] developed an enhanced anodic photoresist by chemically modifying the MicroChem SU-8 resist through the incorporation of the radical polymer poly(2,2,6,6-tetramethyl-4-piperidinyl-N-oxyl methacrylate) and the ionic conductor lithium perchlorate (Figure 8d). Capable of being photolithographically defined on silicon substrates with a feature resolution of 10 μm, the modified photoresist exhibits stable charge and discharge behavior at around 0.68 V versus the Ag/AgCl electrode. Its nearly 100% coulombic efficiency highlights excellent electrochemical reversibility and cycling stability. This enhancement not only broadens the application scope of traditional photoresists but also significantly improves their performance in electrochemical energy storage devices. By integrating radical polymers with superior solubility, optical transparency, and radical stability, along with ionic conductors that enhance ion conductivity, this approach offers new strategies and technical means for designing on-chip energy storage devices. Furthermore, this method demonstrates potential applications in microelectromechanical systems and other miniaturized electronic components, thereby advancing the development of integrated micro-energy systems.

In laser scribing technology, a high-energy laser beam is focused onto the surface of the workpiece, inducing localized melting and vaporization of the targeted region. This enables precise material removal and the formation of well-defined patterns with high spatial resolution. Unlike photolithography, which relies on the selective removal of photoresist layers, laser scribing exploits the localized thermal effects to directly fabricate interdigitated microelectrodes of various dimensions based on pre-designed patterns. Due to its simplicity, high precision, and fast processing speed, laser scribing has been widely implemented in the fabrication of MBs. To further enhance the energy density of interdigitated MBs, Jin et al. [116] integrated laser scribing, templating, and an in situ electrodeposition strategy to fabricate flexible aqueous zinc–iodine MBs without the need for conventional additives such as binders, conductive agents, or toxic solvents. The working mechanism of this microdevice operates as follows: during the charging process, zinc ions acquire electrons and undergo reduction to form metallic zinc, which is deposited on the anode. Simultaneously, iodide ions present in the polyacrylamide-based polyelectrolyte lose electrons and are oxidized at the cathode, generating iodine species such as molecular iodine and triiodide anions. In summary, laser scribing has emerged as an effective technique for the fabrication of high-performance interdigitated MBs, particularly when integrated with complementary approaches such as electrodeposition. However, this technology imposes specific constraints on the surface roughness, thickness, and thermal stability of the electrode materials. Furthermore, the potential for thermal-induced degradation or structural damage to the active materials must be carefully considered. Therefore, the development of high-precision, low-heat laser systems is critically important to minimize damage to the electrode architecture during processing and to preserve the structural integrity and electrochemical performance of the final device.

High-performance miniaturized power sources are also poised to significantly impact the advancement of microelectronic systems. For instance, Pikul et al. [62] demonstrated lithium-ion MBs achieving power densities as high as 7.4 mW cm^{-2} mm^{-1}—matching or surpassing those of leading supercapacitors—and marking a 2000-fold improvement compared to previously reported MBs. The key finding of this study is that rational optimization of the battery microarchitecture can concurrently improve both ionic and electronic transport properties, thereby enabling high-power performance. This performance enhancement is achieved through the implementation of 3D bicontinuous

16163028, 2026, 33, Downloaded from https://advanced.onlinelibrary.wiley.com/doi/10.1002/adfm.202524957 by Nanjing University, Wiley Online Library on [03/11/2026]. See the Terms and Conditions (https://onlinelibrary.wiley.com/terms-and-conditions) on Wiley Online Library for rules of use; OA articles are governed by the applicable Creative Commons License

interdigitated microelectrodes. By utilizing this unique microarchitecture, the batteries can simultaneously achieve high power and energy densities, thereby providing a high-performance energy solution. Importantly, the fabrication approach is compatible with large-area scaling, enabling its application across a broad spectrum of devices. The innovative design not only addresses the limitations of traditional MBs but also paves the way for the development of more powerful and compact electronic devices. This breakthrough could significantly advance the field of integrated microelectronics by enabling higher performance in miniaturized systems. Figure 8f,g shows the fabrication process schematic, with the nickel scaffold serving as the structural template for the battery architecture. Electrodeposition enables integration of both electrodes on one substrate. As illustrated in Figure 8h, the nanoporous electrodes consist of electrochemically active layers (red and yellow) on a conductive nickel scaffold (blue), which acts as the current collector. A nickel–tin alloy (red) serves as the anode, and lithiated manganese oxide (yellow) functions as the cathode. The use of the nickel scaffold ensures efficient electron transport and mechanical stability, while the nanoporous structure facilitates rapid ion diffusion within the electrolytically active layers. This design enables high-performance energy storage with optimized power and energy density, making it suitable for advanced microelectronic applications. Overall, this fabrication method provides a robust and scalable approach for integrating high-capacity electrodes into compact MBs systems, enhancing their potential for use in miniaturized electronic devices.

The optimization of MBs footprint stands as a pivotal challenge in advancing miniaturization and high integration, with its historical progression marked by breakthroughs in material innovation, architectural design, and fabrication methodologies (Table 1) [140]. Early-generation thin-film batteries (1980s–2000s) employed a planar thin-film electrode architecture, typically measuring below 100 μm in thickness, fabricated via vacuum deposition techniques such as magnetron sputtering on substrate surfaces. These devices exhibited an operational footprint generally ranging from several square millimeters to 1 cm^2. However, constrained by the inherent limitations of their 2D planar configuration, the active material loading capacity within electrodes remained severely restricted, resulting in persistently low areal capacities of 0.1–0.5 mAh cm^{-2}. Such subcritical energy density characteristics rendered these early iterations inadequate for addressing the sustained power delivery demands of emerging microelectronic systems, particularly in application-critical domains like wearable electronics and implantable medical devices, where their restricted energy storage capabilities fundamentally bottlenecked practical deployment scalability [46]. The basic on-chip MBs are structured as a thin-film battery (Figure 9a) that mirrors the configuration of full-sized batteries, comprising multiple layers of solid films stacked together. Furthermore, devices integrated on-chip are commonly fabricated in parallel, necessitating uniform deposition of each film across an entire wafer (e.g., a 200mm wafer, Figure 9b).

Typically, the total thickness of such thin-film batteries is less than 100μm, which is even thinner than a single electrode layer found in full-sized batteries. The 2010s witnessed groundbreaking advancements in MBs technology through the integration of 3D macroporous frameworks. By leveraging electrochemical deposition and template-assisted synthesis, researchers successfully engineered composite electrodes (e.g., carbon nanotube/graphene hybrids) with hierarchical pore architectures. These structures amplified the specific surface area by 5–10 times compared to conventional planar thin-film electrodes, achieving a breakthrough in areal capacity exceeding 1 mAh cm^{-2}. A landmark example emerged in 2018, when an MIT-led team developed a MBs featuring a 3D porous silicon anode. This innovation delivered an exceptional areal capacity of 1.8 mAh cm^{-2} within a compact 0.5 cm^2 footprint, while its interconnected porous network enabled a threefold enhancement in volumetric energy density over traditional thin-film counterparts. This advancement has effectively mitigated key limitations in energy density, opening new pathways for high-performance power solutions tailored to wearable electronics and miniaturized sensor systems. With the increasing demand for 3D integration of electronic components, through-silicon via (TSV) technology has emerged as the most promising and practical approach for realizing the 3D assembly of single-crystalline device elements, despite the presence of several remaining processing challenges (Figure 9c).

Although monolithic three-dimensional (M3D) integration approaches offer significant potential for advancing semiconductor device architectures, the realization of seamless single-crystalline semiconductor connections without the use of intermediate wafers has not yet been achieved. Such difficulties are rooted in the fundamental limitations associated with low-temperature epitaxial growth on amorphous or polycrystalline surfaces—a prerequisite for back-end-of-the-line compatibility in order to avoid damaging the underlying circuitry during device fabrication. Consequently, the development of a reliable, growth-based methodology enabling M3D integration of single-crystalline materials remains an outstanding challenge in the field. Kim et al. [141] propose a novel approach for the low-temperature synthesis of single-crystalline transition metal dichalcogenides on amorphous and polycrystalline substrates, while preserving the functionality of underlying electronic devices. By employing this novel approach, the authors achieved the monolithic integration of vertically aligned single-crystalline logic transistor arrays, representing a major advancement toward the realization of sophisticated 3D device architectures. This breakthrough enables the realization of novel vertical complementary metal–oxide–semiconductor (CMOS) architectures incorporating single-crystalline channel materials. By demonstrating scalable and integrable growth of high-quality crystals on non-single-crystalline substrates, this advancement opens new pathways toward M3D integration of a wide range of electronic components using single-crystalline materials, thereby advancing the development of next-generation high-performance electronic systems.

The 2020s have witnessed transformative advancements in MBs miniaturization and energy density enhancement through self-curling and multilayer stacking strategies. The Swiss-roll architecture, enabled by stress-induced thin-film self-assembly, leverages intrinsic built-in strain to autonomously transform planar electrodes into microscale cylindrical configurations, dramatically reducing device footprint. A landmark demonstration in 2022 by researchers at Chemnitz University of Technology achieved a silicon-based MBs with an area < 1 mm^2 (comparable

16163028, 2026, 33, Downloaded from https://advanced.onlinelibrary.wiley.com/doi/10.1002/adfm.202524957 by Nanjing University, Wiley Online Library on [03/11/2026]. See the Terms and Conditions (https://onlinelibrary.wiley.com/terms-and-conditions) on Wiley Online Library for rules of use; OA articles are governed by the applicable Creative Commons License

TABLE 1 | MBs fabrication techniques and comparative analysis of their pros and cons.

Method	Material	Advantages	Disadvantages	Refs.
Sputtering	a-Silicon thin film	A broad range of materials and substrates	High cost, low efficiency, slow deposition, and poor conformity.	[61, 122–125]
E-beam evaporation	a-Silicon thin film	An efficient process enabling the deposition of high-melting-point materials.	High cost and low conformity	[126]
LPCVD	Poly-Silicon thin film	Conformal deposition, high purity, and high deposition rate	Precursor-dependent material limits and toxic byproducts	[127]
VLS growth	c-Silicon NWs	Low-cost, feasible fabrication of ultrasmall nanostructures.	Irregular nanostructures and poor uniformity control.	[128]
3D printing	Silicon/C	Flexible design and fabrication of unique 3D structures.	Limited choice of ink materials	[129]
Dry etching	nanopillar arrays	Highly regular structures and well-established industrial processes.	High investment in the equipment	[130–132]
MACE	c-Silicon NWs	High NW density, low production cost, and a simple process.	Irregular NWs and hazardous etching substance	[83]
Electrochemical etching	c-Silicon	Low-cost, fast process with well-controlled nanostructure geometry.	High surface roughness	[133–135]
Screen Printing	c-Silicon	High conductivity, Flexibility, Transparency	Dispersion issues	[136]
Inkjet Printer	CNTs	High precision, Versatility, Customization	Stability challenges	[137]
Photolithography	c-Silicon NWs	High resolution, Precision	Costly equipment	[138]
Mask-assisted filtration	CNTs	High pattern precision, Scalable	Limited resolution	[139]

to a grain of salt) using this technique, delivering a remarkable areal energy density of 0.5 mWh cm^{-2}—a breakthrough overcoming spatial limitations of conventional planar designs. Parallel progress in substrate-free vertical electrode stacking has unlocked exponential growth in areal energy storage capacity via precisely engineered interlayer ion/electron transport pathways [142]. A representative example is the four-layer stacked PEDOT-MnO_2 battery, which achieves an areal energy density of 3.87 mWh cm^{-2}, quadrupling that of single-layer counterparts. This 3D integration approach not only preserves electrode material activity but also enhances power output efficiency through shortened ion diffusion paths [143]. Collectively, these innovations provide ultracompact, high-energy-density solutions for next-generation wearable electronics and implantable medical devices, marking a paradigm shift in MBs architecture design. The micro-origami self-assembly technique revolutionizes MBs fabrication by transforming planar thin films into micrometer-scale Swiss-roll architectures, effectively addressing the longstanding challenge of integrating high-energy-density power sources with microelectronic devices. This on-chip compatible methodology exploits inherent built-in strain to spontaneously fold metallic Ti/Au sheets into hollow helical current collectors that emulate the optimized electrode topology of conventional bulk batteries.

Pioneering work by Li et al. [144] demonstrated this concept through an innovative twin-tube configuration: two perforated Ti/Au layers undergo coordinated self-rolling on a single substrate, forming interdigitated tubular electrodes. Subsequent electrodeposition of MnO_2 (0.8 μg loading via 7-min deposition) and Zn onto these Swiss-roll scaffolds creates air-stable, high-performance MBs. Structural characterization via top/side-view imaging confirms uniform material deposition within the helical channels. The resulting MBs achieves remarkable metrics within a 0.11 mm^2 footprint, delivering 136 μAh cm^{-2} capacity and 181 μWh cm^{-2} energy density–performance metrics rivaling state-of-the-art counterparts while reducing manufacturing costs by an order of magnitude. Crucially, cycling stability matches leading MBs technologies, with potential for further enhancement through integration of high-capacity materials like silicon or germanium. This scalable platform enables parallel fabrication of battery arrays in single processing runs, positioning Swiss-roll architectures as a transformative solution for powering next-generation autonomous microsystems.

Tang's [126] research team pioneered a helical microelectrode system through stress-engineered self-assembly of Si–Ge

16163028, 2026, 33, Downloaded from https://advanced.onlinelibrary.wiley.com/doi/10.1002/adfm.202524957 by Nanjing University, Wiley Online Library on [03/11/2026]. See the Terms and Conditions (https://onlinelibrary.wiley.com/terms-and-conditions) on Wiley Online Library for rules of use; OA articles are governed by the applicable Creative Commons License

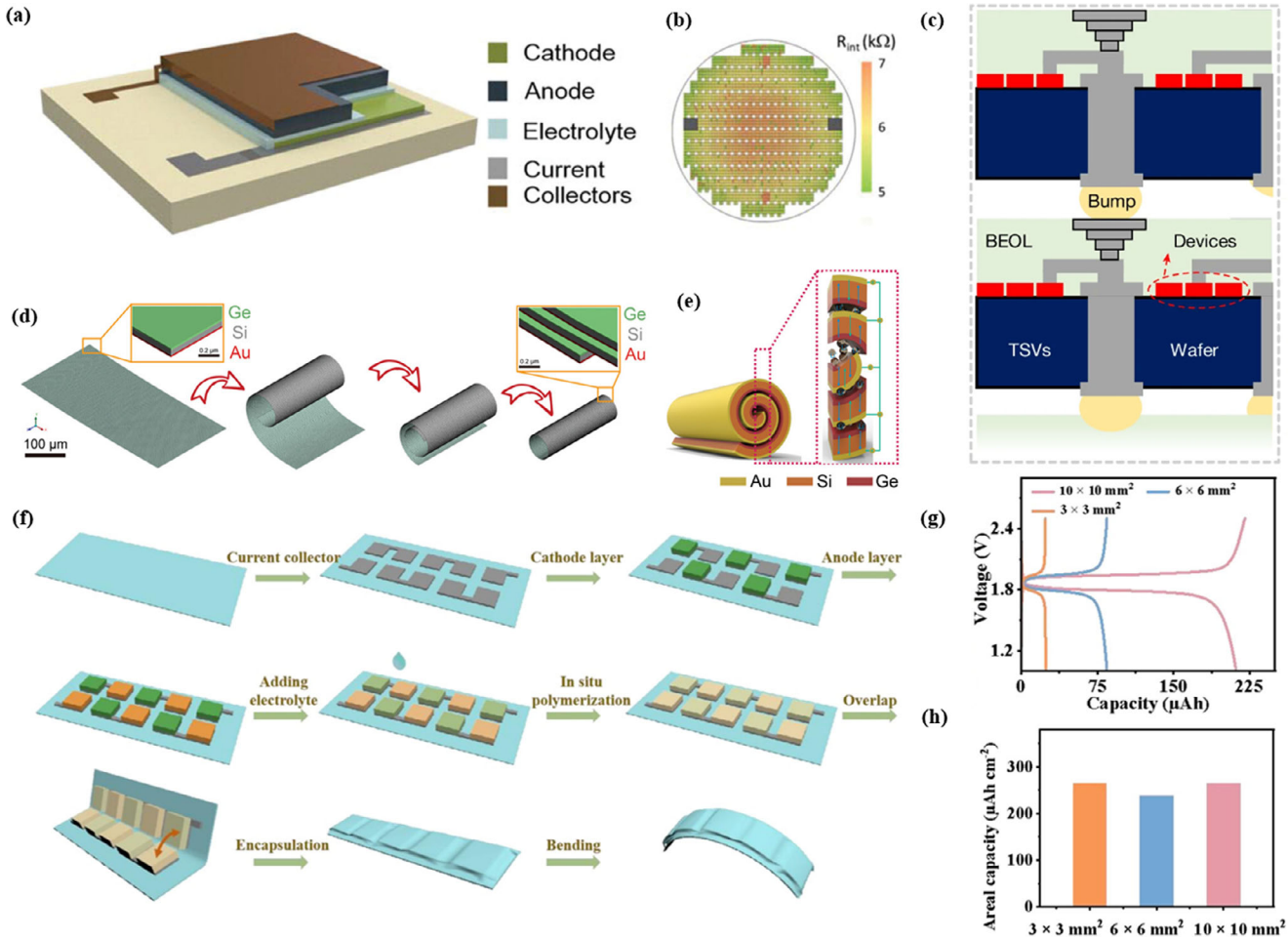


FIGURE 9 | (a) Schematic illustration of a thin film battery structure. Reproduced with permission [145]. Copyright 2022, Wiley-VCH. (b) Wafer-scale sheet resistance mapping of solid-state electrolyte layer on silicon substrate. Reproduced with permission [146]. Copyright 2019, IEEE. (c) TSV-enabled 3D integration schematic depicting multistrata stacking architecture with vertically aligned TSV arrays at wafer-level scale. Reproduced with permission [141]. Copyright 2024, Springer Nature. (d) FEA of Si(60nm)/Ge(20nm) heterostructure with Au(5nm) current collector: Multiphysics simulation of thermomechanical and charge transport behavior. (e) Multiphysics schematic of Archimedean spiral electrode: Multiscale Li^+ diffusion pathways | charge percolation highways via spiral-structured topological optimization. Reproduced with permission [126]. Copyright 2020, Wiley-VCH. (f) Screen-printing schematic for monolithic LIMB integration: Layered electrode–electrolyte architectures with interdigitated current collectors. (g) Areal capacity measured at 50 μA cm^{-2}. (h) LIMBs with geometric variants. Reproduced with permission [66]. Copyright 2020, Wiley-VCH.

nanocomposites, demonstrating a breakthrough in overcoming charge transport limitations inherent to thick-film electrodes. The spontaneous formation of spiral geometry originates from precisely controlled stress gradients within the multilayered nanomembrane architecture. This geometry inherently preserves nanoscale charge-transfer pathways while circumventing kinetic bottlenecks observed in conventional dense electrodes – a critical advancement validated through coupled experimental and computational analyses. As illustrated in Figure 9d, finite element modeling (FEM) simulations of the self-rolling dynamics reveal quasi-stacked helical configurations with tunable interlayer gap dimensions (sub-50 nm winding thickness), directly attributable to built-in stress modulation during nanomembrane fabrication. Figure 9e further demonstrates the structural superiority: the helical topology enables sub-millisecond charge carrier migration across the electrode–electrolyte interface, achieving 3-order-of-magnitude faster transport kinetics compared to planar counterparts. Zhu et al. [66] reported a scalable screen-printing approach for the fabrication of planar, monolithically integrated, solid-state LIMBs. The devices exhibited notable electrochemical performance, including a high areal capacity of 1431 μAh cm^{-2}, excellent output voltage, and remarkable mechanical flexibility. Furthermore, they demonstrated outstanding cycling stability, with negligible capacity degradation after 8000 cycles, along with exceptional adaptability in terms of dimensional design. The superior flexibility of these devices is attributed to the inherent mechanical compliance of all constituent components—particularly the solid-state electrolyte—as well as the robust interfacial integration between the electrodes and electrolyte. As a result, the LIMBs maintain stable electrochemical performance even after repeated bending cycles. The fabrication steps of the monolithically integrated solid-state LIMBs are summarized in Figure 9f. As the device size was increased, the GCD curves remained nearly unchanged in shape, and the overall capacity scaled accordingly, demonstrating excellent scalability (Figure 9g). As shown in Figure 9h, a consistent areal capacity of around 250 μAh cm^{-2} was maintained across varying device sizes, confirming the scalable nature of the screen-printed LIMBs. The

16163028, 2026, 33, Downloaded from https://advanced.onlinelibrary.wiley.com/doi/10.1002/adfm.202524957 by Nanjing University, Wiley Online Library on [03/11/2026]. See the Terms and Conditions (https://onlinelibrary.wiley.com/terms-and-conditions) on Wiley Online Library for rules of use; OA articles are governed by the applicable Creative Commons License

flexibility to customize electrode shapes and dimensions further enhances their suitability for application-specific energy storage needs.

Advanced MBs fabrication processes, through interdisciplinary integration across multiple length scales, have overcome fundamental limitations inherent in conventional battery systems regarding micro/nano-scale integration and interfacial regulation. These processes serve as the core driving force behind the development of high-energy-density miniaturized energy storage devices. By innovatively combining precision semiconductor manufacturing techniques with the intrinsic properties of energy materials, such fabrication methodologies enable the controllable construction of sub-micron electrode architectures and the synergistic optimization of nanoscale interfacial engineering. This has significantly enhanced carrier transport kinetics and the stability of mechano–electrochemical coupling.

2.6 | Indicators and Parameters

The integration of MBs into modern energy systems and microelectronic devices necessitates a rigorous evaluation of their operational indicators and performance parameters. These parameters not only delineate the electrochemical properties of MBs but also dictate their suitability for a wide range of applications, spanning from implantable biomedical devices to grid-scale energy storage solutions. As the demand for miniaturized, high-efficiency power sources grows, the interplay between technical parameters-such as energy density, cycle life, SOC, and safety thresholds and application-specific requirements becomes pivotal in achieving optimal system integration. MBs, characterized by their microscale architecture and high energy density, must balance trade-offs between capacity retention, thermal stability, and mechanical flexibility. For instance, in wearable electronics and IoT sensors, volumetric energy density (>10 mWh cm^{-3}) and cycle stability (>5000 cycles) are prioritized to ensure long-term autonomy under dynamic mechanical stress. Conversely, in implantable biosensors, biocompatibility and low self-discharge rates (<1%/month) emerge as critical parameters to minimize invasive maintenance and enhance patient safety. Meanwhile, grid-connected energy storage systems emphasize scalable parameters like power density (>1 Kw kg^{-1}) and bidirectional efficiency (>95%) to support rapid charge–discharge cycles and grid resilience. The standardization of these indicators is further complicated by heterogeneous application environments. For example, temperature-dependent parameters such as internal resistance and capacity fade require adaptive management strategies, as demonstrated in 3D-printed sodium-ion MBs where multi-scale thermal regulation extended operational lifespan by 40% under fluctuating loads. Additionally, emerging metrics like "energy per footprint" (Wh cm^{-2}) and "dynamic response time" (<10 ms) are redefining integration frameworks for MBs in smart grids and autonomous robotics.

Chen et al. [147] introduced a single-layer (SL) MoS_2/graphene heterostructure designed for application in zinc-ion MBs. This architecture delivers multiple performance-enhancing features: it provides strong binding sites for Zn ions, enables epitaxial nucleation along the Zn (002) direction through favorable lattice matching, and ensures a more uniform current density distribution, thereby improving cycling stability and efficiency. The developed MoS_2/graphene-based Zn||MnO_2 MBs exhibit reversible, dendrite-free zinc plating/stripping processes, delivering an areal capacity of 0.16 mAh cm^{-2} at a current density of 0.5 mA cm^{-2}. These devices show stable performance over 470 cycles in an area of less than 0.1 mm^2. Moreover, through the use of single-crystalline MoS_2/graphene films, the integration of these MBs with transistors on-chip has been achieved via lithographic methods, enabling the creation of compact, self-powered field-effect transistors and photodetectors. The monolithically integrated, self-powered microsystem based on SL MoS_2/graphene heterostructures represents a promising strategy for achieving multifunctionality and miniaturization in next-generation electronic devices. The SL MoS_2 microelectrode was fabricated by transferring an individual SL MoS_2 flake onto a pre-patterned graphene layer, which was electrically connected to Au leads, forming a partially overlapping heterojunction. As illustrated in the cross-sectional schematic of Figure 10a, the microelectrode is designed with a SU-8 photoresist-defined opening that selectively exposes three distinct areas—graphene, single-layer MoS_2, and their heterojunction—to the electrolyte environment. This setup allows for a direct comparison of Zn electrochemical nucleation behaviors across these surfaces under the same experimental settings. As illustrated in Figure 10b, the authors successfully co-fabricated an SL MoS_2/graphene-based Zn||MnO_2 MB and a FET on a single chip through a series of photolithographic, transfer, etching, metal deposition, and electrodeposition processes. Utilizing a monolithic crystalline SL MoS_2/graphene film, they further developed a prototype self-powered "smart dust" device that integrates a battery, sensor, and logic circuits within a unified architecture, as shown in Figure 10c. This integrated, self-sustaining system holds great promise for deployment in ubiquitous sensing networks, enabling real-time monitoring of critical environmental parameters such as air and water quality, temperature, and humidity—factors essential for effective environmental and public health management. Additionally, the system operates as a wireless biomedical sensor, capable of measuring key physiological signals including heart rate, body temperature, blood pressure, and glucose levels. Consequently, it provides extensive applicability in both wearable and implantable health-monitoring systems, enhancing its versatility and impact across multiple domains.

Dai et al. [148] presented a dual-plating method for the facile fabrication of zinc–bromine microbatteries (Zn–Br_2 MBs) based on a liquid catholyte system. This approach offers both high areal energy density and enhanced charge–discharge rate capability. The fabricated Zn–Br_2 MBs delivered an areal energy density of 3.6 mWh cm^{-2}, which is notably about ten times greater than that of existing planar MBs, marking a major advancement in the field. Additionally, these devices demonstrate polarity-switchable behavior, which allows tolerance against misidentification of cathode and anode during operation. The proposed strategy is also extendable to other aqueous MB chemistries, such as Zn–I_2 and Zn–MnO_2 systems. This research not only provides a viable design methodology for achieving high-performance MBs but also pushes the boundaries of miniaturized energy storage technologies. As depicted in Figure 10d, the fabrication procedure involves first mounting a thin, flexible, and hydrophilic

16163028, 2026, 33, Downloaded from https://advanced.onlinelibrary.wiley.com/doi/10.1002/adfm.202524957 by Nanjing University, Wiley Online Library on [03/11/2026]. See the Terms and Conditions (https://onlinelibrary.wiley.com/terms-and-conditions) on Wiley Online Library for rules of use; OA articles are governed by the applicable Creative Commons License

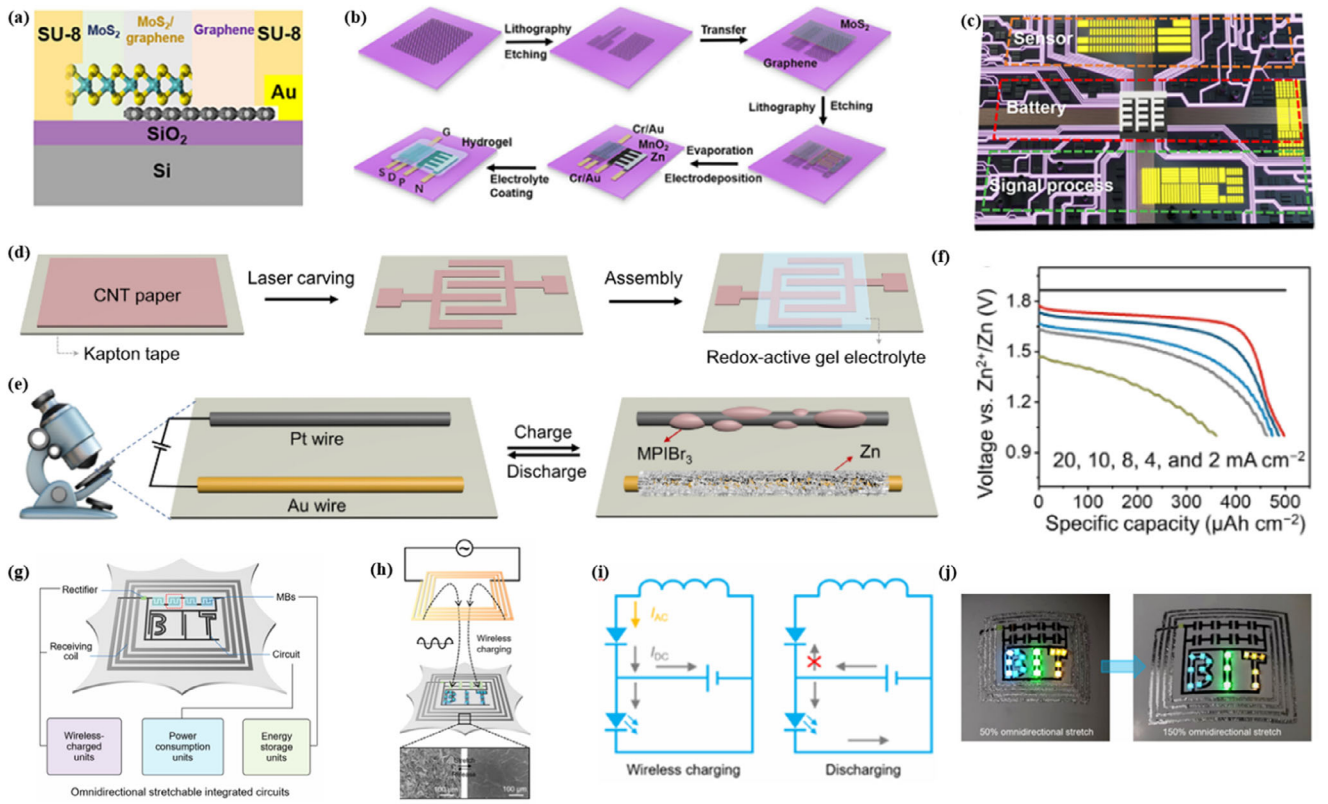


FIGURE 10 | (a) Integrated van der Waals heterostructure microdevice: Schematic architecture of monolayer MoS_2/graphene hybrid system; Optical micrographs of fabricated devices vs. Si/SiO_2 alignment markers (scale bars: 10 μm). (b) Integrated manufacturing strategy for constructing MoS_2/graphene-based FET and MB devices. (c) System-level integration strategy for 2D material-based smart chips: SL-MoS_2/graphene heterostructure enabling co-localized battery power supply, biochemical sensing, and in-memory computing functionalities in ultra-compact systems. Reproduced with permission [147]. Copyright 2025, Elsevier. (d) Fabrication process of the Zn–Br_2 MBs. (e) In operando microscopic visualization of dualmetal electrodeposition dynamics with Pt and Au as spatially resolved anode/cathode current collectors. (f) Cycling performance. Reproduced with permission [148]. Copyright 2025, American Association for the Advancement of Science. (g) Schematic of the IC architecture delineating structural configuration and functional domains. (h) Wireless charging IC schematic with SEM-imaged stretchable Ag coils. (i) Schematic of wireless power transfer-integrated IC architecture during concurrent energy harvesting and load provisioning cycles. (j) Mechanical robustness demonstration of stretchable IC-integrated micro-LED arrays (threshold operating voltage: 2–3.2 V) under biaxial tensile strain (50%–150%). Reproduced with permission [67]. Copyright 2025, American Association for the Advancement of Science.

CNT paper (~10 μm) onto an insulating tape surface. Laser ablation is then applied to define interdigitated electrode structures, yielding a total active area of approximately 0.18 cm^2. To probe the real-time plating and stripping dynamics of Zn–Br_2 MBs, operando microscopy was conducted during device operation (Figure 10e). A well-defined discharge plateau at around 1.7 V versus Zn^{2+}/Zn was recorded at a current density of 2 mA cm^{-2}. The battery also displayed superior rate capability, maintaining approximately 72% of its initial capacity at 20 mA cm^{-2} (Figure 10f), with a peak power density reaching ~26.2 mW cm^{-2}. These results provide strong evidence of the fast electrochemical reaction kinetics enabled by the oily $MPIBr_3$ cathode material. These in-plane, wirelessly rechargeable MBs, with their conformable geometry and high energy output, hold considerable promise for enabling next-generation, shape-adaptive electronic systems.

However, the seamless integration of MBs into flexible electronic systems remains a significant challenge, requiring careful structural design and materials engineering at the microscale to ensure both high compatibility and robust mechanical stability. Wang et al. [67] have developed stretchable and wirelessly rechargeable dual-plating MBs that can be seamlessly integrated into electronic circuits through an omnidirectional stretch-contraction process combined with mask-assisted printing. The implementation of strain-induced folding structures, along with a design strategy focused on minimizing active material loss, endows these MBs with exceptional mechanical robustness, enabling them to withstand up to approximately 200% omnidirectional strain. These devices also exhibit power and energy densities about one order of magnitude higher than conventional in-plane MBs, signifying a significant leap forward in the development of flexible power sources for next-generation electronics. Owing to their exceptional compatibility and elastic properties, the proposed wireless-charging stretchable MBs enable the integration of complex flexible systems such as stretchable display circuits and intelligent electronic skin capable of mimicking human tactile perception—detecting parameters including object weight, temperature, and shape. The omnidirectional stretch–contraction strategy offers unique advantages, as prestretched elastomeric substrates can generate uniform and multidirectional contraction forces during relaxation, effectively transferring well-defined stress profiles

16163028, 2026, 33, Downloaded from https://advanced.onlinelibrary.wiley.com/doi/10.1002/adfm.202524957 by Nanjing University, Wiley Online Library on [03/11/2026]. See the Terms and Conditions (https://onlinelibrary.wiley.com/terms-and-conditions) on Wiley Online Library for rules of use; OA articles are governed by the applicable Creative Commons License

to the surface patterns. This attribute enables the design of miniaturized, stretchable in-plane circuits with intricate layouts while maintaining structural integrity and operational stability. A schematic representation of a stretchable integrated circuit, comprising wireless charging modules, energy storage devices, and power-consuming components, is shown in Figure 10g, highlighting the potential for fully integrated, flexible electronic systems. Featuring exceptional mechanical flexibility and structural integrity, an omnidirectionally stretchable integrated circuit has been successfully realized, incorporating three fundamental functional units: a wireless charging module (including a receiving coil and rectifier), an energy storage module (designed as a series–parallel microbattery array), and a power-consuming module (comprising patterned conductive circuits). A circuit diagram illustrating the wireless charging process is shown in Figure 10h, depicting how the rectified DC current serves dual purposes: charging the MB array and supplying power to the LED array. Experimental verification of this operation mode is provided in Figure 10i. Upon reaching the target voltage, the MBs are disconnected from the wireless charger, and the stored energy is used to power the LED array. As illustrated in Figure 10j, the LED array continues to operate normally even after being stretched by 50% and 150%, confirming the system's high mechanical durability and ability to function under significant deformation.

Mechanistically, the spiral architecture's high surface-to-volume ratio (exceeding 10^3 cm^{-1}) and continuous ion diffusion channels synergistically address the traditional trade-off between electrode mass loading and charge transfer efficiency. This stress-guided self-assembly paradigm establishes a scalable platform for developing high-rate MBs, particularly promising for applications requiring rapid charge–discharge cycling in miniaturized electrochemical microdevices. As the demands for higher energy density and smaller physical sizes grow, developing dependable safety technologies for rechargeable batteries has become essential. A key focus in battery safety is understanding and managing thermal runaway—a condition marked by uncontrollable heat generation from a series of exothermic reactions within the cell. Conducting comprehensive full-cell safety evaluations is challenging due to the requirement for large cell capacities—typically exceeding one ampere-hour—for Accelerating Rate Calorimetry (ARC) tests, which are crucial for analyzing thermal runaway events. The implementation of effective safety screening protocols is also difficult due to high material usage and elevated manufacturing costs. Seongjae et al. [149] designed cylindrical pouch-type miniature batteries (~21 mAh, ~0.1 g cathode active material) with distinct thermal generation features, allowing for laboratory-scale accelerating rate calorimetry (ARC) testing at the full-cell level (Figure 11a–d). This methodology enables rapid safety evaluation and offers early-stage insights for iterative design improvements, thus expediting the development of high-safety battery systems.

The evolution of MBs technology has not kept up with advancements in MEMS, leading to a significant limitation for MEMS applications. Many currently available MBs, including solar cells and micro fuel cells, do not fulfill the necessary energy density and operational lifespan requirements of MEMS devices. In contrast, betavoltaic MBs, characterized by their long operational lifetimes and high energy densities, have emerged as one of the most significant research avenues in MBs development. These devices hold substantial promise as power sources for MEMS applications. Liu et al. [150] proposed a sandwich-structured ^{63}Ni-Si betavoltaic MB, with a comprehensive analysis of the optimization of its physical parameters using various substrates, supported by MCNP simulation studies. The fabricated device features a shallow junction configuration. Temperature is identified as a key factor affecting the electrical performance of betavoltaic MBs, particularly in extreme and remote environments such as those encountered in space-based sensing applications. While prior studies have suggested a linear temperature dependence of the open-circuit voltage (Voc) in Si PN junction betavoltaic devices, this relationship is shown to deviate under certain operational conditions. Consequently, this study investigates the temperature effects on betavoltaic performance through both experimental and simulation approaches. The computational model for a betavoltaic device featuring a sandwich structure and bidirectional ^{63}Ni isotope layers was developed using MCNP (Figure 11e). Figure 11f shows the temperature dependence of Voc and Jsc for optimized sandwich-structured betavoltaic devices on p- and n-type substrates (junction depth: 0.05 μm). Experimental results, depicted in Figure 11g, closely match the simulated trends.

In addition, Liu et al. [151] conducted a theoretical analysis of the temperature-dependent behavior of ^{63}Ni-Si betavoltaic MBs, taking into account radiation sources with different thicknesses and activity levels across a temperature range of 170–340 K. The study also included experimental investigations into the thermal characteristics of both monolayer and interbedded ^{63}Ni-Si structures between 213.15 and 333.15 K. The findings indicated that the temperature sensitivity of the betavoltaic performance diminishes with increasing source thickness, activity density, and average energy. Specifically, increasing the temperature was found to induce a linear decline in open-circuit voltage and maximum power output at lower temperatures, followed by an exponential drop at higher temperatures across upper, lower, and interbedded device configurations. As illustrated in Figure 11h, a theoretical monolayer calculation model of the ^{63}Ni-Si betavoltaic MBs was developed using the MCNP5 Monte Carlo code to investigate its temperature dependence. To simulate the device's electrical performance, this computational model was developed using actual structural parameters from experimental samples, such as source thickness, ECU thickness, junction depth, doping concentration, and air gap. The simulation aimed to compare these calculated performances with the experimentally measured results, as depicted in Figure 11i. Furthermore, Figure 11j highlights the variation of the Voc with temperature for various thicknesses of ^{63}Ni. Butera et al. [152] report on the performance of a fabricated prototype $Al_{0.2}Ga_{0.8}As^{55}Fe$ radioisotope MBs PV cell, evaluated over a temperature range from −20°C to 50°C. This study employed two 400 μm-diameter p^+–i–n^+ $Al_{0.2}Ga_{0.8}As$ mesa photodiodes, each featuring a 3 μm intrinsic layer, as energy conversion elements in an innovative X-ray MB prototype. The investigation focused on the temperature-dependent behavior of key device parameters, revealing a consistent decline in Voc, maximum output power, and internal conversion efficiency with increasing temperature. At −20 °C, the photodiodes recorded an open-circuit voltage of 0.2 V and a maximum output power of 0.04 pW. Under the same conditions, the prototype demonstrated an internal power conversion efficiency of up to 0.95%.

16163028, 2026, 33, Downloaded from https://advanced.onlinelibrary.wiley.com/doi/10.1002/adfm.202524957 by Nanjing University, Wiley Online Library on [03/11/2026]. See the Terms and Conditions (https://onlinelibrary.wiley.com/terms-and-conditions) on Wiley Online Library for rules of use; OA articles are governed by the applicable Creative Commons License

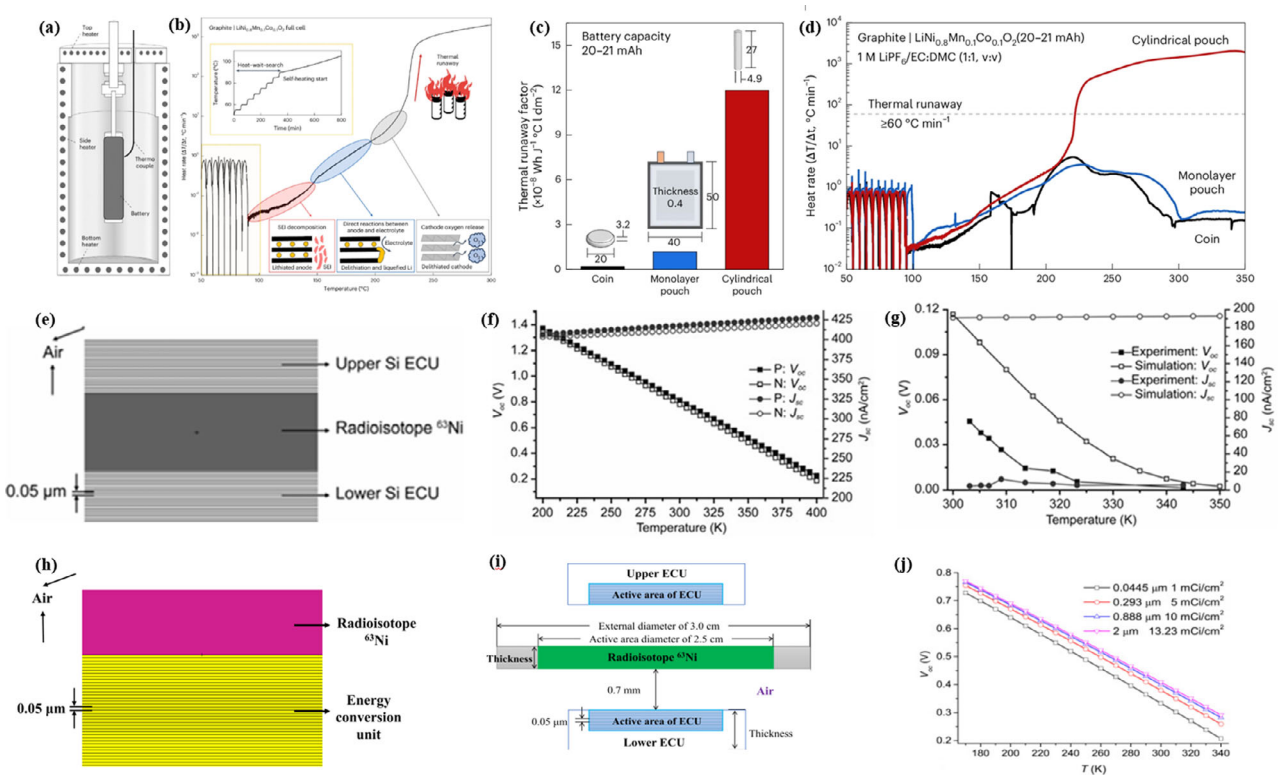


FIGURE 11 | (a) Illustration of a standard ARC module employed for full-cell-level safety testing. (b) ARC analysis reveals thermal runaway via self-sustaining exothermic reactions in $LiNi_{0.8}Mn_{0.1}Co_{0.1}O_2$/graphite full cells. (c) Thermal runaway observed in lab-scale battery systems. (d) Comparative ARC evaluation of three distinct cell chemistries. Reproduced with permission [149]. Copyright 2025, Springer Nature. (e) Calculation model of Si betavoltaic MBs. (f) Temperature-dependent open-circuit voltage and short-circuit current density characteristics of betavoltaic devices with 50-nm junction depth. (g) Temperature dependences of Voc and Jsc in experiment and simulation. Reproduced with permission [150]. Copyright 2014, Science China Press. (h) MCNP5-modeled monolayer ^{63}Ni-Si betavoltaic MBs investigate thermal response characteristics. (i) MCNP5-simulated thermal response model validated against experimental measurements. (j) Changes in V_o as a function of temperature for different thicknesses of ^{63}Ni. Reproduced with permission [151]. Copyright 2018, Elsevier.

A thorough understanding and precise control of key operational parameters in MBs are essential for advancing their design and application. Such parametric insight not only facilitates a comprehensive assessment of electrochemical performance and system stability but also enables the rational optimization of device functionality across diverse operating conditions. The integration of these multidimensional parameters with AI-driven analytical frameworks opens new avenues for performance enhancement through data-informed modeling and adaptive control strategies. This synergistic, data-centric paradigm provides a robust foundation for the development of next-generation MBs technologies, paving the way toward intelligent system design, predictive degradation monitoring, and high-efficiency energy storage solutions tailored for autonomous microsystems.

3 | The Applications and Integration of Microbatteries

The rapid advancement of miniaturized electronics and the growing demand for autonomous, portable, and sustainable power sources have positioned MBs as pivotal components in modern technological ecosystems. As technology advances, the applications of MBs have expanded far beyond traditional roles, permeating fields such as the IoT, wearable devices, medical implants, smart sensors, and micro-electromechanical systems (MEMS) [153–163]. Their integration into these systems, however, presents unique challenges, including energy density optimization, scalable manufacturing, and compatibility with heterogeneous substrates. This chapter explores the transformative applications of MBs across interdisciplinary domains and delves into the innovative strategies employed to seamlessly embed these power sources into multifunctional platforms. By bridging the gap between energy storage and device functionality, the integration of MBs is redefining the boundaries of compact, self-sustaining technologies and paving the way for next-generation innovations in both consumer and industrial landscapes.

3.1 | Manufacturing Constraints and Integration Requirements

The structure and design of a battery play a crucial role in achieving high energy and power densities in microenergy systems. Thin-film batteries, in many respects, serve as the foundation for such systems. In a typical fabrication process, a LiPON solid electrolyte layer is sputtered onto a predeposited cathode (usually $LiCoO_2$ or $LiMn_2O_4$), followed by thermal evaporation of a lithium-metal anode, completing a planar three-layer stack. While thin-film batteries exhibit excellent rate performance, their

16163028, 2026, 33, Downloaded from https://advanced.onlinelibrary.wiley.com/doi/10.1002/adfm.202524957 by Nanjing University, Wiley Online Library on [03/11/2026]. See the Terms and Conditions (https://onlinelibrary.wiley.com/terms-and-conditions) on Wiley Online Library for rules of use; OA articles are governed by the applicable Creative Commons License

planar geometry limits areal energy density because only a few micrometers of active material can be deposited before mechanical stress and transport bottlenecks become significant. To increase areal energy density and deliver the peak current bursts required for data transmission in IoT devices, commercial solid-state batteries often parallel-stack multiple thinfilm layers and connect them to form a single MB cell. Bipolar stacking reduces electron transport distance, minimizes interconnection-related losses, and decreases inactive mass, resulting in a compact, high-energy, high-power MB. Beyond stacked thin-film layouts, researchers have also explored entirely new cell geometries, most notably 3D electrodes. By adopting highaspectratio 3D architectures, such as pillars or interdigitated patterns, these designs increase the electrode/electrolyte interfacial area, shorten iontransport pathways, and enhance activematerial utilization without compromising energy density. This shift from planar to 3D architectures enables MBs to meet the stringent energy and power demands of miniaturized IoT devices [164].

Different nanowire fabrication methods, such as bottom–up growth and top–down etching, impose inherent constraints on material selection and structural characteristics, which in turn directly govern the core electrochemical and mechanical properties of the resulting devices. Bottom–up growth approaches (e.g., vapor–liquid–solid mechanism, solution-phase synthesis) are typically limited by growth kinetics and crystal-phase compatibility, often restricting material choices to those suitable for specific catalystmediated or template-guided processes, such as certain semiconductors, metals, or oxides. In contrast, top–down etching techniques (e.g., lithographic patterning, reactiveion etching) enable precise dimensional control, yet their accessible material systems are largely constrained by the compatibility with existing lithography and etching processes, leading to a narrower range of achievable compositions and crystallographic orientations. Structurally, growth methods can produce nanowires with high aspect ratios and tunable diameters and lengths, but they often exhibit variations in alignment, uniformity, and interface abruptness. Etching-based routes, while capable of producing ordered arrays and complex architectures, may introduce surface defects, stress concentrations, or limited aspect ratios due to processinduced damage. These material and structural constraints imposed by the fabrication process further directly influence key device properties, including electrochemical performance (e.g., capacity, rate capability, cycling stability) and mechanical behavior (e.g., stiffness, fracture strength, interfacial adhesion). Consequently, the choice of nanowire fabrication fundamentally delineates the accessible materialstructure space and sets intrinsic boundaries on the ultimate functional performance of the devices [165, 166].

From a systems perspective, the specific demands for power and energy imposed by integration scenarios translate into rigorous performance metrics for MB devices—such as instantaneous power density, sustained operational duration, and cycling stability. These metrics, in turn, map directly onto precise constraints on the intrinsic properties of their constituent materials. For instance, IoT sensor nodes require MBs to achieve energy autonomy for several years under dynamic loads ranging from nanowatts to microwatts. This imposes near-limit requirements on the low self-discharge rate of electrode materials and the ultralong-term electrochemical stability of electrolytes. Conversely, pulsed operating loads in wearable devices—such as milliampere-level current peaks during wireless communication—demand electrode materials with excellent rate capability and rapid iondiffusion kinetics, while the solid electrolyte interphase must withstand such repeated current surges without degradation [167–169].

The evolution of MB technology is consistently governed by the synergistic constraints imposed by materials at both the "manufacturing" and "integration" levels. At the manufacturing level, the inherent properties of materials—such as the significant volume expansion of silicon anodes, low conductivity, and the low tap density of nanomaterials—directly dictate viable processing pathways and the theoretical performance limits of the final devices. In response, research efforts have focused on material nanostructure engineering (e.g., porous silicon, nanowires) and advanced manufacturing techniques (e.g., lithography, 3D printing) to address these challenges. At the integration level, materials must achieve deep compatibility with the target microsystem in terms of process temperature, electrochemical window, thermal expansion coefficient, and mechanical stress. Failure to meet these requirements can lead to circuit interference, interface failure, or reliability issues. Corresponding strategies involve the development of process-integrated designs (e.g., monolithic integration of transistors and batteries based on two-dimensional material heterojunctions), novel device architectures (e.g., interdigitated structures that eliminate separators), and multifunctional material systems. The key to future breakthroughs lies in developing new materials that can simultaneously meet the dual requirements of manufacturability and integrability. By breaking the chain of constraints linking "manufacturing, materials, and integration," the ultimate goal is to realize high-performance, highly reliable on-chip energy system integration.

Consequently, system-level energy and power budgets essentially define a multidimensional boundary of material performance, compelling complex tradeoffs and multiobjective optimization among: the intrinsic volume expansion of high-energy-density materials (e.g., silicon anodes), the interfacial stability of highly ion-conductive solid electrolytes, and the construction of highly conductive networks required for high-power output. This constraint dimension, derived inversely from application scenarios, intertwines with the "feasibility" constraints imposed by manufacturing processes. Together, they delineate the theoretical upper limits and practical bottlenecks of material and device performance under current technological pathways.

3.2 | Related Application Systems

The convergence of IoT ecosystems, implantable biomedical devices, and advanced wearables necessitates breakthrough advancements in multifunctional integration and energy-density optimization for next-generation microscale electronics. These technologies require compact yet powerful solutions to support their increasingly sophisticated functionalities. SoC, as a highly integrated single-chip system, has achieved deep integration of functional modules in computing, communication, and sensing domains. However, its energy supply still relies on traditional batteries or external power sources, which limit device autonomy

16163028, 2026, 33, Downloaded from https://advanced.onlinelibrary.wiley.com/doi/10.1002/adfm.202524957 by Nanjing University, Wiley Online Library on [03/11/2026]. See the Terms and Conditions (https://onlinelibrary.wiley.com/terms-and-conditions) on Wiley Online Library for rules of use; OA articles are governed by the applicable Creative Commons License

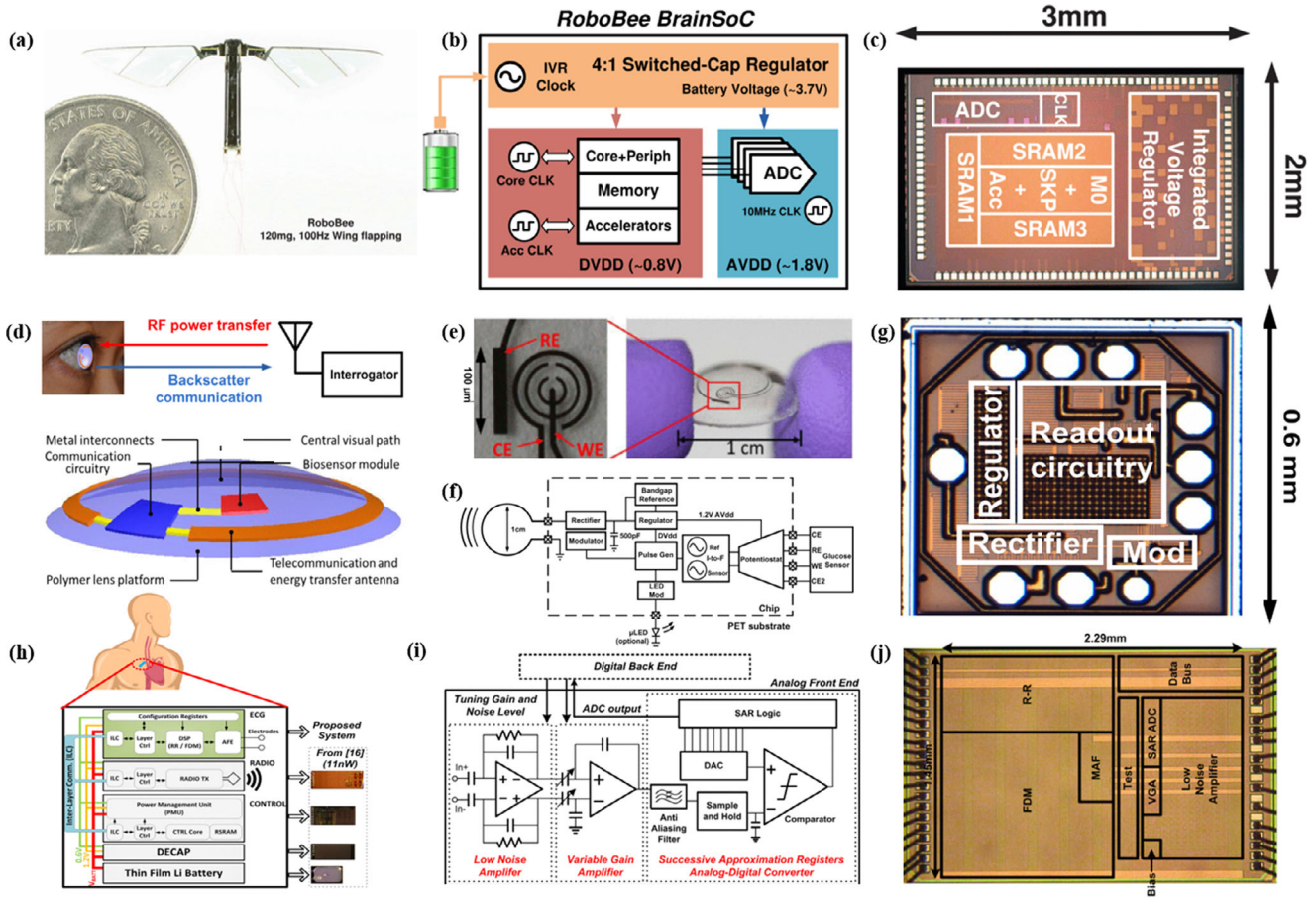


FIGURE 12 | (a) RoboBee is a bio-inspired, bee-sized micro-robot. (b) Illustration of the system architecture for the Self-Sustained BrainSoC. (c) BrainSoC die photograph. Reproduced with permission [42]. Copyright 2017, IEEE. (d) Schematic representation of an active contact lens system designed for wireless health monitoring. (e) Design, development, and fabrication of a Glucose Sensor (f) System architecture of the readout IC. (g) Micrograph of readout IC. Reproduced with permission [170]. Copyright 2012, IEEE. (h) ultralow-power sensor node peripherals. (i) Top-level diagram of the analog front end. (j) Die image of the proposed SoC fabricated in 65 nm low-power CMOS technology. Reproduced with permission [171]. Copyright 2015, IEEE.

and further miniaturization. MBs, as a form of miniaturized energy storage technology, offer high energy density, flexibility, compatibility, and low self-discharge characteristics, making them a crucial solution for powering miniature devices. Their ability to provide reliable energy storage in compact form factors addresses key challenges in powering microelectronic systems. Zhang et al. [42] present a fully integrated SoC specifically optimized for insect-scale flapping-wing pico-aerial vehicles, such as a bee-sized robot (Figure 12a). This SoC meets autonomous flight requirements with minimal weight (<3 mg after thinning), low power consumption, and real-time performance. The system integrates embedded voltage regulation, data conversion, clock generation, as well as general-purpose and accelerated computing units. The self-contained system operates directly from a lithium battery, enabling microscale applications (Figure 12b,c). Experimental results demonstrate that the SoC controls open-loop wing flapping and achieves enhanced energy efficiency through hardware acceleration. Additionally, the use of adaptive clocking ensures supply resilience, further improving the system's performance. These advancements highlight the potential for miniaturized, autonomous flying devices capable of complex tasks in various applications.

Additionally, Liao et al. [170] demonstrated a wirelessly powered noninvasive sensing platform integrating a loop antenna, glucose sensor, and a 0.36 mm^2 CMOS chip co-housing power management, signal readout, wireless interface, LED driver, and on-chip capacitors. The system achieves continuous glucose monitoring from 0.05 to 1 mM with 0.18 $A{\cdot}mm{\cdot}mM^{-1}$ sensitivity and 400 $Hz{\cdot}mM^{-1}$ resolution, eliminating external components through monolithic integration. The system operates at a regulated supply voltage of 1.2 V and consumes only 3 μW of power. As illustrated in Figure 12d, a wireless health monitoring concept based on an active contact lens is proposed, integrating a glucose sensor, loop antenna, communication interface, and readout circuitry onto a flexible polymer lens substrate. The contact lens-integrated glucose sensor wirelessly transmits tear analyte data to an NFC-enabled mobile-integrated platform, demonstrating potential for point-of-care diagnostics. Figure 12e details the electrochemical cell architecture: concentric ring topology for working (50 μm width) and counter (75 μm width) electrodes with 50 μm pitch spacing—optimized for reduced interfacial impedance and enhanced sensitivity—alongside a proximal 1.6mm×0.25mm rectangular reference electrode positioned ≤200 μm from the sensing zone. Figure 12f presents the sensor readout architecture.

16163028, 2026, 33, Downloaded from https://advanced.onlinelibrary.wiley.com/doi/10.1002/adfm.202524957 by Nanjing University, Wiley Online Library on [03/11/2026]. See the Terms and Conditions (https://onlinelibrary.wiley.com/terms-and-conditions) on Wiley Online Library for rules of use; OA articles are governed by the applicable Creative Commons License

The IC incorporates a power management unit, readout circuitry, a wireless interface, an LED driver, and on-chip capacitive energy storage within a compact 0.36 mm^2 CMOS chip, eliminating the need for any external components such as crystals, inductors, capacitors, or batteries. The system is wirelessly powered via RF energy harvested from an external interrogator. Key design challenges in RF power-harvesting ICs include the co-design of an efficient rectifier with a low-power voltage regulator (LPVR), as well as ensuring sufficient on-chip capacitance to support energy buffering. Fabricated in 0.13 μm CMOS, the integrated system (Figure 12g) occupies 0.36 mm^2 silicon area while implementing these functional blocks.

Chen et al. [171] introduced the development of a syringe-implantable electrocardiography (ECG) monitoring system optimized for ultralow-power operation and high measurement accuracy. The analog front-end (AFE) incorporates noise optimization techniques and advanced circuit design, achieving a remarkably low current consumption of 31 nA. Complementing the AFE, the digital back end employs a minimum-energy computation strategy, reducing digital energy consumption by approximately 40%. The proposed SoC, implemented in a 65 nm CMOS process, consumes only 64 nW of power. Functional validation was carried out through ECG simulation, in vivo experiments in live sheep, and ex vivo testing on isolated sheep hearts, confirming the system's capability to accurately detect atrial fibrillation and record associated arrhythmic waveforms. The effectiveness of the system in achieving both low power consumption and reliable arrhythmia detection is significantly influenced by the efficiency of its embedded algorithms. The system architecture comprises analog signal acquisition and digital back-end modules. Bioelectrical signals are acquired through electrodes and processed via an AFE, which includes filtering, amplification, and digitization stages. The dedicated digital signal processing (DSP) module executes an in-depth analysis of the waveform over a 10-s interval, enabling the precise identification and classification of anomalous cardiac events. Upon detection of an anomaly, the device stores the corresponding downsampled (by a factor of 10) 10-s waveform segment in on-chip memory. This recorded data can later be transmitted to an external device via a wireless transceiver for further clinical evaluation. As shown in Figure 12h,i, the system integrates an ultralow-power AFE consisting of an LNA, VGA, and SAR ADC operating at 0.6 V, and supports interfacing with other low-power sensor nodes. Except for the ADC's clocked comparator, all blocks operate in the subthreshold region to reduce power and improve efficiency. A chip microphotograph is provided in Figure 12j.

3.3 | Implantable Microbatteries

The emergence of microscale electronic systems has revolutionized wearable medical device design through functional miniaturization, leading to the realization of advanced, personalized, and highly integrated healthcare solutions—such as biosensing and diagnostics—but has also catalyzed significant advancements in the domain of implantable biomedical electronics. Since their introduction, implantable bioelectronic devices have been deployed across a wide array of applications, ranging from symptom mitigation in chronic diseases (e.g., Parkinson's disease), functional restoration of impaired physiological processes (e.g., auditory rehabilitation via cochlear implants), to real-time metabolic monitoring through integrated sensor technologies. These developments hold substantial promises for revolutionizing healthcare delivery and significantly enhancing the quality of patient care.

Enhancing quality of life depends on the development of fully compliant, personalized, advanced healthcare electronic systems. A key enabler of such systems is a physically flexible, high-performance, and biocompatible battery that can reliably power devices while conforming to the complex contours of the human body. Such batteries must also withstand mechanical deformations without sacrificing performance or safety. However, current options fail to simultaneously meet all these criteria, and there is an absence of effective integration strategies for incorporating these components into complex architectures, such as those found in orthodontic applications within the human body. Kutbee et al. [43] demonstrated a mechanically flexible lithium-ion MB with a mass of just 236 μg, exhibiting a remarkable volumetric energy density of 200 $mWh{\cdot}cm^{-3}$ following 120 cycles of continuous operation. Biocompatibility assessments revealed a 90% cell viability rate, confirming the battery's compatibility with biological environments. Furthermore, the study showcases the successful incorporation of this battery into an optoelectronic system integrated within a 3D-printed smart dental brace. This novel orthodontic system marks a substantial advancement in personalized healthcare, with promising applications in accelerating bone regeneration and enhancing enamel protection, thereby contributing to a reduction in overall healthcare expenditure. All-solid-state battery materials are essential for realizing biocompatibility and thermal endurance up to 90°C, thereby ensuring device safety and reliability in implanted or wearable configurations. As shown in Figure 13a,b, this enables efficient integration of an optoelectronic system based on a chip-scale battery and NIR-LED arrays with a 1.8 V turn-on voltage and 640 nm emission. Integrated into a 3D-printed dental brace, the system forms a wearable phototherapy device. The battery exhibits a volumetric energy density of 200 mWh cm^{-3}, retaining this performance after 120 charge–discharge cycles, thus indicating exceptional electrochemical stability. Cell viability tests conducted on the battery surface suggest the potential for developing biocompatible energy storage solutions. This prospect appears feasible even for lithium-based systems, provided they are adequately encapsulated.

Moreover, a fully hydrogel-based flexible MB has been demonstrated, compatible with both lithium-ion and zinc-ion chemistries. This development significantly broadens the design space for biocompatible and wearable power sources. Miniaturized energy storage devices offering high energy output and biocompatibility are poised to significantly advance eco-friendly, safe, and nontoxic in vivo diagnostics and therapeutic methods. Such technologies are particularly promising for applications like non-invasive monitoring or interventions within the gastrointestinal tract, where significant technical challenges persist. Chen et al. [172] reported the development of an ingestible zinc-ion hybrid micro-supercapacitor (ZMSC) designed to supply electrical energy as well as nutritional ions. The device incorporates an edible activated carbon microcathode and a zinc microanode and is housed within a standard-sized capsule to enable safe oral administration and targeted

16163028, 2026, 33, Downloaded from https://advanced.onlinelibrary.wiley.com/doi/10.1002/adfm.202524957 by Nanjing University, Wiley Online Library on [03/11/2026]. See the Terms and Conditions (https://onlinelibrary.wiley.com/terms-and-conditions) on Wiley Online Library for rules of use; OA articles are governed by the applicable Creative Commons License

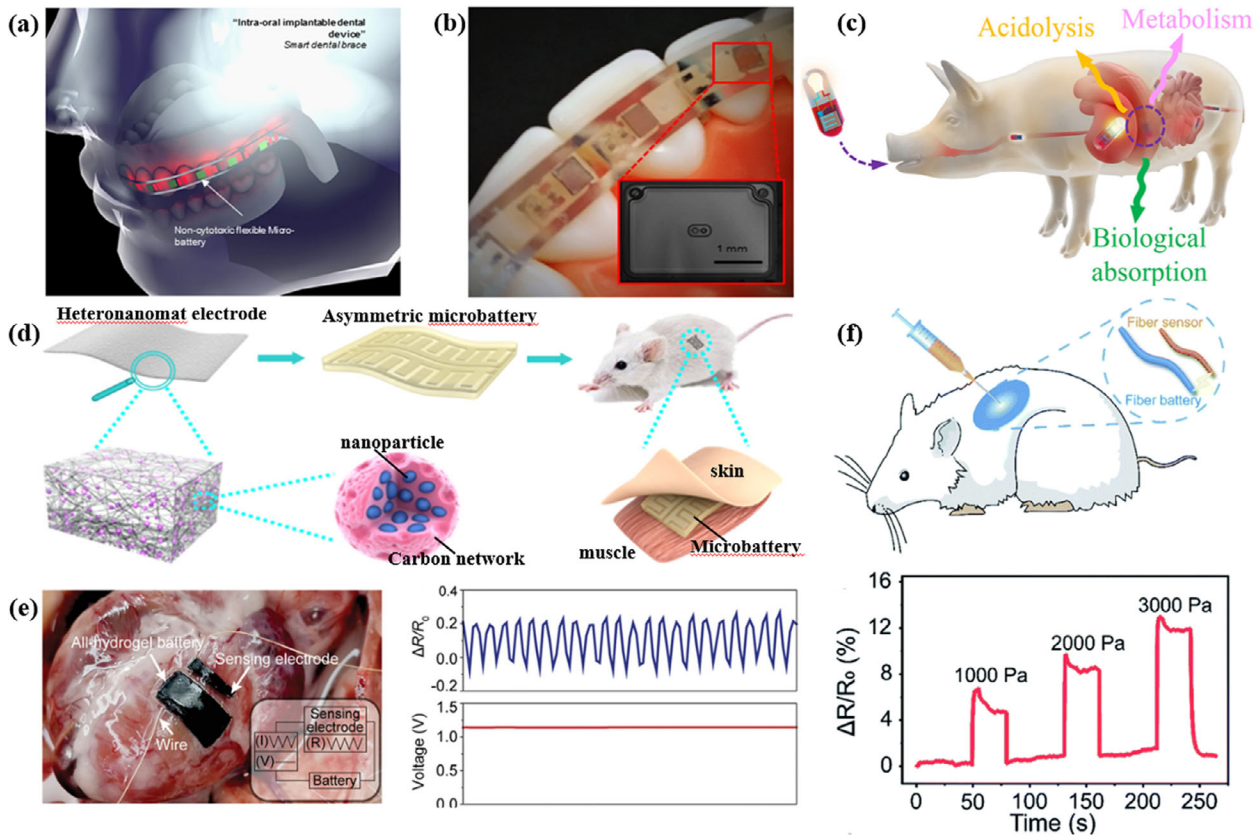


FIGURE 13 | (a) Biocompatible deformable energy storage system enabling conformal integration of intraoral phototherapeutic platforms with anatomical curvature-adaptive adhesion to dental arches. (b) Optical images of an intra-oral implantable device utilizing a millimeter-sized, flexible, biocompatible lithium-ion battery as a rapid power source. Reproduced with permission [43]. Copyright 2017, Springer Nature. (c) A nutritive and edible zinc-ion MB featuring high energy density. Reproduced with permission [172]. Copyright 2022, American Chemical Society. (d) A MB made from biocompatible materials, suitable for direct implantation within the body. Reproduced with permission [173]. Copyright 2018, American Chemical Society. (e) Pressure monitoring. Reproduced with permission [174]. Copyright 2022, Wiley-VCH. (f) Heartbeat monitoring. Reproduced with permission [175]. Copyright 2021, The Royal Society of Chemistry.

deployment in the stomach of a porcine model. (Figure 13c). The microdevice exhibits several advantageous features, including mechanical flexibility, lightweight construction, and shape adaptability. This ZMSC achieves an areal energy density of 215.1 μWh cm^{-2} and an areal capacitance of 605 mF cm^{-2} at 1.8 V, outperforming commercial button batteries and other biocompatible SCs/MSCs. In vitro and in vivo studies confirm its biocompatibility and safety. The device can directly power on-board electronics in the porcine stomach without voltage boosting, while also providing zinc nutrient supplementation.

Furthermore, during the discharging process, these devices exhibit potent antibacterial activity against Escherichia coli. The growing global life expectancy has accelerated the development of implantable bioelectronic devices aimed at improving long-term healthcare outcomes. However, the reliance on traditional battery technologies—marked by limited cycle life, rigid physical structures, and suboptimal energy density—continues to be a significant obstacle to attaining reliable, safe, and efficient performance in the intricate physiological setting of the human body. To address these limitations, Zhang et al. [173] developed a novel flexible symmetric sodium-ion MB utilizing heteronanomat electrodes and biocompatible electrolytes (Figure 13d). Featuring a spherical-in-network structure, the film electrodes are fabricated using a synergistic combination of electrospinning and electrospraying techniques, followed by carbonization. This approach enables the uniform integration of active material/carbon spheres within a carbon nanofiber matrix, yielding heteronanomat electrodes with enhanced structural integrity, efficient electron and ion transport kinetics, and high mass loading density. The resultant flexible MBs employ interdigitated microelectrode architectures and biocompatible electrolytes, making them promising candidates for powering implantable bioelectronics. A proof-of-concept study demonstrated symmetric sodium-ion MBs using $Na_2VTi(PO_4)_3$-based heteronanomat bifunctional electrodes and biocompatible electrolytes. These systems demonstrate excellent electrochemical reversibility, rapid charge-transfer kinetics, and superior energy density in biocompatible environments, highlighting their outstanding performance characteristics. In addition, long-term in vivo experiments carried out over 30 days in live Sprague–Dawley rats confirmed outstanding capacity retention (>98%) and stable electrochemical performance, demonstrating the device's suitability for prolonged diagnostic operations within physiological environments. This work presents a novel spherical-in-network heteronanomat structure that enhances electrode performance, facilitating the creation of high-energy, biocompatible, and safe power solutions for next-generation implantable bioelectronics.

16163028, 2026, 33, Downloaded from https://advanced.onlinelibrary.wiley.com/doi/10.1002/adfm.202524957 by Nanjing University, Wiley Online Library on [03/11/2026]. See the Terms and Conditions (https://onlinelibrary.wiley.com/terms-and-conditions) on Wiley Online Library for rules of use; OA articles are governed by the applicable Creative Commons License

Dynamic and intricate geometries of biological tissues, while inducing minimal immune responses. This necessitates the development of power sources that possess tissue-mimetic mechanical properties, enabling both conformability and biocompatibility. However, conventional batteries typically lack the required softness due to the high Young's moduli of their materials, including metals, carbon-based materials, conductive polymers, and composite electrodes. Consequently, developing truly tissue-like, soft, and flexible batteries remains a critical challenge in bio-integrated electronics. Ye et al. [174] have demonstrated the first fully ultrasoft batteries constructed entirely from hydrogel-based materials, presenting a promising strategy to address the mechanical mismatch between conventional energy storage systems and soft biological tissues (Figure 13e). These all-hydrogel batteries have Young's moduli as low as 80 kPa, closely matching soft biological tissues. The lithium-ion type offers a specific capacity of 82 mAh g^{-1}, while the zinc-ion variant achieves 370 mAh g^{-1} at 0.5 A g^{-1}. In addition to their excellent electrochemical performance, these devices demonstrate long-term stability and favorable biocompatibility, highlighting their potential for integration into wearable and implantable bioelectronic platforms. The realization of biodegradable, rechargeable, flexible, and safe power sources for in vivo applications has long been a critical unmet need—addressed effectively by this pioneering work. Mei et al. [175] reported the development of a fully biocompatible battery system, consisting of a polydopamine/polypyrrole composite anode, a MnO_2 cathode, and a biodegradable chitosan membrane as the separator. The use of bodily fluids as the electrolyte further ensures biocompatibility and enables safe operation within physiological environments. This design utilizes biodegradable fibrous conductors, enabling minimally invasive implantation and seamless tissue integration with minimal immune response. The device offers a specific capacity of 25.6 mA h g^{-1} and retains 69.1% of its initial capacity after 200 cycles, demonstrating robust electrochemical performance and cycling stability. These features establish its potential as a reliable power source for implantable biomedical devices, as evidenced by the success in vivo powering of biosensors. Upon completion of its operational lifetime, the battery undergoes complete biodegradation, thereby eliminating the need for surgical retrieval. To illustrate its practical applicability, the fiber-shaped battery was integrated with a pressure-sensing fiber device to monitor mechanical changes at the implantation site (Figure 13f). Following fulfillment of its power delivery function, the battery degraded as designed through hydrolytic and enzymatic processes. Specifically, the polyglycolic acid, polydopamine, and chitosan components were fully broken down in situ. Implantable MBs are pivotal in advancing biomedical technologies by serving as compact and dependable power sources for neuroprosthetics, cardiac pacemakers, targeted drug delivery systems, and real-time biosensors. The sustained performance and safety of these devices are fundamentally dependent on the biocompatibility and environmental sustainability of their underlying power systems.

3.4 | Integrated Solar Cell and Storage Systems

The synergistic integration of photovoltaic energy harvesting architectures with solid-state electrochemical storage systems has become a critical enabler for overcoming the intrinsic intermittency of renewable sources while meeting next-generation decentralized energy demands. Recent advancements in MB technology, characterized by high energy density architectures and microscale fabrication techniques, present unprecedented opportunities to develop compact, self-sustaining power systems. In 2002, researchers led by Geoffrey at the John Glenn Research Center (USA) introduced the concept of integrating TFB diodes into solar cell panels as a means of offering reverse bias protection for cells affected by shading. This innovative approach was designed to improve the robustness and performance of solar arrays in environments where partial shading is a common issue. Leveraging the foundational idea, researchers at the University of Michigan took a significant step forward in 2010 by developing and documenting the first millimeter-scale energy-autonomous sensor system. This innovative system incorporated stacked TFB diodes alongside photovoltaic (PV) cells, thereby facilitating autonomous operation and eliminating the dependency on external power sources. The breakthrough underscored the potential for fully self-sustaining sensor networks capable of functioning in various operational contexts. Figure 14a illustrates an 8.75 mm^3 sensor platform powered by two 1 mm^2 solar cells arranged in series, coupled with a Cymbet TFB diode, and controlled by an integrated power management unit (PMU). This arrangement ensures optimal energy conversion efficiency while safeguarding the system against potential reverse bias conditions [176]. The functional characteristics of the microsystem are presented in Figure 14b. Fabricated using 1P6M 0.18 μm CMOS technology, the integrated circuitry operates at a nominal voltage of 1.8 V (Figure 14c). To ensure extended system operation and minimize energy consumption during idle periods, the architecture incorporates ultralow-power sleep modes. In the active state, the TFB supplies the necessary power, as the on-chip solar cells fail to deliver the required microwatt-level output. Conversely, during low-power sleep mode, the TFB is replenished by harvesting ambient light indoors or outdoors. The system's energy-autonomous performance across alternating cycles of activity and dormancy is confirmed by experimental monitoring of battery voltage and charge/discharge currents.

Kuriyama et al. [177] propose an integrated emergency power supply solution—referred to as a micro uninterruptible power supply (μUPS)—by on-chip integration of a rechargeable energy storage device to overcome the intermittent power delivery limitations of PV cells. Integral to the μUPS architecture, the authors present comprehensive details regarding the fabrication process and electrical characterization of series-connected TFBs. Under illumination, the series-connected photovoltaic (PV) cells fulfill a dual function: generating multiple voltage rails to power the microsystem and concurrently recharging the on-chip battery. In the case of partial shading or a complete power outage, the stored energy within the battery is automatically utilized to maintain system operation, thereby ensuring continuous functionality and enhancing overall operational robustness. The proposed design is compatible with CMOS-MEMS post-processing techniques used for fabricating series-connected PV cells. In their implementation, fourteen series-connected battery cells were realized, achieving a total output voltage of 51.3 V. This demonstrates the feasibility and effectiveness of integrating a μUPS system to ensure reliable power delivery in PV-powered applications. Among various energy harvesting sources, PV cells are particularly promising due to their relatively high-power output—solar irradiance provides approximately 100 mW cm^{-2}

16163028, 2026, 33, Downloaded from https://advanced.onlinelibrary.wiley.com/doi/10.1002/adfm.202524957 by Nanjing University, Wiley Online Library on [03/11/2026]. See the Terms and Conditions (https://onlinelibrary.wiley.com/terms-and-conditions) on Wiley Online Library for rules of use; OA articles are governed by the applicable Creative Commons License

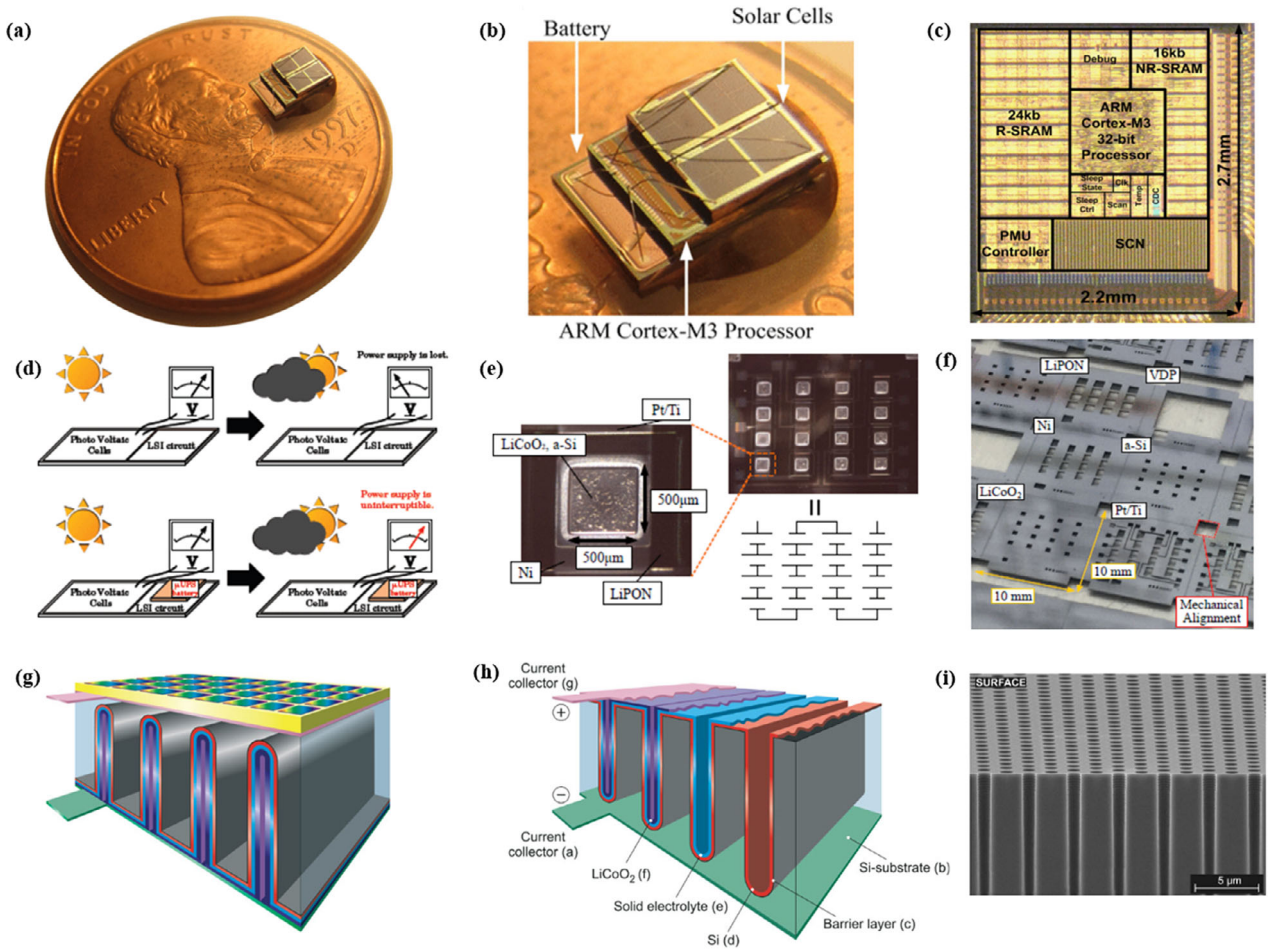


FIGURE 14 | (a,b) System overview and waveforms of a near-perpetual sensor with integrated solar cells, TFB, and microprocessor. (c) Chip micrograph. Reproduced with permission [176]. Copyright 2013, IEEE. (d) Comparison of monolithic integration: photovoltaic cells and LSI circuits are shown without TFBs (top) and with TFBs (bottom). (e) Schematic of a 16-series-connected battery arrangement and its equivalent circuit. (f) Shadow mask utilized for patterning thin-film battery layers. Alignment is accomplished mechanically by aligning holes in the mask with pins on the substrate. Reproduced with permission [177]. Copyright 2018, IEEE. (g) Schematic illustration of the integration between a Si solar cell and a 3D TFB. (h) Schematic of a 3D-integrated all-solid-state Li-ion battery, featuring surface area enlargement achieved through electrochemical or reactive ion etching (RIE) of the silicon substrate. (i) Holes etched into a single-crystalline silicon substrate. Reproduced with permission [44]. Copyright 2007, Wiley-VCH.

under standard conditions. When configured in series, PV cells are capable of generating output voltages exceeding 10 V, while simultaneously supplying multiple voltage levels from a single chip. This capability enables the co-integration of LSIs, sensors, and MEMS actuators with diverse voltage requirements on a unified platform. However, the power output of such harvesters is inherently susceptible to environmental variations, such as solar irradiance fluctuations caused by cloud-induced shading, as illustrated in Figure 14d. To address this instability, we propose the on-chip integration of an emergency power supply in the form of a μUPS. Under illumination, the series-connected PV cells supply multiple voltage levels directly to the system while simultaneously charging the on-chip battery. In the event of shading or reduced light intensity, the stored energy in the battery seamlessly supports continuous system operation. Figure 14e demonstrates a series-connected array of 16 micro-batteries (500×500 μm^2 unit cells) delivering 51.3 V output sufficient for MEMS actuation, while Figure 14f details DRIE-fabricated 200 μm-thick Si shadow masks with corner-alignment apertures for precision substrate registration.

Recent advances in self-sustaining microsystems leverage heterogeneous integration of TFBs with cross-domain functional modules—encompassing energy harvesting components and multi-physics sensing elements—to enable next-generation autonomous devices. These integrated solutions improve energy efficiency and extend device functionality. Figure 14g illustrates a schematic of an integrated system proposed by Notten et al. [44], which combines a Si-solar cell with a 3D TFB. The engineered self-sustaining microsystem architecture targets next-generation autonomous platforms through symbiotic integration of energy harvesting and storage modalities, addressing dynamic cross-domain power requirements. A novel all-solid-state, three-dimensionally integrated battery architecture has been developed by capitalizing on the superior lithium intercalation behavior of thin-film silicon electrodes. As depicted in Figure 14h, the concept is based on a unique structural design that maximizes volumetric efficiency. Figure 14i showcases representative trench and hole structures fabricated via Reactive Ion Etching (RIE), achieving a significant surface area enhancement—up to 25-fold. The conformal coating of functional layers within these

16163028, 2026, 33, Downloaded from https://advanced.onlinelibrary.wiley.com/doi/10.1002/adfm.202524957 by Nanjing University, Wiley Online Library on [03/11/2026]. See the Terms and Conditions (https://onlinelibrary.wiley.com/terms-and-conditions) on Wiley Online Library for rules of use; OA articles are governed by the applicable Creative Commons License

high-aspect-ratio geometries is accomplished using Low-Pressure Chemical Vapor Deposition (LPCVD), which ensures uniform coverage and enhances overall device performance. The choice of energy harvesting or transduction element—such as solar cells for light energy, piezoelectric devices for mechanical pressure, or thermoelectric generators for thermal gradients—is dictated by the available energy source. Efficient storage of the harvested energy is essential for sustained system operation. However, conventional batteries and supercapacitors often exhibit poor integration compatibility with miniaturized energy conversion platforms. As a result, TFBs represent the most promising energy storage solution for highly integrated, multifunctional microsystems.

3.5 | On-Chip Integration

The convergence of monolithically integrated transparent modules—an electrochemical storage unit, signal processing elements, and photon detection components—into a unified microsystem architecture establishes unprecedented multidimensional functionality in transparent electronics. This integration strategy enables advanced functionalities while maintaining optical transparency. Jia et al. [178] explore the use of indium gallium zinc oxide (InGaZnO) for fabricating these devices and the integrated system, leveraging its versatile multifunctional properties. A transparent lithium-ion battery utilizing InGaZnO as the anode material has been developed, delivering a specific capacity of approximately 9.8 μAh cm^{-2}. This battery serves as an on-chip power source, providing both transparency and energy storage capability. A thin-film transistor with InGaZnO as the channel showed a mobility of ~23.3 cm^2 V^{-1} s^{-1}, and a photodetector using the same material achieved a responsivity of ~0.35 A W^{-1}. All components were integrated on a common substrate to form a transparent microsystem. The TFT functions as a rectifier for AC signal conversion and energy storage in the battery, and the photodetector operates efficiently when powered by the battery, demonstrating full system functionality. The integrated transparent microsystem architecture is shown in Figure 15a, with Figure 15b presenting its equivalent circuit model that details electrical connectivity and operational mechanisms. The fabricated device (Figure 15c) employs indium tin oxide (ITO) interconnects to simultaneously achieve optical transparency and electrical conductivity. In light of the imperative to develop alternatives to traditional LIBs, significant attention has been directed toward the exploration of innovative chemistries and advanced fabrication methodologies for solid-state lithium-ion conductors. Historically, such materials have been produced in the form of millimeter-scale pellets utilizing conventional ceramic processing techniques.

However, thin-film lithium-ion conductors transcend conventional energy storage paradigms, enabling solid-state iontronic applications in neuromorphic engineering, memristive computing, and adaptive sensing architectures. Zhu et al. [179] systematically investigated the chemical properties and thin-film processing techniques of lithium oxides, exploring both the challenges and opportunities associated with their integration into MBs for energy storage, neuromorphic devices capable of emulating human brain functions, and sensors designed for the detection of toxic substances and greenhouse gases (Figure 15d). In two-terminal systems, a variety of switching mechanisms have been observed (Figure 15e,f), ranging from filamentary-like to more homogeneous processes. For instance, devices based on $LixCoO_2$ layered compounds exhibit a stochastic and poorly controlled exchange mechanism with Si electrodes. This behavior underscores the necessity for further research aimed at reducing switching variability and operation voltage, as well as enhancing switching speed. Layered materials featuring two-dimensional lithium migration pathways may also suffer from inherently anisotropic ionic transport, which can limit their performance in practical applications. Nonetheless, the resistive switching characteristics observed in $LixCoO_2$-based devices have generated significant interest in lithium-based memristive technologies for next-generation electronic systems. The electrochemical characteristics of $Li_{4+3X}Ti_5O_{12}$—a benchmark anode material—originate from its Li-concentration-dependent permittivity and the inherent $Li_4Ti_5O_{12}$(insulator)/$Li_7Ti_5O_{12}$(metal) miscibility gap, which drives spontaneous phase separation. This decomposition process, governed by electrical bias-mediated shifts in spinodal/binodal boundaries, enables dynamic control of the device's macroscopic conductivity through spatial phase redistribution. Miskin et al. [45] developed CMOS-compatible electrochemical actuators operating at record-low voltages (≥200 μV) and power consumption (≥10 nW) through voltage-gated ion intercalation mechanisms, achieving full integration with conventional semiconductor foundry processes. To showcase their functionality and potential applications in microscale robotics, lithographic patterning and release techniques were employed to fabricate sub-100 μm walking robotic prototypes. Each step of the fabrication process is executed in parallel, facilitating the batch production of over one million microscale robots from a single four-inch wafer. These findings represent a significant milestone toward the scalable manufacturing of functional, silicon-based microrobots that are not visible to the naked eye. Figure 15g presents an optical image of a microscopic robot still anchored to its substrate, with all constituent components fabricated simultaneously through the same monolithic process. A close-up view of a chip segment containing thousands of such microrobots on a diced wafer is shown in Figure 15h. Figure 15i quantifies the robot's motion dynamics, showing peak/average velocities of 30 and 1 μm s^{-1}, respectively, translating to ~1 body length/min locomotion.

The primary objective of MB research is to enable the operation of microelectronic devices (MEDs) and, ultimately, to advance the realization of the IoT. To meet this goal, MBs must satisfy two key requirements. First, their physical dimensions should be compatible with those of the targeted MEDs. Second, their energy and power output must be appropriately matched to the operational needs of the associated devices. The specific quantitative requirements for various IoT-related applications in terms of MB performance are summarized in Table 2.

4 | Prospect

MBs have emerged as a cornerstone technology for the next generation of miniaturized electronic devices, owing to their exceptional capability to deliver high energy densities within

16163028, 2026, 33, Downloaded from https://advanced.onlinelibrary.wiley.com/doi/10.1002/adfm.202524957 by Nanjing University, Wiley Online Library on [03/11/2026]. See the Terms and Conditions (https://onlinelibrary.wiley.com/terms-and-conditions) on Wiley Online Library for rules of use; OA articles are governed by the applicable Creative Commons License

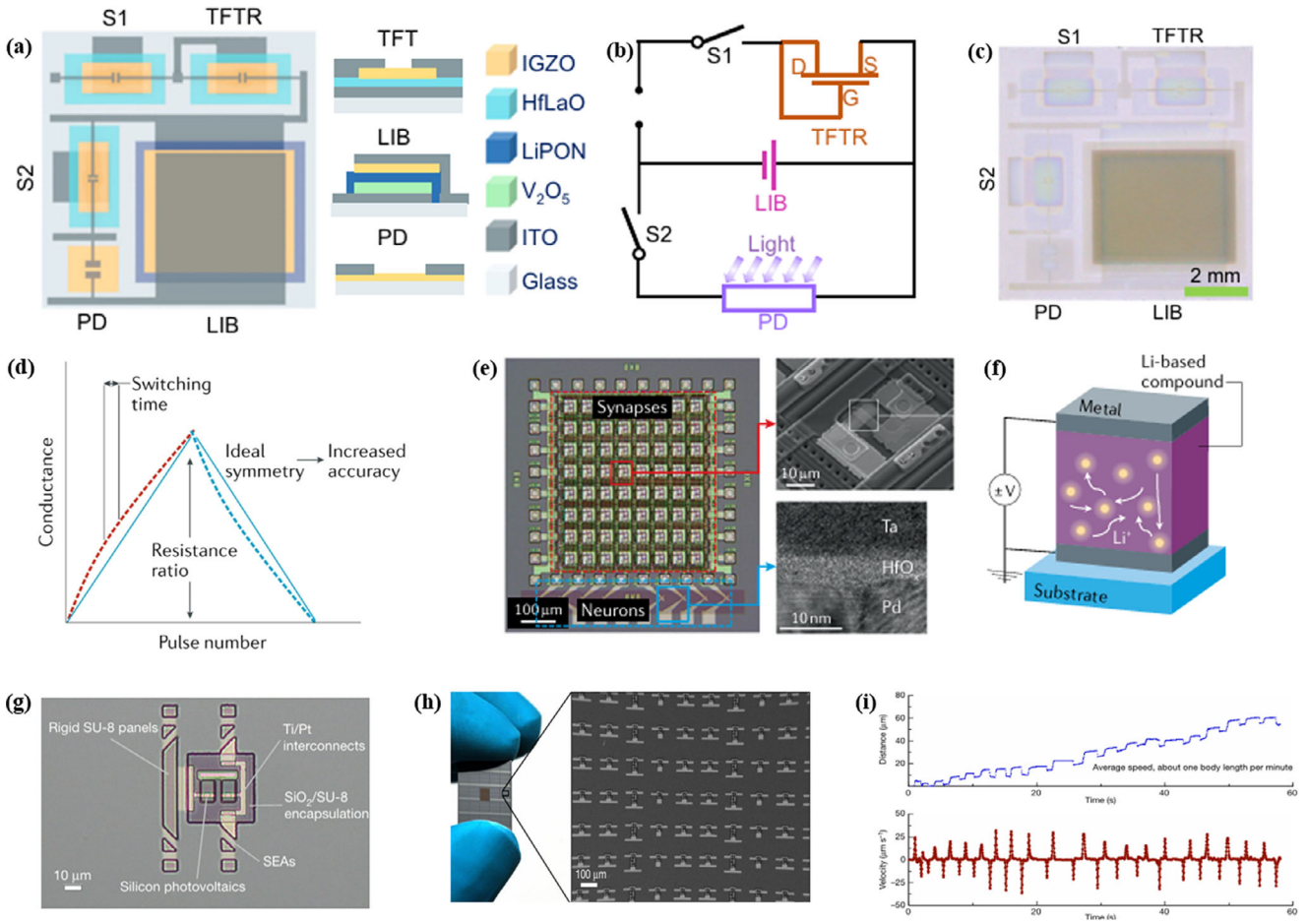


FIGURE 15 | (a) Schematic representations depicting the integrated microsystem design with constituent elements. (b) Electro-functional equivalent circuit representation for the integrated microsystem. (c) Macro-scale photographs of the packaged microsystem device with interface ports. Reproduced with permission [178]. Copyright 2023, Springer Nature. (d) Memristive synaptic fidelity is governed by three pivotal characteristics: switching velocity, resistance contrast magnitude, and potentiation–depression symmetry, collectively determining neuromorphic operational precision. Reproduced with permission [179]. Copyright 2021, Springer Nature. (e) Artificial neural network based on memristors. Reproduced with permission [187]. Copyright 2018, Springer Nature. (f) Two-terminal Li-based memristive device. (g) Pseudocolor-enhanced microscopy image showing the micro-robot's functional segmentation-control core versus propulsion actuators. (h) Optical micrograph of a die segment diced from a 100-mm wafer, demonstrating 10^3-scale micro-robot integration within the original 10^6-unit wafer-scale array. (i) Top: Displacement of the robot's center of mass over time, measured relative to a fixed reference point. Bottom: Corresponding instantaneous velocity obtained by numerical differentiation of the displacement data. Peak speeds of up to 30 μm s^{-1} are observed. Reproduced with permission [45]. Copyright 2020, Springer Nature.

TABLE 2 | Energy and power specifications of MBs for diverse applications.

Application domain	Power range	Energy density	Refs.
Wearable Electronics	1–10 mW	~200–500 Wh/L	[180]
	0.1–5 mW(Avg.)	~200–500 Wh/L	[181]
Implantable Medical Devices	10–100μW(Avg.)	~1000 Wh/L	[182]
Wireless Sensor Nodes	10 μW – 1 mW	N/A	[183]
Energy Storage & Harvesting	1 – 100 mW	~200–500 Wh/L	[184]
	~1 – 100 μW/cm^2	~1 – 100 μW/cm^2	[185]
	~0.001–1 μW/cm^2	~0.001–1μW/cm^2	[186]

16163028, 2026, 33, Downloaded from https://advanced.onlinelibrary.wiley.com/doi/10.1002/adfm.202524957 by Nanjing University, Wiley Online Library on [03/11/2026]. See the Terms and Conditions (https://onlinelibrary.wiley.com/terms-and-conditions) on Wiley Online Library for rules of use; OA articles are governed by the applicable Creative Commons License

ultra-compact form factors. Over the past decade, significant advancements in materials science and micro/nanofabrication technologies have facilitated the transition of MBs designs from conventional thin-film architectures to more sophisticated 3D configurations. Initial iterations, such as lithium-based thin-film batteries, established the foundation for scalable integration but were constrained by limitations in energy density and mechanical flexibility. Subsequent innovations, including the utilization of nanowire-structured electrodes and solid-state electrolytes, have dramatically improved capacity retention and cycle stability, enabling MBs to function reliably under conditions of dynamic mechanical stress and extreme temperatures. In integrated systems, MBs now serve as an indispensable component of self-sustaining microelectronics. For example, their synergy with energy harvesters, such as perovskite solar cells, facilitates uninterrupted power delivery for IoT nodes. Moreover, bioresorbable MBs are revolutionizing implantable medical devices by offering transient energy solutions while minimizing biological impact. Additionally, the incorporation of MBs into flexible and stretchable substrates has spurred significant advancements in wearable health monitors and electronic skins, where attributes like energy autonomy and mechanical compliance are paramount.

Nevertheless, despite substantial progress, several unresolved challenges continue to constrain the full potential of MBs in highly integrated systems. Material-level constraints, such as interfacial instability between solid-state electrolytes and electrodes, persistently hinder long-term cyclability. The trade-offs inherent in structural design between energy density and mechanical flexibility demand further optimization, especially for applications requiring extreme deformations (>200% strain). At the system-integration level, the co-design of MBs alongside multifunctional electronics necessitates breakthroughs in thermal management and cross-material compatibility. Thermal expansion mismatches between silicon-based circuits and battery materials can lead to mechanical delamination, thereby degrading performance in on-chip configurations. Furthermore, the development of adaptive power management algorithms is essential to optimize energy flow among MBs, energy harvesters, and ultralow-power sensors, ensuring peak efficiency across a wide range of operational scenarios.

The evolution of MBs manufacturing processes is poised to undergo a paradigm shift, moving beyond mere miniaturization toward intelligent, precision engineering of materials and architectures at the micro and nanoscale. This progression will be pivotal in unlocking their full potential for next-generation integrated systems. The frontier of future MB manufacturing is poised to evolve synergistically along three core dimensions. First, advanced techniques such as precision additive printing (e.g., electrochemical 3D printing) and atomic-level subtractive etching (e.g., atomic layer etching) will enable nanoscale-precision control over the spatial distribution and loading of active cathode/anode materials [188–191]. This allows for the programmable design of overall battery capacity and interfacial properties. Second, the manufacturing scale will advance further from the microscale to the nanoscale. Utilizing nanoscale templating and self-assembly techniques, three-dimensional ordered architectures integrating electrodes and electrolytes will be constructed directly at the nanoscale, fundamentally enhancing ion transport kinetics and material utilization efficiency. Ultimately, these processes will achieve deep convergence with back-end-of-line microelectronic fabrication. By developing fully low-temperature, highly compatible thin-film process packages, wafer-level monolithic integration of MBs onto sensors, processors, and other chips will be realized. This integration builds "plug-and-play" miniaturized on-chip energy systems, a technical pathway aimed at addressing the fundamental challenges of capacity, power, and system integration for MBs at the manufacturing **source**.

Within the precision manufacturing strategy for microbatteries, additive and subtractive processes will function in a complementary manner. Additive techniques, such as next-generation electrochemical 3D printing, will enable the sub-micron-scale in situ heterogeneous printing of cathode, anode, and solid electrolyte materials. This allows for the programmable construction of three-dimensional architectures with pre-designed capacity. Concurrently, subtractive techniques like atomic layer etching can be employed for the selective removal or modification of electrode films at the single-atomic-layer level, thereby achieving precise control over their thickness, porosity, and surface states. The synergistic combination of these approaches ultimately facilitates nanoscale-precision control over the mass, distribution, and interfacial characteristics of active electrode materials, ensuring accurate performance matching at the full-cell level.

The nanoscaling of manufacturing dimensions will propel a fundamental paradigm shift in MBs, transitioning from merely "using nanomaterials" to "constructing at the nanoscale." The core pathway involves first utilizing techniques such as block copolymer self-assembly to create highly ordered nano-templates. Subsequently, methods like atomic layer deposition are employed to conformally construct integrated three-dimensional nano-architectures of electrodes and electrolytes within these templates, thereby intrinsically enhancing electrochemical performance. To achieve system integration, cross-scale heterogeneous integration technologies, such as nano-transfer printing, are further required. These techniques enable the precise transfer and interconnection of the aforementioned nano-functional units onto microscale system circuits, ultimately accomplishing the reliable manufacturing of macroscopic functional devices from nano-active structures.

Envisioning the future, the advancement of MBs will be guided by several critical trends to address the escalating demands of innovative applications. (1) Primarily, the imperative for miniaturization necessitates not only a reduction in physical dimensions while preserving or augmenting energy density but also entails meticulous refinements in manufacturing methodologies. (2) Second, nanotechnology is poised to be instrumental in the evolution of MBs. By exploiting the distinctive attributes of nanomaterials, significant enhancements can be achieved in electrode performance and electrolyte stability, paving novel avenues for high-performance MBs configurations. (3) Thirdly, enhancing the efficacy of MBs hinges on the development of high-specific-energy materials alongside pioneering structural designs. Leveraging artificial intelligence (AI)-facilitated material screening and performance optimization processes can expedite this progression, ensuring optimal congruence between selected

16163028, 2026, 33, Downloaded from https://advanced.onlinelibrary.wiley.com/doi/10.1002/adfm.202524957 by Nanjing University, Wiley Online Library on [03/11/2026]. See the Terms and Conditions (https://onlinelibrary.wiley.com/terms-and-conditions) on Wiley Online Library for rules of use; OA articles are governed by the applicable Creative Commons License

materials and architectural designs. This synergy effectively elevates overall battery performance. Particularly, flexible nanowire-based MBs and their integrated systems have demonstrated substantial potential in state-of-the-art applications such as active wireless high-definition stretchable displays, where superior flexibility and adaptability are paramount. (4) Last, the increasing complexity of electronic devices mandates the trend toward high-density integration. Employing advanced packaging technologies and 3D integration strategies facilitates the incorporation of multifunctional components within confined spaces, thereby enhancing system efficiency and reliability. In conclusion, the convergence of these four pivotal research domains—miniaturization, nanotechnology application, performance enhancement, and high-density integration—will collectively propel the field of MBs technology to unprecedented levels, catering to the diverse requirements of an intelligent and interconnected future. Interdisciplinary collaboration and application-oriented research and development remain indispensable to fully actualizing the latent potential of MBs.

Acknowledgements

The authors acknowledge the National Natural Science Foundation of China for Distinguished Young Scholars No. 62325403, the National Natural Science Foundation of China (62504103), Natural Science Foundation of Jiangsu Province (BK20230498 and BK20251214), and Jiangsu Funding Program for Excellent Postdoctoral Talent (2024ZB427). The China Postdoctoral Science Foundation under Grant Numbers 2025T180143 and 2025M770547.

Conflicts of Interest

The authors declare no conflicts of interest.

Data Availability Statement

No primary research results, software, or codes have been included, and no new data were generated or analyzed as part of this review.

References

1. H. Tang, Y. Yin, Y. Huang, et al., "Battery-Everywhere Design Based on a Cathodeless Configuration With High Sustainability and Energy Density," *ACS Energy Letters* 6, no. 5 (2021): 1859–1868, https://doi.org/10.1021/acsenergylett.1c00555.

2. F. L. Cras, B. Pecquenard, V. Dubois, V. Phan, and D. Guy-Bouyssou, "All-Solid-State Lithium-Ion Microbatteries Using Silicon Nanofilm Anodes: High Performance and Memory Effect," *Advanced Energy Materials* 5, no. 19 (2015): 1501061, https://doi.org/10.1002/aenm.201501061.

3. J. H. Pikul and H. Ning, "Powering the Internet of Things," *Joule* 2, no. 6 (2018): 1036–1038, https://doi.org/10.1016/j.joule.2018.06.005.

4. H. Hassanin, G. Sheikholeslami, P. Sareh, and R. B. Ishaq, "Microadditive Manufacturing Technologies of 3D Microelectromechanical Systems," *Advanced Engineering Materials* 23, no. 12 (2021): 2100422, https://doi.org/10.1002/adem.202100422.

5. X. Mei, D. Ye, F. Zhang, and C. Di, "Implantable Application of Polymer-Based Biosensors," *Journal of Polymer Science* 60, no. 3 (2022): 328–347, https://doi.org/10.1002/pol.20210543.

6. K. Suresh, V. Jeoti, S. Soeung, M. Drieberg, M. Goh, and M. Z. Aslam, "A Comparative Survey on Silicon Based and Surface Acoustic Wave (SAW)-Based RFID Tags: Potentials, Challenges, and Future Directions," *IEEE Access* 8 (2020): 91624–91647, https://doi.org/10.1109/ACCESS.2020.2976533.

7. S. Wang, J. Liu, X. Song, and H. Xu, "Failure Mechanisms and Design Strategies for Low-Temperature Solid-State Metal Batteries," *Journal of Materials Chemistry A* 13 (2025): 10388–10414, https://doi.org/10.1039/D4TA07644C.

8. F. Bu, W. Zhou, Y. Xu, Y. Du, C. Guan, and W. Huang, "Recent Developments of Advanced Micro-Supercapacitors: Design, Fabrication and Applications," *NPJ Flexible Electronics* 4, no. 1 (2020): 31, https://doi.org/10.1038/s41528-020-00093-6.

9. H. Zhang, Y. Cao, M. O. L. Chee, P. Dong, M. Ye, and J. Shen, "Recent Advances in Micro-Supercapacitors," *Nanoscale* 11, no. 13 (2019): 5807–5821, https://doi.org/10.1039/C9NR01090D.

10. D. Qi, Y. Liu, Z. Liu, L. Zhang, and X. Chen, "Design of Architectures and Materials in In-Plane Micro-supercapacitors: Current Status and Future Challenges," *Advanced Materials* 29, no. 5 (2017): 1602802, https://doi.org/10.1002/adma.201602802.

11. Z. Zhu, R. Kan, S. Hu, et al., "Recent Advances in High-Performance Microbatteries: Construction, Application, and Perspective," *Small* 16, no. 39 (2020): 2003251, https://doi.org/10.1002/smll.202003251.

12. J. Ni, A. Dai, Y. Yuan, L. Li, and J. Lu, "Three-Dimensional Microbatteries Beyond Lithium Ion," *Matter* 2, no. 6 (2020): 1366–1376, https://doi.org/10.1016/j.matt.2020.04.020.

13. H. Yoo, M. Mahato, W. Oh, et al., "Exploring Role of Microbatteries in Enhancing Sustainability and Functionality of Implantable Biosensors and Bioelectronics," *Biosensors and Bioelectronics* 260 (2024): 116419, https://doi.org/10.1016/j.bios.2024.116419.

14. A. Jetybayeva, A. Umirzakov, B. Uzakbaiuly, Z. Bakenov, and A. Mukanova, "Towards Li–S Microbatteries: A Perspective Review," *Journal of Power Sources* 573 (2023): 233158, https://doi.org/10.1016/j.jpowsour.2023.233158.

15. J. Ma, R. Quhe, W. Zhang, et al., "Zn Microbatteries Explore Ways for Integrations in Intelligent Systems," *Small* 19, no. 26 (2023): 2300230, https://doi.org/10.1002/smll.202300230.

16. M. Moghadami, A. Massoudi, and M. Nangir, "Unveiling the Recent Advances in Micro-Electrode Materials and Configurations for Sodium-Ion Micro-Batteries," *Journal of Materials Chemistry A* 12 (2024): 17923–17957, https://doi.org/10.1039/D4TA02096K.

17. W. Yang, L. Xu, W. Luo, et al., "3D Macroporous Frame Based Microbattery With Ultrahigh Capacity, Energy Density, and Integrability," *Advanced Energy Materials* 13, no. 24 (2023): 2300574, https://doi.org/10.1002/aenm.202300574.

18. Q. Liu, G. Zhang, N. Chen, et al., "The First Flexible Dual-Ion Microbattery Demonstrates Superior Capacity and Ultrahigh Energy Density: Small and Powerful," *Advanced Functional Materials* 30, no. 38 (2020): 2002086, https://doi.org/10.1002/adfm.202002086.

19. N. A. Kyeremateng and R. Hahn, "Attainable Energy Density of Microbatteries," *ACS Energy Letters* 3, no. 5 (2018): 1172–1175, https://doi.org/10.1021/acsenergylett.8b00500.

20. S. Zheng, X. Shi, P. Das, Z. Wu, and X. Bao, "The Road Towards Planar Microbatteries and Micro-Supercapacitors: From 2D to 3D Device Geometries," *Advanced Materials* 31, no. 50 (2019): 1900583, https://doi.org/10.1002/adma.201900583.

21. J. Ma, S. Zheng, Y. Fu, X. Wang, J. Qin, and Z. Wu, "The Status and Challenging Perspectives of 3D-Printed Micro-Batteries," *Chemical Science* 15, no. 15 (2024): 5451–5481, https://doi.org/10.1039/D3SC06999K.

22. A. Alsubhi, R. G. Anaraky, S. Babatunde, et al., "User-Centered Perspectives on the Design of Batteryless Wearables," *International Journal of Human–Computer Interaction* 40, no. 23 (2024): 8025–8046, https://doi.org/10.1080/10447318.2023.2276528.

23. K. Han, D. Zhang, W. Zhuang, Y. Wan, and P. Yang, "Integrated Multimodal Microfluidic E-Skin Powered by Synergistic Tandem Nanogenerators for Sweat-Based Health Monitoring and Skin-Temperature

16163028, 2026, 33, Downloaded from https://advanced.onlinelibrary.wiley.com/doi/10.1002/adfm.202524957 by Nanjing University, Wiley Online Library on [03/11/2026]. See the Terms and Conditions (https://onlinelibrary.wiley.com/terms-and-conditions) on Wiley Online Library for rules of use; OA articles are governed by the applicable Creative Commons License

Analysis," *Journal of Materials Chemistry A* 11, no. 32 (2023): 17112–17124, https://doi.org/10.1039/D3TA01755A.

24. X. Song, Y. Gu, S. Wang, and J. Wang, "Nanowire-Based Flexible Sensors for Wearable Electronics, Brain–Computer Interfaces, and Artificial Skins," *Electron* 3, no. 2 (2025): 77, https://doi.org/10.1002/elt2.77.

25. J. Li, Y. Dong, J. H. Park, and J. Yoo, "Body-Coupled Power Transmission and Energy Harvesting," *Nature Electronics* 4, no. 7 (2021): 530–538, https://doi.org/10.1038/s41928-021-00592-y.

26. A. Shaju, R. Ummer, S. Thomas, and B. Kandasubramanian, "Novel Approaches in 3D Printing Techniques for the Development of High-Performance Micro-Batteries," *Journal of Electronic Materials* (2024): 1–22, https://doi.org/10.1007/s11664-024-11659-9.

27. S. Ferrari, M. Loveridge, S. D. Beattie, M. Jahn, R. J. Dashwood, and R. Bhagat, "Latest Advances in the Manufacturing of 3D Rechargeable Lithium Microbatteries," *Journal of Power Sources* 286 (2015): 25–46, https://doi.org/10.1016/j.jpowsour.2015.03.133.

28. N. Naresh, Y. Zhu, J. Luo, et al., "Advanced 3D Micro-Electrodes for On-Chip Zinc-Ion Micro-Batteries," *Advanced Functional Materials* 35, no. 3 (2025): 2413777, https://doi.org/10.1002/adfm.202413777.

29. L. Deng, Q. Lin, Z. Li, J. Cao, K. Sun, and T. Wei, "Cathodes for Zinc-Ion Micro-Batteries: Challenges, Strategies, and Perspectives," *Batteries* 11, no. 2 (2025): 57, https://doi.org/10.3390/batteries11020057.

30. X. Yue, A. C. Johnson, S. Kim, et al., "A Nearly Packaging-Free Design Paradigm for Light, Powerful, and Energy-Dense Primary Microbatteries," *Advanced Materials* 33, no. 35 (2021): 2101760, https://doi.org/10.1002/adma.202101760.

31. Z. Su, S. Li, L. Ma, et al., "Quenching-Induced Defects Liberate the Latent Reversible Capacity of Lithium Titanate Anode," *Advanced Materials* 35, no. 5 (2023): 2208573, https://doi.org/10.1002/adma.202208573.

32. S. Kim, A. Patra, R. R. Kohlmeyer, et al., "Serially Integrated High-Voltage and High Power Miniature Batteries," *Cell Reports Physical Science* 4, no. 1 (2023): 101205, https://doi.org/10.1016/j.xcrp.2022.101205.

33. P. Dehghanzadeh, J. Huan, R. R. Kalavakonda, S. Mandal, and S. Bhunia, "On-Chip Batteries as Distributed Energy Sources in Heterogeneous 2.5 D/3D Integrated Circuits," *IEEE Access* 11 (2023): 89896–89906, https://doi.org/10.1109/ACCESS.2023.3305593.

34. J. Ni, X. Zhu, Y. Yuan, et al., "Rooting Binder-Free Tin Nanoarrays Into Copper Substrate via Tin-Copper Alloying for Robust Energy Storage," *Nature Communications* 11, no. 1 (2020): 1212, https://doi.org/10.1038/s41467-020-15045-x.

35. J. Ni, X. Li, M. Sun, et al., "Durian-Inspired Design of Bismuth–Antimony Alloy Arrays for Robust Sodium Storage," *ACS Nano* 14, no. 7 (2020): 9117–9124, https://doi.org/10.1021/acsnano.0c04366.

36. Y. Wang, D. Chao, Z. Wang, J. Ni, and L. Li, "An Energetic CuS–Cu Battery System Based on CuS Nanosheet Arrays," *ACS nano* 15, no. 3 (2021): 5420–5427, https://doi.org/10.1021/acsnano.1c00075.

37. A. Armutlulu, Y. Fang, S. H. Kim, C. H. Ji, S. A. Bidstrup Allen, and M. G. Allen, "A MEMS-Enabled 3D Zinc–Air Microbattery With Improved Discharge Characteristics Based on a Multilayer Metallic Substructure," *Journal of Micromechanics and Microengineering* 21, no. 10 (2011): 104011, https://doi.org/10.1088/0960-1317/21/10/104011.

38. S. Zheng, Z. Wu, F. Zhou, et al., "All-Solid-State Planar Integrated Lithium Ion Micro-Batteries With Extraordinary Flexibility and High-Temperature Performance," *Nano Energy* 51 (2018): 613–620, https://doi.org/10.1016/j.nanoen.2018.07.009.

39. X. Pan, X. Hong, L. Xu, Y. Li, M. Yan, and L. Mai, "On-Chip Micro/Nano Devices for Energy Conversion and Storage," *Nano Today* 28 (2019): 100764, https://doi.org/10.1016/j.nantod.2019.100764.

40. A. D. Refino, C. Eldona, R. F. H. Hernandha, et al., "Advances in 3D Silicon-Based Lithium-Ion Microbatteries," *Communications Materials* 5, no. 1 (2024): 22, https://doi.org/10.1038/s43246-024-00459-7.

41. Q. Meng, Y. Huang, L. Li, F. Wu, and R. Chen, "Smart Batteries for Powering the Future," *Joule* 8, no. 2 (2024): 344–373, https://doi.org/10.1016/j.joule.2024.01.011.

42. X. Zhang, M. Lok, T. Tong, et al., "A Fully Integrated Battery-Powered System-on-Chip in 40-nm CMOS for Closed-Loop Control of Insect-Scale Pico-Aerial Vehicle," *IEEE Journal of Solid-State Circuits* 52, no. 9 (2017): 2374–2387, https://doi.org/10.1109/JSSC.2017.2705170.

43. A. Kutbee, R. R. Bahabry, K. Alamoudi, et al., "Flexible and Biocompatible High-Performance Solid-State Micro-Battery for Implantable Orthodontic System," *npj Flexible Electronics* 1, no. 1 (2017): 7, https://doi.org/10.1038/s41528-017-0008-7.

44. P. Notten, F. Roozeboom, R. Niessen, and L. Baggetto, "3-D Integrated All-Solid-State Rechargeable Batteries," *Advanced Materials* 19, no. 24 (2007): 4564–4567, https://doi.org/10.1002/adma.200702398.

45. M. Z. Miskin, A. J. Cortese, K. Dorsey, et al., "Electronically Integrated, Mass-Manufactured, Microscopic Robots," *Nature* 584, no. 7822 (2020): 557–561, https://doi.org/10.1038/s41586-020-2626-9.

46. Y. Ma, S. Wang, and Z. Wu, "Photolithographic Microfabrication of Microbatteries for On-Chip Energy Storage," *Nano-Micro Letters* 17, no. 1 (2025): 105, https://doi.org/10.1007/s40820-024-01625-9.

47. J. Zhu, W. Hu, J. Ni, and L. Li, "Zinc Micro-Energy Storage Devices Powering Microsystems," *National Science Open* 3, no. 5 (2024): 20230078, https://doi.org/10.1360/nso/20230078.

48. S. Behboudikhiavi, J. O. Omale, B. Babu, L. Piraux, and A. Vlad, "Electrodeposition of Li-Ion Cathode Materials: The Fascinating Alternative for Li-Ion Micro-Batteries Fabrication," *Journal of The Electrochemical Society* 170, no. 2 (2023): 020509, https://doi.org/10.1149/1945-7111/acb6b9.

49. R. Mehek, N. Iqbal, T. Noor, et al., "Metal–Organic Framework Based Electrode Materials for Lithium-Ion Batteries: A Review," *RSC Advances* 11, no. 47 (2021): 29247–29266, https://doi.org/10.1039/D1RA05073G.

50. H. Zhang, Z. Qu, H. Tang, et al., "On-Chip Integration of a Covalent Organic Framework-Based Catalyst Into a Miniaturized Zn–Air Battery With High Energy Density," *ACS Energy Letters* 6, no. 7 (2021): 2491–2498, https://doi.org/10.1021/acsenergylett.1c00768.

51. A. Marincaș and P. Ilea, "Enhancing Lithium Manganese Oxide Electrochemical Behavior by Doping and Surface Modifications," *Coatings* 11, no. 4 (2021): 456, https://doi.org/10.3390/coatings11040456.

52. H. Adenusi, G. A. Chass, S. Passerini, K. V. Tian, and G. Chen, "Lithium Batteries and the Solid Electrolyte Interphase (SEI)—Progress and Outlook," *Advanced Energy Materials* 13, no. 10 (2023): 2203307, https://doi.org/10.1002/aenm.202203307.

53. U. Ulusoy, "A Review of Particle Shape Effects on Material Properties for Various Engineering Applications: From Macro to Nanoscale," *Minerals* 13, no. 1 (2023): 91, https://doi.org/10.3390/min13010091.

54. A. Jandyal, I. Chaturvedi, I. Wazir, A. Raina, and M. I. Ul Haq, "3D printing–A Review of Processes, Materials and Applications in Industry 4.0," *Sustainable Operations and Computers* 3 (2022): 33–42, https://doi.org/10.1016/j.susoc.2021.09.004.

55. J. I. Hur, L. C. Smith, and B. Dunn, "High Areal Energy Density 3D Lithium-Ion Microbatteries," *Joule* 2, no. 6 (2018): 1187–1201, https://doi.org/10.1016/j.joule.2018.04.002.

56. F. Wang, Z. Liu, P. Zhang, et al., "Dual-Graphene Rechargeable Sodium Battery," *Small* 13, no. 47 (2017): 1702449, https://doi.org/10.1002/smll.201702449.

57. M. Koo, K. Park, S. H. Lee, et al., "Bendable Inorganic Thin-Film Battery for Fully Flexible Electronic Systems," *Nano Letters* 12, no. 9 (2012): 4810–4816, https://doi.org/10.1021/nl302254v.

58. Z. Hao, L. Xu, Q. Liu, et al., "On-Chip Ni–Zn Microbattery Based on Hierarchical Ordered Porous Ni@Ni(OH)$_2$ Microelectrode With Ultrafast

16163028, 2026, 33, Downloaded from https://advanced.onlinelibrary.wiley.com/doi/10.1002/adfm.202524957 by Nanjing University, Wiley Online Library on [03/11/2026]. See the Terms and Conditions (https://onlinelibrary.wiley.com/terms-and-conditions) on Wiley Online Library for rules of use; OA articles are governed by the applicable Creative Commons License

Ion and Electron Transport Kinetics," *Advanced Functional Materials* 29, no. 16 (2019): 1808470, https://doi.org/10.1002/adfm.201808470.

59. K. Wu, J. Huang, J. Yi, et al., "Recent Advances in Polymer Electrolytes for Zinc Ion Batteries: Mechanisms, Properties, and Perspectives," *Advanced Energy Materials* 10, no. 12 (2020): 1903977, https://doi.org/10.1002/aenm.201903977.

60. W. Lai, Y. Wang, Z. Lei, et al., "High Performance, Environmentally Benign and Integratable Zn//MnO_2 Microbatteries," *Journal of Materials Chemistry A* 6, no. 9 (2018): 3933–3940, https://doi.org/10.1039/C7TA10936A.

61. D. Ruzmetov, V. P. Oleshko, P. M. Haney, et al., "Electrolyte Stability Determines Scaling Limits for Solid-State 3D Li Ion Batteries," *Nano Letters* 12, no. 1 (2012): 505–511, https://doi.org/10.1021/nl204047z.

62. J. H. Pikul, H. Gang Zhang, J. Cho, P. V. Braun, and W. P. King, "High-Power Lithium Ion Microbatteries From Interdigitated Three-Dimensional Bicontinuous Nanoporous Electrodes," *Nature Communications* 4, no. 1 (2013): 1732, https://doi.org/10.1038/ncomms2747.

63. J. Trask, A. Anapolsky, B. Cardozo, et al., "Optimization of 10-μm, Sputtered, $LiCoO_2$ Cathodes to Enable Higher Energy Density Solid State Batteries," *Journal of Power Sources* 350 (2017): 56–64, https://doi.org/10.1016/j.jpowsour.2017.03.017.

64. D. Cao, Y. Xing, K. Tantratian, et al., "3D Printed High-Performance Lithium Metal Microbatteries Enabled by Nanocellulose," *Advanced Materials* 31, no. 14 (2019): 1807313, https://doi.org/10.1002/adma.201807313.

65. M. Sadeq Saleh, M. HamidVishkasougheh, H. Zbib, and R. Panat, "Polycrystalline Micropillars by a Novel 3-D Printing Method and Their Behavior Under Compressive Loads," *Scripta Materialia* 149 (2018): 144–149, https://doi.org/10.1016/j.scriptamat.2018.02.027.

66. Y. Zhu, S. Wang, Y. Ma, et al., "High-Voltage Monolithically Integrated Solid-State Microbatteries With Exceptional Flexibility and Superior Areal Capacity," *Energy Storage Materials* 76 (2025): 104146, https://doi.org/10.1016/j.ensm.2025.104146.

67. Y. Wang, Y. Zhao, L. Yu, et al., "Deformation-Tolerant, Wireless-Charging Microbatteries for Seamlessly Integrated Omnidirectional Stretchable Electronics," *Science Advances* 11, no. 8 (2025): ads6892, https://doi.org/10.1126/sciadv.ads6892.

68. W. C. West, J. F. Whitacre, V. White, and B. V. Ratnakumar, "Fabrication and Testing of all Solid-State Microscale Lithium Batteries for Microspacecraft Applications," *Journal of Micromechanics and Microengineering* 12, no. 1 (2001): 58, https://doi.org/10.1088/0960-1317/12/1/309.

69. L. Mai, Y. Dong, L. Xu, and C. Han, "Single Nanowire Electrochemical Devices," *Nano Letters* 10, no. 10 (2010): 4273–4278, https://doi.org/10.1021/nl102845r.

70. D. Voiry, R. Fullon, J. Yang, et al., "The Role of Electronic Coupling Between Substrate and 2D MoS_2 Nanosheets in Electrocatalytic Production of Hydrogen," *Nature Materials* 15, no. 9 (2016): 1003–1009, https://doi.org/10.1038/nmat4660.

71. V. K. Bandari and O. G. Schmidt, "System-Engineered Miniaturized Robots: From Structure to Intelligence," *Advanced Intelligent Systems* 3, no. 10 (2021): 2000284, https://doi.org/10.1002/aisy.202000284.

72. A. S. Algamili, M. H. M. Khir, J. O. Dennis, et al., "A Review of Actuation and Sensing Mechanisms in MEMS-Based Sensor Devices," *Nanoscale research letters* 16 (2021): 1–21, https://doi.org/10.1186/s11671-021-03481-7.

73. H. C. Ates, P. Q. Nguyen, L. Gonzalez-Macia, et al., "End-to-End Design of Wearable Sensors," *Nature Reviews Materials* 7, no. 11 (2022): 887–907, https://doi.org/10.1038/s41578-022-00460-x.

74. J. Baranwal, B. Barse, G. Gatto, G. Broncova, and A. Kumar, "Electrochemical Sensors and Their Applications: A Review," *Chemosensors* 10, no. 9 (2022): 363, https://doi.org/10.3390/chemosensors10090363.

75. F. Tan, H. An, N. Li, J. Du, and Z. Peng, "A Study on $Li_{0.33}La_{0.55}TiO_3$ Solid Electrolyte With High Ionic Conductivity and Its Application in Flexible All-Solid-State Batteries," *Nanoscale* 13, no. 26 (2021): 11518–11524, https://doi.org/10.1039/D1NR02427B.

76. G. D. Salian, C. Lebouin, A. Galeyeva, A. P. Kurbatov, and T. Djenizian, "Electrodeposition of Polymer Electrolyte Into Porous LiNi0. 5Mn1. 5O4 for High Performance All-Solid-State Microbatteries," *Frontiers in Chemistry* 6 (2019): 675, https://doi.org/10.3389/fchem.2018.00675.

77. N. Plylahan, M. Letiche, M. K. S. Barr, and T. Djenizian, "All-Solid-State Lithium-Ion Batteries Based on Self-Supported Titania Nanotubes," *Electrochemistry communications* 43 (2014): 121–124, https://doi.org/10.1016/j.elecom.2014.03.029.

78. M. Nasreldin, R. Delattre, C. Calmes, et al., "High Performance Stretchable Li-Ion Microbattery," *Energy Storage Materials* 33 (2020): 108–115, https://doi.org/10.1016/j.ensm.2020.07.005.

79. Q. Xia, S. Sun, J. Xu, et al., "Self-Standing 3D Cathodes for All-Solid-State Thin Film Lithium Batteries With Improved Interface Kinetics," *Small* 14, no. 52 (2018): 1804149, https://doi.org/10.1002/smll.201804149.

80. H. Kim, J. B. Cook, H. Lin, et al., "Oxygen Vacancies Enhance Pseudocapacitive Charge Storage Properties of MoO_{3-X}," *Nature Materials* 16, no. 4 (2017): 454–460, https://doi.org/10.1038/nmat4810.

81. H. Xia, Q. Xia, B. Lin, J. Zhu, J. K. Seo, and Y. S. Meng, "Self-Standing Porous $LiMn_2O_4$ Nanowall Arrays as Promising Cathodes for Advanced 3D Microbatteries and Flexible Lithium-Ion Batteries," *Nano Energy* 22 (2016): 475–482, https://doi.org/10.1016/j.nanoen.2016.01.022.

82. K. Yu, X. Pan, G. Zhang, et al., "Nanowires in Energy Storage Devices: Structures, Synthesis, and Applications," *Advanced Energy Materials* 8, no. 32 (2018): 1802369, https://doi.org/10.1002/aenm.201802369.

83. A. D. Refino, E. Adhitama, M. M. Bela, et al., "Impact of Exposing Lithium Metal to Monocrystalline Vertical Silicon Nanowires for Lithium-Ion Microbatteries," *Communications Materials* 4, no. 1 (2023): 58, https://doi.org/10.1038/s43246-023-00385-0.

84. A. D. Refino, N. Yulianto, S. Priyono, et al., "Carbon-Coating Effect on the Performance of Photolithographically-Structured Si Nanowires for Lithium-Ion Microbattery Anodes," *Communications Materials* 6, no. 1 (2025): 32, https://doi.org/10.1038/s43246-025-00755-w.

85. X. Song, J. Fan, B. Sun, et al., "Direct Growth and Integration of Silicon Nanowire Transistors on Polymer Substrates," *ACS Applied Materials & Interfaces* 17, no. 34 (2025): 48503–48510, https://doi.org/10.1021/acsami.5c11278.

86. Z. Li, J. Allen, M. Allen, H. H. Tan, C. Jagadish, and L. Fu, "Review on III-V Semiconductor Single Nanowire-Based Room Temperature Infrared Photodetectors," *Materials* 13, no. 6 (2020): 1400, https://doi.org/10.3390/ma13061400.

87. Z. Yang, T. Albrow-Owen, H. Cui, et al., "Single-Nanowire Spectrometers," *Science* 365, no. 6457 (2019): 1017–1020, https://doi.org/10.1126/science.aax8814.

88. J. Deng, Y. Su, D. Liu, P. Yang, B. Liu, and C. Liu, "Nanowire Photoelectrochemistry," *Chemical Reviews* 119, no. 15 (2019): 9221–9259, https://doi.org/10.1021/acs.chemrev.9b00232.

89. E. Garnett, L. Mai, and P. Yang, "Introduction: 1D Nanomaterials/Nanowires," *Chemical Reviews* 119, no. 15 (2019): 8955–8957, https://doi.org/10.1021/acs.chemrev.9b00423.

90. C. Jia, Z. Lin, Y. Huang, and X. Duan, "Nanowire Electronics: From Nanoscale to Macroscale," *Chemical Reviews* 119, no. 15 (2019): 9074–9135, https://doi.org/10.1021/acs.chemrev.9b00164.

91. I. Holzman and Y. Ivry, "Superconducting Nanowires for Single-Photon Detection: Progress, Challenges, and Opportunities," *Advanced Quantum Technologies* 2, no. 3-4 (2019): 1800058, https://doi.org/10.1002/qute.201800058.

92. M. Jansson, V. V. Nosenko, Y. Torigoe, et al., "High-Performance Multiwavelength GaNAs Single Nanowire Lasers,"

16163028, 2026, 33, Downloaded from https://advanced.onlinelibrary.wiley.com/doi/10.1002/adfm.202524957 by Nanjing University, Wiley Online Library on [03/11/2026]. See the Terms and Conditions (https://onlinelibrary.wiley.com/terms-and-conditions) on Wiley Online Library for rules of use; OA articles are governed by the applicable Creative Commons License

ACS Nano 18, no. 2 (2024): 1477–1484, https://doi.org/10.1021/acsnano.3c07980.

93. L. Yu, M. Oudwan, O. Moustapha, F. Fortuna, and P. Roca i Cabarrocas, "Guided Growth of In-Plane Silicon Nanowires," *Applied Physics Letters* 95, no. 11 (2009), https://doi.org/10.1063/1.3227667.

94. R. Yuan, W. Qian, Y. Zhang, et al., "Orthogonal-Stacking Integration of Highly Conductive Silicide Nanowire Network as Flexible and Transparent Thin Films," *Advanced Electronic Materials* 9, no. 7 (2023): 2201185, https://doi.org/10.1002/aelm.202201185.

95. X. Song, L. Wu, Y. Liang, et al., "High-Performance Transparent Silicon Nanowire Thin Film Transistors Integrated on Glass Substrates via a Room Temperature Solution Passivation," *Advanced Electronic Materials* 9, no. 4 (2023): 2201236, https://doi.org/10.1002/aelm.202201236.

96. X. Song, T. Zhang, L. Wu, et al., "Highly Stretchable High-Performance Silicon Nanowire Field Effect Transistors Integrated on Elastomer Substrates," *Advanced Science* 9, no. 9 (2022): 2105623, https://doi.org/10.1002/advs.202105623.

97. X. Song, Y. Gu, S. Wang, J. Fan, J. An, and L. Yan, "Scalable Integration of High Sensitivity Strain Sensors Based on Silicon Nanowire Spring Array Directly Grown on Flexible Polyimide Films," *Nano Letters* 25, no. 6 (2025): 2290–2297, https://doi.org/10.1021/acs.nanolett.4c05553.

98. L. Wu, Z. Hu, L. Liang, R. Hu, J. Wang, and L. Yu, "Step-Necking Growth of Silicon Nanowire Channels for High Performance Field Effect Transistors," *Nature Communications* 16, no. 1 (2025): 965, https://doi.org/10.1038/s41467-025-56376-x.

99. J. Yan, Y. Zhang, Z. Liu, J. Wang, J. Xu, and L. Yu, "Ultracompact Single-Nanowire-Morphed Grippers Driven by Vectorial Lorentz Forces for Dexterous Robotic Manipulations," *Nature Communications* 14, no. 1 (2023): 3786, https://doi.org/10.1038/s41467-023-39524-z.

100. X. Xu, M. Yan, X. Tian, et al., "In Situ Investigation of Li and Na Ion Transport With Single Nanowire Electrochemical Devices," *Nano Letters* 15, no. 6 (2015): 3879–3884, https://doi.org/10.1021/acs.nanolett.5b00705.

101. S. R. Gowda, A. Leela Mohana Reddy, X. Zhan, and P. M. Ajayan, "Building Energy Storage Device on a Single Nanowire," *Nano Letters* 11, no. 8 (2011): 3329–3333, https://doi.org/10.1021/nl2017042.

102. L. Zheng, S. Zhang, H. Huang, et al., "Artificial Intelligence-Driven Rechargeable Batteries in Multiple Fields of Development and Application Towards Energy Storage," *Journal of Energy Storage* 73 (2023): 108926, https://doi.org/10.1016/j.est.2023.108926.

103. D. Shi, J. Zhao, C. Eze, et al., "Cloud-Based Artificial Intelligence Framework for Battery Management System," *Energies* 16, no. 11 (2023): 4403, https://doi.org/10.3390/en16114403.

104. T. Vegge, J. Tarascon, and K. Edström, "Toward Better and Smarter Batteries by Combining AI With Multisensory and Self-Healing Approaches," *Advanced Energy Materials* 11, no. 23 (2021): 2100362, https://doi.org/10.1002/aenm.202100362.

105. S. Wang, J. Liu, X. Song, et al., "Artificial Intelligence Empowers Solid-State Batteries for Material Screening and Performance Evaluation," *Nano-Micro Letters* 17, no. 1 (2025): 287, https://doi.org/10.1007/s40820-025-01797-y.

106. Q. Zheng, X. Shi, Y. Cai, L. An, and D. Zhang, "Artificial Intelligence-Empowered Modeling and Management of Flow Batteries: A Mini-Review," *Future Batteries* 7 (2025): 100107, https://doi.org/10.1016/j.fub.2025.100107.

107. A. Jose, C. A. D. Cook, J. Palacios, et al., "Recent Advancements in Artificial Intelligence in Battery Recycling," *Batteries* 10, no. 12 (2024): 440, https://doi.org/10.3390/batteries10120440.

108. Q. Hu, J. Lu, J. Hui, Z. Rao, Y. Ren, and H. Wang, "Artificial Intelligence-Driven Development in Rechargeable Battery Materials: Progress, Challenges, and Future Perspectives," *Advanced Functional Materials* 35 (2025): 08438, https://doi.org/10.1002/adfm.202508438.

109. T. Zahid, K. Xu, W. Li, C. Li, and H. Li, "State of Charge Estimation for Electric Vehicle Power Battery Using Advanced Machine Learning Algorithm Under Diversified Drive Cycles," *Energy* 162 (2018): 871–882, https://doi.org/10.1016/j.energy.2018.08.071.

110. T. Kono, Y. Taito, and H. Hidaka, "Essential Roles, Challenges and Development of Embedded MCU Micro-Systems to Innovate Edge Computing for the IoT/AI Age," *IEICE Transactions on Electronics* E103C, no. 4 (2020): 132–143, https://doi.org/10.1587/transele.2019CDI0001.

111. H. Zhou, H. Zhang, R. Zhang, X. Yuan, and H. Chang, "AI-Driven Photonic Noses: From Conventional Sensors to Cloud-to-Edge Intelligent Microsystems," *Microsystems & Nanoengineering* 11, no. 1 (2025): 209, https://doi.org/10.1038/s41378-025-01058-3.

112. H. Tsai, S. Podder, and P. Chen, "Microsystem Advances Through Integration With Artificial Intelligence," *Micromachines* 14, no. 4 (2023): 826, https://doi.org/10.3390/mi14040826.

113. X. Wang, S. Zheng, F. Zhou, et al., "Scalable Fabrication of Printed $Zn//MnO_2$ Planar Micro-Batteries With High Volumetric Energy Density and Exceptional Safety," *National Science Review* 7, no. 1 (2020): 64–72, https://doi.org/10.1093/nsr/nwz070.

114. S. Lawes, Q. Sun, A. Lushington, B. Xiao, Y. Liu, and X. Sun, "Inkjet-Printed Silicon as High Performance Anodes for Li-Ion Batteries," *Nano Energy* 36 (2017): 313–321, https://doi.org/10.1016/j.nanoen.2017.04.041.

115. L. Cao, G. Fang, H. Cao, and X. Duan, "Photopatterning and Electrochemical Energy Storage Properties of an On-Chip Organic Radical Microbattery," *Langmuir* 35, no. 49 (2019): 16079–16086, https://doi.org/10.1021/acs.langmuir.9b02079.

116. X. Jin, L. Song, C. Dai, et al., "A Flexible Aqueous Zinc–Iodine Microbattery With Unprecedented Energy Density," *Advanced Materials* 34, no. 15 (2022): 2109450, https://doi.org/10.1002/adma.202109450.

117. A. Farmani and T. A. Nguyen, "Battery-on-a-Chip," in *Nanobatteries and Nanogenerators* (Elsevier, 2021), 447–461.

118. L. Liu, Q. Weng, X. Lu, X. Sun, L. Zhang, and O. G. Schmidt, "Advances on Microsized On-Chip Lithium-Ion Batteries," *Small* 13, no. 45 (2017): 1701847, https://doi.org/10.1002/smll.201701847.

119. L. Romano Brandt, K. Nishio, E. Salvati, et al., "Improving Ultra-Fast Charging Performance and Durability of all Solid State Thin Film Li-NMC Battery-on-Chip Systems by in Situ TEM Lamella Analysis," *Applied Materials Today* 26 (2022): 101282, https://doi.org/10.1016/j.apmt.2021.101282.

120. Y. Chen, H. Liao, Y. Cheng, J. Huang, and C. Liu, "Scalable Interlayer Nanostructure Design for High-Rate (10C) Submicron Silicon-Film Electrode by Incorporating Silver Nanoparticles," *ACS Applied Materials & Interfaces* 15, no. 15 (2023): 18845–18856, https://doi.org/10.1021/acsami.2c23279.

121. S. Sun, Z. Han, W. Liu, et al., "Lattice Pinning in MoO_3 via Coherent Interface With Stabilized Li^+ Intercalation," *Nature Communications* 14, no. 1 (2023): 6662, https://doi.org/10.1038/s41467-023-42335-x.

122. V. P. Phan, B. Pecquenard, and F. Le Cras, "High-Performance All-Solid-State Cells Fabricated With Silicon Electrodes," *Advanced Functional Materials* 22, no. 12 (2012): 2580–2584, https://doi.org/10.1002/adfm.201200104.

123. S. Kanazawa, T. Baba, K. Yoneda, M. Mizuhata, and I. Kanno, "Deposition and Performance of all Solid-State Thin-Film Lithium-Ion Batteries Composed of Amorphous Si/LiPON/VO-LiPO Multilayers," *Thin Solid Films* 697 (2020): 137840, https://doi.org/10.1016/j.tsf.2020.137840.

124. A. A. Talin, D. Ruzmetov, A. Kolmakov, et al., "Fabrication, Testing, and Simulation of All-Solid-State Three-Dimensional Li-Ion Batteries," *ACS Applied Materials & Interfaces* 8, no. 47 (2016): 32385–32391, https://doi.org/10.1021/acsami.6b12244.

125. W. Ko, M. Fang, M. Li, and K. Lin, "Fabrication of Self-Standing Si–TiO_2 Web-Nanowired Anodes for High Volumetric Capacity Lithium Ion Microbatteries," *Nano Express* 1, no. 3 (2020): 030014, https://doi.org/10.1088/2632-959X/abc295.

16163028, 2026, 33, Downloaded from https://advanced.onlinelibrary.wiley.com/doi/10.1002/adfm.202524957 by Nanjing University, Wiley Online Library on [03/11/2026]. See the Terms and Conditions (https://onlinelibrary.wiley.com/terms-and-conditions) on Wiley Online Library for rules of use; OA articles are governed by the applicable Creative Commons License

126. H. Tang, D. D. Karnaushenko, V. Neu, et al., "Stress-Actuated Spiral Microelectrode for High-Performance Lithium-Ion Microbatteries," *Small* 16, no. 35 (2020): 2002410, https://doi.org/10.1002/smll.202002410.

127. L. Baggetto, R. A. H. Niessen, F. Roozeboom, and P. H. L. Notten, "High Energy Density All-Solid-State Batteries: A Challenging Concept Towards 3D Integration," *Advanced Functional Materials* 18, no. 7 (2008): 1057–1066, https://doi.org/10.1002/adfm.200701245.

128. B. Laïk, L. Eude, J. Pereira-Ramos, C. S. Cojocaru, D. Pribat, and E. Rouvière, "Silicon Nanowires as Negative Electrode for Lithium-Ion Microbatteries," *Electrochimica Acta* 53, no. 17 (2008): 5528–5532, https://doi.org/10.1016/j.electacta.2008.02.114.

129. H. Beydaghi, S. Abouali, S. B. Thorat, et al., "3D Printed Silicon-Few Layer Graphene Anode for Advanced Li-Ion Batteries," *RSC Advances* 11, no. 56 (2021): 35051–35060, https://doi.org/10.1039/D1RA06643A.

130. M. Sternad, G. Hirtler, M. Sorger, et al., "A Lithium-Silicon Microbattery With Anode and Housing Directly Made From Semiconductor Grade Monocrystalline Si," *Advanced Materials Technologies* 7, no. 3 (2022): 2100405, https://doi.org/10.1002/admt.202100405.

131. A. D. Refino, N. Yulianto, I. Syamsu, et al., "Versatilely Tuned Vertical Silicon Nanowire Arrays by Cryogenic Reactive Ion Etching as a Lithium-Ion Battery Anode," *Scientific Reports* 11, no. 1 (2021): 19779, https://doi.org/10.1038/s41598-021-99173-4.

132. A. P. Nugroho, N. H. Hawari, B. Prakoso, et al., "Vertically Aligned n-Type Silicon Nanowire Array as a Free-Standing Anode for Lithium-Ion Batteries," *Nanomaterials* 11, no. 11 (2021): 3137, https://doi.org/10.3390/nano11113137.

133. X. Zhao, N. Kalidas, and V. Lehto, "Self-Standing Mesoporous Si Films as Anodes for Lithium-Ion Microbatteries," *Journal of Power Sources* 529 (2022): 231269, https://doi.org/10.1016/j.jpowsour.2022.231269.

134. V. Chaudoy, E. Luais, F. Ghamouss, et al., "Anode Based on Porous Silicon Films Using Polymer Electrolyte for Lithium-Ion Microbatteries," *ECS Transactions* 66, no. 8 (2015): 31, https://doi.org/10.1149/06608.0031ecst.

135. E. Luais, F. Ghamouss, J. Wolfman, et al., "Mesoporous Silicon Negative Electrode for Thin Film Lithium-Ion Microbatteries," *Journal of Power Sources* 274 (2015): 693–700, https://doi.org/10.1016/j.jpowsour.2014.10.084.

136. P. He, J. Cao, H. Ding, et al., "Screen-Printing of a Highly Conductive Graphene Ink for Flexible Printed Electronics," *ACS Applied Materials & Interfaces* 11, no. 35 (2019): 32225–32234, https://doi.org/10.1021/acsami.9b04589.

137. K. Zub, S. Hoeppener, and U. S. Schubert, "Inkjet Printing and 3D Printing Strategies for Biosensing, Analytical, and Diagnostic Applications," *Advanced Materials* 34, no. 31 (2022): 2105015, https://doi.org/10.1002/adma.202105015.

138. W. Liu, J. Wang, X. Xu, C. Zhao, X. Xu, and P. S. Weiss, "Single-Step Dual-Layer Photolithography for Tunable and Scalable Nanopatterning," *Acs Nano* 15, no. 7 (2021): 12180–12188, https://doi.org/10.1021/acsnano.1c03703.

139. Q. Zhang, J. Yan, X. Ma, L. Zhao, P. Song, and L. Xia, "Self-Calibrated Paper-Based Nanoarrays for Background-Free Quantitative Detection of Pesticides Using Self-Assembly and Mask-Assisted Techniques," *Journal of Hazardous Materials* 480 (2024): 136195, https://doi.org/10.1016/j.jhazmat.2024.136195.

140. Z. Qu, M. Zhu, Y. Yin, et al., "A Sub-Square-Millimeter Microbattery With Milliampere-Hour-Level Footprint Capacity," *Advanced Energy Materials* 12, no. 28 (2022): 2200714, https://doi.org/10.1002/aenm.202200714.

141. K. S. Kim, S. Seo, J. Kwon, et al., "Growth-Based Monolithic 3D Integration of Single-Crystal 2D Semiconductors," *Nature* 636, no. 8043 (2024): 615–621, https://doi.org/10.1038/s41586-024-08236-9.

142. Y. Liang, W. Wu, D. Li, et al., "Highly Stable Lithium Metal Batteries by Regulating the Lithium Nitrate Chemistry With a Modified Eutectic Electrolyte," *Advanced Energy Materials* 12, no. 47 (2022): 2202493, https://doi.org/10.1002/aenm.202202493.

143. Y. Cheng, X. Guo, and V. F. Pavlidis, "Emerging Monolithic 3D Integration: Opportunities and Challenges From the Computer System Perspective," *Integration* 85 (2022): 97–107, https://doi.org/10.1016/j.vlsi.2022.04.004.

144. Y. Li, M. Zhu, D. D. Karnaushenko, et al., "Microbatteries With Twin-Swiss-Rolls Redefine Performance Limits in the Sub-Square Millimeter Range," *Nanoscale Horizons* 8, no. 1 (2023): 127–132, https://doi.org/10.1039/D2NH00472K.

145. Y. Li, M. Zhu, V. K. Bandari, et al., "On-Chip Batteries for Dust-Sized Computers," *Advanced Energy Materials* 12, no. 13 (2022): 2103641, https://doi.org/10.1002/aenm.202103641.

146. S. Oukassi, A. Bazin, C. Secouard, et al., "Millimeter Scale Thin Film Batteries for Integrated High Energy Density Storage," IEEE International Electron Devices Meeting (IEDM), (2019), https://doi.org/10.1109/IEDM19573.2019.8993483.

147. J. Chen, W. Zhao, Y. Gao, et al., "Single-Layer MoS2/Graphene-Based Stable on-Chip Zn-Ion Microbattery for Monolithically Integrated Electronics," *Science Bulletin* 70, no. 4 (2025): 508–517, https://doi.org/10.1016/j.scib.2024.11.023.

148. C. Dai, L. Hu, X. Jin, et al., "Fast Constructing Polarity-Switchable Zinc-Bromine Microbatteries With High Areal Energy Density," *Science Advances* 8, no. 28 (2022): abo6688, https://doi.org/10.1126/sciadv.abo6688.

149. S. Ko, H. Otsuka, S. Kimura, et al., "Rapid Safety Screening Realized by Accelerating Rate Calorimetry With Lab-Scale Small Batteries," *Nature Energy* 10 (2025): 707–714, https://doi.org/10.1038/s41560-025-01751-7.

150. Y. Liu, X. Tang, Z. Xu, L. Hong, P. Wang, and D. Chen, "Optimization and Temperature Effects on Sandwich Betavoltaic Microbattery," *Science China Technological Sciences* 57 (2014): 14–18, https://doi.org/10.1007/s11431-013-5413-0.

151. L. Yunpeng, G. Xiao, J. Zhangang, and T. Xiaobin, "Temperature Dependence of ^{63}Ni–Si Betavoltaic Microbattery," *Applied Radiation and Isotopes* 135 (2018): 47–56, https://doi.org/10.1016/j.apradiso.2018.01.017.

152. S. Butera, M. D. C. Whitaker, G. Lioliou, and A. M. Barnett, "AlGaAs$_{55}$Fe X-Ray Radioisotope Microbattery," *Scientific Reports* 6, no. 1 (2016): 38409, https://doi.org/10.1038/srep38409.

153. V. Pachkawade, "Bioinspired Micro-Electromechanical Systems/Nano-Electromechanical Systems: An Overview, Applications, and Perspective," *Nature-Derived Sensors* (2025): 267–293, https://doi.org/10.1016/B978-0-443-22002-9.00011-7.

154. P. Pulugu, S. Ghosh, S. Rokade, K. Choudhury, N. Arya, and P. Kumar, "A Perspective on Implantable Biomedical Materials and Devices for Diagnostic Applications," *Current Opinion in Biomedical Engineering* 18 (2021): 100287, https://doi.org/10.1016/j.cobme.2021.100287.

155. N. Hossain, M. Z. A. Mahmud, A. Hossain, et al., "Advances of Materials Science in MEMS Applications: A Review," *Results in Engineering* 22 (2024): 102115, https://doi.org/10.1016/j.rineng.2024.102115.

156. A. Sohail, A. Ali, H. Shaukat, et al., "Integrating Self-Powered Medical Devices With Advanced Energy Harvesting: A Review," *Energy Strategy Reviews* 52 (2024): 101328, https://doi.org/10.1016/j.esr.2024.101328.

157. J. A. Khatokar, N. Vinay, A. S. Bale, et al., "A Study on Improved Methods in Micro-Electromechanical Systems Technology," *Materials Today: Proceedings* 43 (2021): 3784–3790, https://doi.org/10.1016/j.matpr.2020.10.993.

158. M. Mariello, I. Eş, and C. M. Proctor, "Soft and Flexible Bioelectronic Micro-Systems for Electronically Controlled Drug Delivery," *Advanced Healthcare Materials* 13, no. 24 (2024): 2302969, https://doi.org/10.1002/adhm.202302969.

159. J. Park, B. Seo, Y. Jeong, and I. Park, "A Review of Recent Advancements in Sensor-Integrated Medical Tools," *Advanced Science* 11, no. 20 (2024): 2307427, https://doi.org/10.1002/advs.202307427.

16163028, 2026, 33, Downloaded from https://advanced.onlinelibrary.wiley.com/doi/10.1002/adfm.202524957 by Nanjing University, Wiley Online Library on [03/11/2026]. See the Terms and Conditions (https://onlinelibrary.wiley.com/terms-and-conditions) on Wiley Online Library for rules of use; OA articles are governed by the applicable Creative Commons License

160. M. I. Hossain, M. S. Zahid, M. A. Chowdhury, M. M. Maruf Hossain, and N. Hossain, "MEMS-Based Energy Harvesting Devices for Low-Power Applications–A Review," *Results in Engineering* 19 (2023): 101264, https://doi.org/10.1016/j.rineng.2023.101264.

161. R. De Fazio, V. M. Mastronardi, M. De Vittorio, and P. Visconti, "Wearable Sensors and Smart Devices to Monitor Rehabilitation Parameters and Sports Performance: An Overview," *Sensors* 23, no. 4 (2023): 1856, https://doi.org/10.3390/s23041856.

162. R. U. S. Ahmad, M. S. Khan, M. E. Hilal, B. Khan, Y. Zhang, and B. L. Khoo, "Advancements in Wearable Heart Sounds Devices for the Monitoring of Cardiovascular Diseases," *SmartMat* 6, no. 1 (2025): 1311, https://doi.org/10.1002/smm2.1311.

163. A. Ali, H. Shaukat, S. Bibi, W. A. Altabey, M. Noori, and S. A. Kouritem, "Recent Progress in Energy Harvesting Systems for Wearable Technology," *Energy Strategy Reviews* 49 (2023): 101124, https://doi.org/10.1016/j.esr.2023.101124.

164. G. Whang, R. Chen, J. T. T. Yu, et al., "Do Micropower Sources Meet the Needs of the Internet of Things?" *Advanced Energy Materials* 15 (2025): 03921, https://doi.org/10.1002/aenm.202503921.

165. T. D. Hedberg, M. E. Sharp, T. M. M. Maw, et al., "Defining Requirements for Integrating Information Between Design, Manufacturing, and Inspection," *International Journal of Production Research* 60, no. 11 (2022): 3339–3359, https://doi.org/10.1080/00207543.2021.1920057.

166. A. Khang, R. Sita, and V. Shah, "Enabling the Future of Manufacturing: Integration of Robotics and IoT to Smart Factory Infrastructure in Industry 4.0," in *Handbook of Research on AI-Based Technologies and Applications in the Era of the Metaverse* (IGI Global, 2023), 25–50.

167. D. Gu, X. Shi, R. Poprawe, D. L. Bourell, R. Setchi, and J. Zhu, "Material-Structure-Performance Integrated Laser-Metal Additive Manufacturing," *Science* 372, no. 6545 (2021): abg1487, https://doi.org/10.1126/science.abg1487.

168. R. Singh and N. Bhanot, "An Integrated DEMATEL-MMDE-ISM Based Approach for Analysing the Barriers of IoT Implementation in the Manufacturing Industry," *International Journal of Production Research* 58, no. 8 (2020): 2454–2476, https://doi.org/10.1080/00207543.2019.1675915.

169. I. Y. Wuni and G. Q. Shen, "Developing Critical Success Factors for Integrating Circular Economy Into Modular Construction Projects in Hong Kong," *Sustainable Production and Consumption* 29 (2022): 574–587, https://doi.org/10.1016/j.spc.2021.11.010.

170. Y. Liao, H. Yao, A. Lingley, B. Parviz, and B. P. Otis, "A 3-μW CMOS Glucose Sensor for Wireless Contact-Lens Tear Glucose Monitoring," *IEEE Journal of Solid-State Circuits* 47, no. 1 (2011): 335–344, https://doi.org/10.1109/JSSC.2011.2170633.

171. Y. Chen, D. Jeon, Y. Lee, et al., "An Injectable 64 nW ECG Mixed-Signal SoC in 65 Nm for Arrhythmia Monitoring," *IEEE Journal of Solid-State Circuits* 50, no. 1 (2014): 375–390, https://doi.org/10.1109/JSSC.2014.2364036.

172. K. Chen, L. Yan, Y. Sheng, Y. Ma, L. Qu, and Y. Zhao, "An Edible and Nutritive Zinc-Ion Micro-Supercapacitor in the Stomach With Ultrahigh Energy Density," *ACS nano* 16, no. 9 (2022): 15261–15272, https://doi.org/10.1021/acsnano.2c06656.

173. G. Zhang, F. Geng, T. Zhao, et al., "Biocompatible Symmetric Na-Ion Microbatteries With Sphere-in-Network Heteronanomat Electrodes Realizing High Reliability and High Energy Density for Implantable Bioelectronics," *ACS Applied Materials & Interfaces* 10, no. 49 (2018): 42268–42278, https://doi.org/10.1021/acsami.8b14918.

174. T. Ye, J. Wang, Y. Jiao, et al., "A Tissue-Like Soft All-Hydrogel Battery," *Advanced Materials* 34, no. 4 (2022): 2105120, https://doi.org/10.1002/adma.202105120.

175. T. Mei, C. Wang, M. Liao, et al., "A Biodegradable and Rechargeable fiber Battery," *Journal of Materials Chemistry A* 9, no. 16 (2021): 10104–10109, https://doi.org/10.1039/D1TA01507A.

176. M. Fojtik, D. Kim, G. Chen, et al., "A Millimeter-Scale Energy-Autonomous Sensor System With Stacked Battery and Solar Cells," *IEEE Journal of Solid-State Circuits* 48, no. 3 (2013): 801–813, https://doi.org/10.1109/JSSC.2012.2233352.

177. T. Kuriyama, A. Suzuki, Y. Okamoto, I. Kimura, Y. Morikawa, and Y. Mita, "A Micromachined All-Solid on-Chip Thin-Film Battery towards Uninterruptible Photovoltaic Cells. Paper Presented at the 2018 Symposium on Design," in 2018 Symposium on Design, Test, Integration & Packaging of MEMS and MOEMS (DTIP), (IEEE, 2018).

178. B. Jia, C. Zhang, M. Liu, et al., "Integration of Microbattery With Thin-Film Electronics for Constructing an Integrated Transparent Microsystem Based on InGaZnO," *Nature Communications* 14, no. 1 (2023): 5330, https://doi.org/10.1038/s41467-023-41181-1.

179. Y. Zhu, J. C. Gonzalez-Rosillo, M. Balaish, Z. D. Hood, K. J. Kim, and J. L. M. Rupp, "Lithium-Film Ceramics for Solid-State Lithionic Devices," *Nature Reviews Materials* 6, no. 4 (2021): 313–331, https://doi.org/10.1038/s41578-020-00261-0.

180. N. Singh, T. Khan, S. Kumar, et al., "Ultra-Thin Flexible Rectenna Integrated With Power Management Unit for Wireless Power Harvester/Charging of Smartwatch/Wristband," *Scientific Reports* 14, no. 1 (2024): 7447, https://doi.org/10.1038/s41598-024-57639-1.

181. M. Saban, L. D. Medus, S. Casans, O. Aghzout, and A. Rosado, "Sensor Node Network for Remote Moisture Measurement in Timber Based on Bluetooth Low Energy and Web-Based Monitoring System," *Sensors* 21, no. 2 (2021): 491, https://doi.org/10.3390/s21020491.

182. H. Ryu, H. Park, M. Kim, et al., "Self-Rechargeable Cardiac Pacemaker System With Triboelectric Nanogenerators," *Nature Communications* 12, no. 1 (2021): 4374, https://doi.org/10.1038/s41467-021-24417-w.

183. R. Chen, A. Canales, and P. Anikeeva, "Neural Recording and Modulation Technologies," *Nature Reviews Materials* 2, no. 2 (2017): 1–16, https://doi.org/10.1038/natrevmats.2016.93.

184. B. Liu, J. Zhuang, and G. Wei, "Recent Advances in the Design of Colorimetric Sensors for Environmental Monitoring," *Environmental Science: Nano* 7, no. 8 (2020): 2195–2213, https://doi.org/10.1039/D0EN00449A.

185. R. Croce and H. van Amerongen, "Light Harvesting in Oxygenic Photosynthesis: Structural Biology Meets Spectroscopy," *Science* 369, no. 6506 (2020): aay2058, https://doi.org/10.1126/science.aay2058.

186. H. H. Ibrahim, M. J. Singh, S. S. Al-Bawri, et al., "Radio Frequency Energy Harvesting Technologies: A Comprehensive Review on Designing, Methodologies, and Potential Applications," *Sensors* 22, no. 11 (2022): 4144, https://doi.org/10.3390/s22114144.

187. Z. Wang, S. Joshi, S. Savel'ev, et al., "Fully Memristive Neural Networks for Pattern Classification With Unsupervised Learning," *Nature Electronics* 1, no. 2 (2018): 137–145, https://doi.org/10.1038/s41928-018-0023-2.

188. A. Jadhav and V. S. Jadhav, "A Review on 3D Printing: An Additive Manufacturing Technology," *Materials Today: Proceedings* 62 (2022): 2094–2099, https://doi.org/10.1016/j.matpr.2022.02.558.

189. S. Wang, X. Chen, X. Han, et al., "A Review of 3D Printing Technology in Pharmaceutics: Technology and Applications, Now and Future," *Pharmaceutics* 15, no. 2 (2023): 416, https://doi.org/10.3390/pharmaceutics15020416.

190. F. Joint, C. Abadie, P. B. Vigneron, et al., "GaAs Manufacturing Processes Conditions for Micro-and Nanoscale Devices," *Journal of Manufacturing Processes* 60 (2020): 666–672, https://doi.org/10.1016/j.jmapro.2020.11.006.

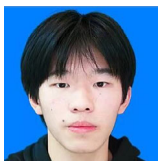
191. I. Levchenko, O. Baranov, M. Keidar, et al., "Additive Technologies and Materials for the Next-Generation CubeSats and Small Satellites," *Advanced Functional Materials* 34, no. 45 (2024): 2407602, https://doi.org/10.1002/adfm.202407602.

16163028, 2026, 33, Downloaded from https://advanced.onlinelibrary.wiley.com/doi/10.1002/adfm.202524957 by Nanjing University, Wiley Online Library on [03/11/2026]. See the Terms and Conditions (https://onlinelibrary.wiley.com/terms-and-conditions) on Wiley Online Library for rules of use; OA articles are governed by the applicable Creative Commons License

Biographies



Sheng Wang received her Ph.D. in Electronic Science and Technology from Nanjing University in 2022. Upon graduation, he was appointed as a Distinguished Young Lecturer at the School of Future Science and Engineering, Soochow University (December 2022 – July 2025). Since July 2025, he has joined the College of Electronic and Optical Engineering & College of Flexible Electronics (Future Technology) at Nanjing University of Posts and Telecommunications. His primary research focuses on solid-state batteries and silicon-nanowire-based flexible electronics.



Huajian Xu received his BS degree from Nantong University in 2023. He is currently pursuing an MS degree at the School of Electronic and Information Engineering, Soochow University. His research focuses on solid-state batteries and micro batteries and their integrated systems.



Xiaopan Song received her Ph.D. in Electronic Science and Technology from Nanjing University in 2023, followed by postdoctoral research at Nanjing University focusing on the precise and controllable growth of silicon-based nanowires and the integration of novel flexible electronic systems, such as high-performance flexible/stretchable transistors, sensors and display devices based on these nanostructures. She is currently appointed as an Associate Researcher at Nanjing University, where she supervises several doctoral and master's students and leads multiple national and provincial-level research projects. Her research is dedicated to developing advanced sensing and display technologies using flexible crystalline silicon nanowires, with applications in next-generation nanoscale human-machine interfaces.



Linwei Yu received his B.S. degree in semiconductor physics in 2001 and his Ph.D. degree in microelectronics from Nanjing University, Nanjing, China, in 2007. From 2007 to 2009, he was a Postdoctoral Researcher at LPICM, Ecole Polytechnique, France, and then joined CNRS as a Permanent Researcher (CR2) in 2009. Since 2013, he has been a Professor with the School of Electronics Science and Engineering, Nanjing University. His research interests include the growth-additive fabrication of silicon-based micro/nano-structures, the development of high-performance FETs and 3D integration technologies, as well as the application of silicon materials for flexible displays, human-machine interfaces, and quantum information technologies.

16163028, 2026, 33, Downloaded from https://advanced.onlinelibrary.wiley.com/doi/10.1002/adfm.202524957 by Nanjing University, Wiley Online Library on [03/11/2026]. See the Terms and Conditions (https://onlinelibrary.wiley.com/terms-and-conditions) on Wiley Online Library for rules of use; OA articles are governed by the applicable Creative Commons License